An Optics Study of Mammal Skin and its Transmission properties

A Thesis presented to the Faculty of the Graduate School
University of Missouri-Columbia

In Partial Fulfillment of the Requirements for the Degree

Master of Science

By

Hisham Abdussamad Abbas

Dr. Gregory E. Triplett Jr., Thesis Supervisor
May 2013

The undersigned, appointed by the Dean of the Graduate School, have examined the thesis entitled

An Optics Study of Mammal Skin and its Transmission properties

Presented by Hisham Abdussamad Abbas

A candidate for the degree of Master of Science

And hereby certify that in their opinion it is worthy of acceptance.

_____

Dr. Gregory Triplett

_____

Dr. Satish Nair

_____

Dr. Kannappan Palaniappan

Acknowledgements

First and foremost, this research would have not been possible without the guidance and support of my advisor Dr. Gregory Triplett. He constantly provided me insight on my research and always wanted me to do better so that I could reach my potential. I also want to thank Dr. Satish Nair and Dr. Kannappan Palaniappan for their advice, encouragement and support.

I would like to thank my lab colleagues Stanley and Hayder for their support and help they provided me during my research.

Last and most importantly, I would like to take this opportunity to thank my family and friends for always supporting me and continuously helping me to make my dreams reality.

Table of Contents

List of Figures

List of Tables

ABSTRACT

A detailed study is performed to understand infrared photonic transmission through skin and the factors that influences transmission at room temperature. Pigskin is the test vehicle of this study since its structure most closely resembles that of human skin. The skin is irradiated using an infrared pulsed source because it can penetrate through thick, fleshy skin more easily and generates light/skin that produces interesting transmission properties. Furthermore, the pulsed beam offers more precise control of thermal generation in the skin. Skin samples of varying thicknesses are also used in this study to emulate multiple skin types. The main objective of this research is to observe the correlated parameters that influence transmission through the layers of skin and to determine a method of effectively improving the associated transmission by minimizing internal losses. The pulse frequency and duty cycle are varied to maximize propagation transmission through the skin layers. The temporal, thermal, spatial and spectral response of the beam spot on the skin's spot are then evaluated.

CHAPTER 1

INTRODUCTION

In the last two decades, the study of electromagnetic irradiation and its influence on live tissue cells have been of great interest. Studies of such interactions help expand the application of photonics in the field of medicine. The study reported in this thesis focuses on the effects of mid-infrared radiation propagation and irradiance on organic tissues.

1.1 Wound Healing

The motivation for this photonics study is enhancement of the wound healing process. Wound healing is a naturally occurring repair phenomenon, which is a highly complicated stepwise process that must be carried out very efficiently. When a wound occurs, the extracellular matrix (ECM), the largest component of dermal skin layer, becomes disturbed. Thus, a reconstruction of ECM is required to enable the wound healing process [1]. Wound healing requires precise coordination between the cell organelles (to evade inadequate wound healing like open wounds, etc.) or it could lead to scars, infections, and in extreme cases amputation, death, etc. The ability to enhance wound healing would be one of the most significant medical discoveries since the invention of the medical ventilator.

Besides the fact that wound healing is a complex repair phenomenon, metabolic disorders like diabetes mellitus fight against the process, which otherwise takes place in a systematic manner. Wound healing in diabetic patients, for example, is suppressed

through the extended inflammatory phase, which postpones the granulation tissue formation, thus resulting to a low tensile strength wound [2]. Diabetic foot ulcers occur in 15% of all diabetes mellitus patients and 84% of those who experience foot ulcers suffer from lower leg amputations [3]. Also, the primary reason for mortality amidst diabetic patients is the suppression of wound healing process [2,4,6].

1.2 Phases of Wound Healing

Wound healing can be divided into four consecutive, but overlapping phases: hemostasis, inflammatory, proliferative, and remodeling. Hemostasis phase is the formation of fibrin clot at the wound site to stop the bleeding. This is done by the aggregation of platelets or thrombocytes at the wound site. Inflammatory phase is the removal of microorganisms (i.e. bacteria). In this process, debris are phagocytized and removed from the wound. This phase overlaps with the proliferative phase-- the division of cells. Proliferative phase is an intricate process demonstrated by the following: angiogenesis, collagen deposition, granular tissue formation, epithelialization, and wound contraction [7]. Angiogenesis is the process of formation of new blood vessels by vascular endothelial cells [8]; granulation tissue formation is the formation of a new temporary extracellular matrix (ECM) by fibroblasts, which provides structural support to the wound by excreting fibronectin and collagen [7] (the fundamental protein of connective tissue); epithelialization is the regrowth of skin over the wound, hence providing concealment for the newly formed tissue and this is accomplished by the action of epithelial cells [9]. Lastly, the wound contracts through the action of myofibroblasts, which establish a grasp on the wound boundaries. When the cells functions are close to complete, unnecessary

cells undergo apoptosis (programmed cell death). In the remodeling phase, collagen is rearranged along tension lines and the cells that are no longer needed are detached by apoptosis. This process is not only complicated, but also unstable and vulnerable to interruption and failure, which leads to chronic non-healing wounds.

1.3 Skin Structure

The human skin comprises of three different regions: the outer layer – epidermis, the middle layer – dermis, and the inner layer- hypodermis. Each layer has varying thicknesses and roles [28]. The following sections describe the role of each and its individual component.

I. Epidermis layer

The epidermis is further divided into 5 layers (from the deepest to the most superficial layer): stratum basale, stratum spinosum, stratum granulosum, stratum lucidum, and the stratum corneum. Stratum basale is the innermost layer present at the dermo-epidermal boundary, where proliferative activity takes place resulting in the generation of new epidermal skin cell. Half of the newly generated skin cells differentiate and move to the next layer to undergo keratinization, while the other half stay in the basal layer and divide over and over again. This layer consists of a single row of columnar or cuboidal cell, which constantly replaces the epidermis as it wears away. Stratum spinosum also known as prickle or spinous cell layer owing to its spiny appearance consists mainly of basal cells produced in the stratum basale, i.e. pushed upward to form prickle cells. Figure 1.1 illustrates the structure of human skin.

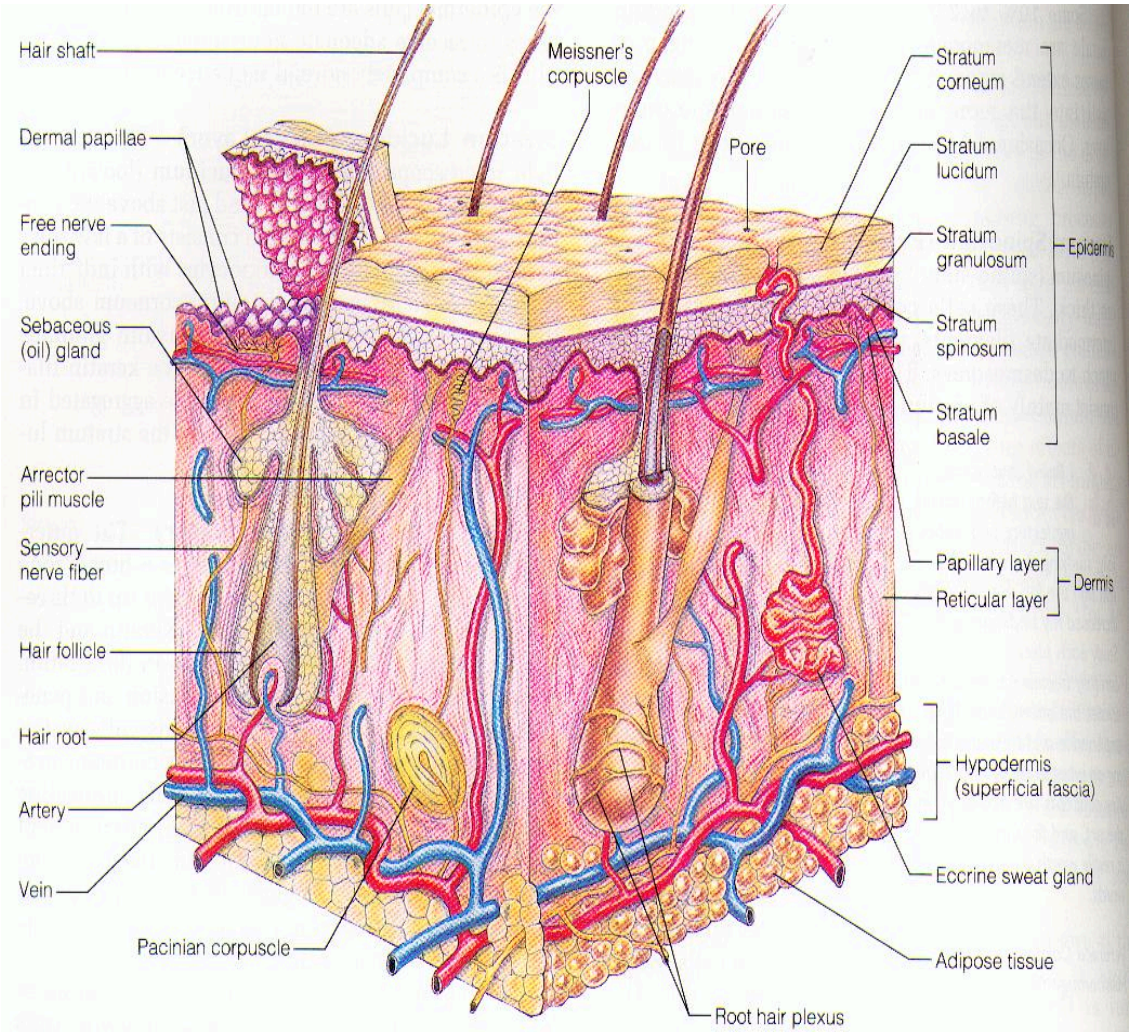

Figure 1.1 Skin structure [32].

The spiny appearance of stratum spinosum is due to the desmosomes that interconnect the cells. It also consists of keratinocytes and langerhans cells. These prickle cells manufacture bipolar lipids, preventing evaporation of water, thus helping the skin to retain its moisture content. The prickles are the points of attachment that join cells, and mitotic division occurs occasionally in this layer. The keratinocytes synthesizes a strong fibrous protein called keratin, which retains skin moisture, while the Langerhans cells

present in this layer detect the penetration of foreign bodies and destroys them. Stratum granulosum is three to five cells thick and is impermeable to water soluble substances. It contains special lamellar granules that secrete a fatty substance that is deposited in between the cells, thus forming a waterproof sealant, which acts as a barrier between the outer dead cells and active epidermis cells. It also contains keratohyalin granules that gives the skin its structure and helps in retaining its moisture content. Stratum lucidum is the layer of dead skin present in certain areas of the epidermis, where the skin is really thick, such as the soles of feet and palms of hands. This layer assists the skin in handling friction and contains three to five layers of dead flattened keratinocytes. Stratum corneum is the outermost layer of epidermis comprising of 15-20 layers of corneocytes (dead cells) held together by corneodesmosomes. Its thickness varies based on the mechanical stress experienced by the body; therefore, it is typically thicker in the palms of hands and soles of feet. Stratum corneum helps in protecting the body from microorganisms and chemicals and helps in retaining elasticity and water content. The ceramide lipid bilayer repels water, which causes water to be stored in between the corneocyte, thus helping the skin to retain its moisture content. In order to preserve the hemostasis of the epidermis, the skin has to be shed periodically to accommodate the newly created keratinocytes. This is carried on by the degradation of corneodesmosomes in a process called as desquamation.

II. Dermis layer

The dermis is the middle layer and made up for roughly 90% of the skin. It provides the skin with tensile strength, controls temperature, stores water and delivers nutrients to the epidermis. It composes of three types of tissues, i.e. collagen, elastic tissue and reticular fibers that are present throughout the dermis. The dermis also includes specialized cells including blood vessels (to deliver nutrients), lymph vessels (for fighting against foreign bodies), sweat glands (apocrine & eccrine), sebaceous glands (oil), collagen (gives skin strength) and elastin (keeps skin flexible). The dermis also contains pain and touch receptors, which transmits irritation, pressure, and information regarding temperature to the skin. The dermis has two-sub layers: the papillary layer that contains a thin arrangement of collagen fibers, which supplies nutrients to the epidermis and regulates the skin temperature by controlling the flow of blood through the skin, and the reticular layer, which contains thicker collagen fibers providing structure and elasticity to the skin. It also supports the hair follicles, sweat glands and sebaceous glands.

III. Hypodermis layer

The hypodermis is the innermost layer of the skin, thus binding it to the tissues beneath i.e. bone and muscle. It is made up of fat and connective tissue and stores nutrients (energy reserve), provides insulation, absorbs shock, and plays an important role in maintaining skin elasticity. The nerve endings sensitive to heat are in the upper and middle dermis, while the nerve endings sensitive to cold are at the lower dermis i.e. at the top of the hypodermis layer. In addition, blood vessels, hair follicles, and nerve endings

all pass through the hypodermis. Of the three skin layers, the dermis and hypodermis play the most important role in the wound healing process, due to the collagen fibers and connective tissue present in them.

CHAPTER 2

STIMULATION OF WOUND HEALING

A Hungarian obstetrician Ignaz Philipp Semmelweis was the first to introduce wound care in the 19th century. Since then, numerous approaches have been explored to accelerate the rate of healing. Though some of them were marginally successful, most failed to provide control over the entire process. Photonic bio-stimulation is a very interesting, yet novel approach to healing that has not been thoroughly investigated. We aim to study the transmission properties of skin to enable further research.

2.1 Photonic bio-stimulation

Photonic bio-stimulation is the action of biological system responding to coherent light produced from a laser source and is one of the many investigated methods of wound healing. The key advantage of a photonic approach is that it's non-invasive and hygienic due to the lack of exposure of internal wounds to atmosphere. Also, the exposure to microorganisms and infections is minimized, as there is no blood involved with irradiation treatment. Thus, by knowing the optical beam power and beam wavelength requirement for transmission, complicated surgeries can be avoided by treating the wound and affected sites with simple irradiation. Figure 2.1 displays the electromagnetic spectrum, where the relationship between energy and wavelength is apparent. We choose infrared because it has lower energy per particle in comparison to UV and visible spectrum, which implies less destructive propagation.

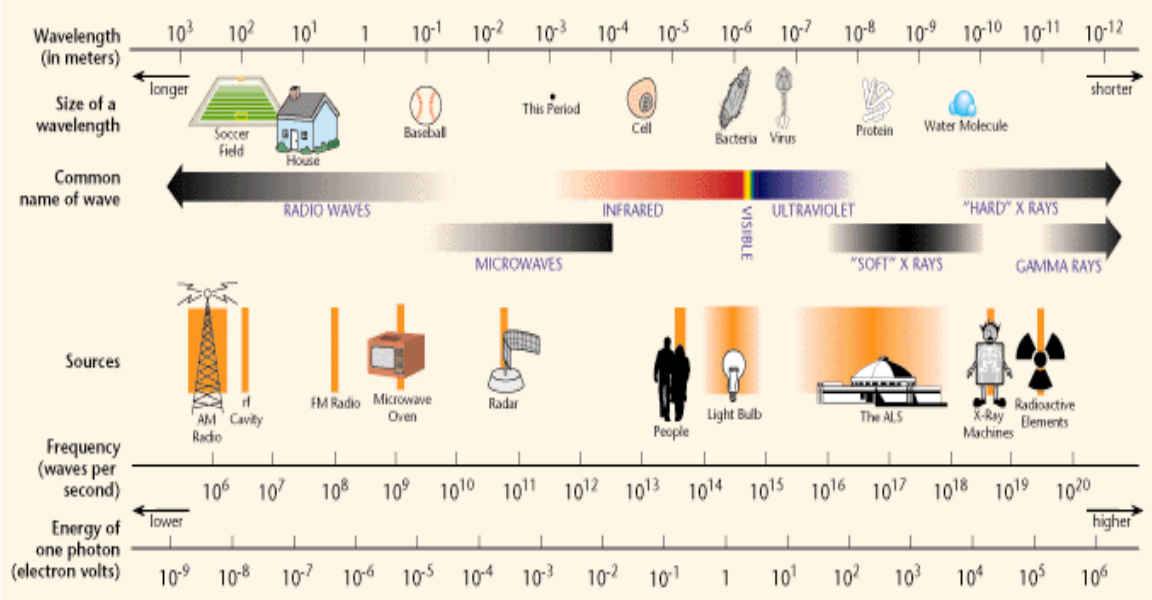

Figure 2.1 Electromagnetic Spectrum showing wavelength and energy [33].

Figure 2.2 displays the absorption properties of human skin, where the relationship between various skin constituents and wavelength is apparent.

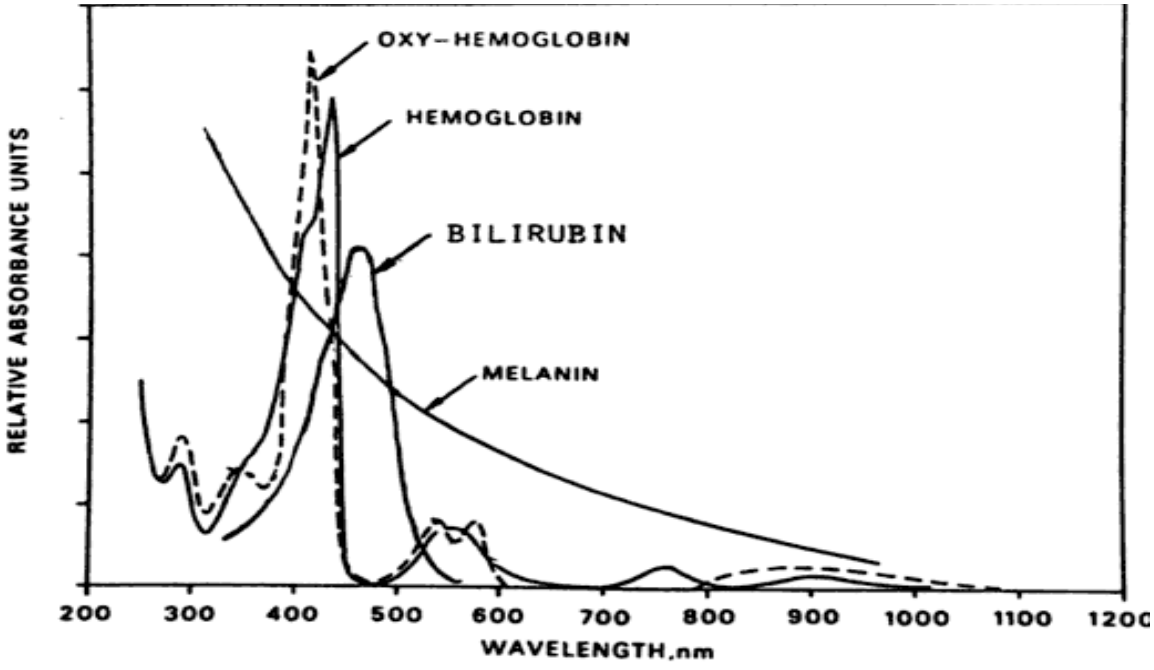

Figure 2.2 Absorption properties of skin vs. wavelength [30].

UV, visible, or IR irradiation could be employed for photonic bio-stimulation; however, due to the limitations and drawbacks of UV and visible regions, they are not ideal for photonic bio-stimulation. UV irradiation can provide large amounts of optical power through the skin, but it is avoided since it is a human carcinogen. The toxic effects of UV from sunlight and therapeutic artificial lamps are a major concern for human health and its effects on human skin include sunburn, inflammation, erythema, tanning, local or systemic immunosuppression [13]. In fact, UVA, UVB, and UVC damage collagen fibers, destroy Vitamin A, and accelerate skin aging [14].

Visible light also possesses certain characteristics, but visible light doesn't penetrate the skin deep enough for stimulation and is absorbed on the skin surface. If visible light penetrates through skin, high optical power must to be delivered, which would inhibit cell growth and decelerate wound healing [11]. Furthermore, visible light is influenced by the absorption and scattering properties of skin primarily due to influence of skin chromophores and the refractive index fluctuations [18, 19, 21]. The main chromophores of human skin are hemoglobin and melanin. Hemoglobin is found in the micro vascular network of the dermis (i.e. 50-500 um below the skin surface) while melanin is located in the epidermis occupying 50-100 um. The melanin concentration varies [18], but both melanin and hemoglobin absorb light strongly in the UV and visible spectrums and have very low absorption in the near infrared. Melanin is also photo-protective causing the skin to get darker and thicker with increasing absorption; therefore, transmission properties are strongly influenced by these concentrations.

These drawbacks are overcome with IR radiation. Since less research has been

conducted in the infrared spectrum, we focus on infrared transmission to determine if this approach is feasible. The infrared spectrum generally has a wavelength and frequency ranging from 0.8μm-1000μm and 1-400 THz, respectively. Since it lies in between the red line of the visible spectrum and microwave spectrum, it corresponds to the thermal irradiation of most objects at room temperature. The properties of infrared irradiation have a wide range of applications that include military, industry, laboratory and medical applications.

When a molecule interacts with the incident infrared radiation, there is a transfer of photonic energy based on frequency of infrared source i.e. the molecule absorbs the incident energy. This absorption characteristic of cellular organelles, in particular, is the basis for wound healing via photonic stimulation. Due to the longer wavelength, low frequency, and low power capabilities in comparison to visible and UV, infrared can penetrate the skin deeper and transmit the needed optical power without causing damage to the tissues [11], thus making infrared transmission suitable for medical applications, as well.

2.2 Prior results of Photonic Bio-stimulation

There have been numerous studies conducted in bio-photonics over the last few decades, although results were inconclusive. A few of the infrared experiments are discussed in the following section.

Mouse fibroblast grew five times faster with a ruby laser ($\lambda = 632.8nm$) concluding it supported mitotic activity [22]. Human skin irradiated at λ =633nm light with a He-Ne laser displayed an increase in number of cell and collagen production.

Further analysis showed that the increased collagen production was not due to cell proliferation, but due to fibroblasts [23]. On exposing human fibroblast cultures with Ga-As at 904 nm, the cell line showed 36-fold increase in pro-collagen production [10]. Recent research also shows that photonic bio-stimulation causes the release of TGF (transforming growth factor) and PDGF (platelet derived growth factor) [24]. TGF plays a role in immunity, cancer, heart disease, diabetes and Marfan syndrome, a genetic disorder of connective tissue while PDGF is a protein that helps in cell growth [10].

Photon bio-stimulation also increases ATP synthesis [10]. It is consumed in endothermic reactions and produced in exothermic reaction, and also transfers energy between metabolic reactions. It is the energy source for majority of cellular functions and maintains cell structure by aiding the assembly and disassembly of elements in cytoskeleton, gives the cell shape, protects the cell, enables cellular motion and plays an important role in cellular transport. Also, ATP supplies the energy required for muscular contraction. [10]

Reports also suggest that photonic bio-stimulation has its greatest effect in the proliferative phase of wound healing [25]. It affects the cellular metabolic process and improves regenerative potential, anti-inflammatory effects, analgesia and vasodilatation [10]. Photons, when used at proper wavelength, density and exposure time, stimulate fibroblast proliferation, collagen synthesis, macrophage and extracellular matrix production [26]. Fibroblast production enhances wound healing, while macrophages (i.e. white blood cells) fight foreign bodies and fasten healing by avoiding delays due to infection.

Extensive efforts show major progress in the NIR-VIS regime with little study of the MIR. One of the reasons for the lack of research in the infrared spectrum is the specialized use associated with infrared lasers. Still, the main challenge with bio-photonics is to find an efficient way to overcome the transmission losses and transmit optical power through the skin. The cells require optical power (stimulation) in a specific range (4-7 J/cm^2) to be delivered, to initiate the healing process [11]. If power delivered is below this specified range, the wound healing process fails to initiate and if power delivered is above the specified range it could lead to harmful side effects. Thus, wavelength and power are important parameters for wound healing.

2.3 Photonic approach to Wound Healing

There are two biological approaches to wound healing, i.e. increasing the collagen synthesis or increasing ATP synthesis. Both facilitate wound healing; however, the latter can help in neuron restoration, which is important for spinal chord surgery. Photon bio-stimulation accelerates the rate of wound healing through a series of stepwise processes. This is illustrated in Figure 2.3.

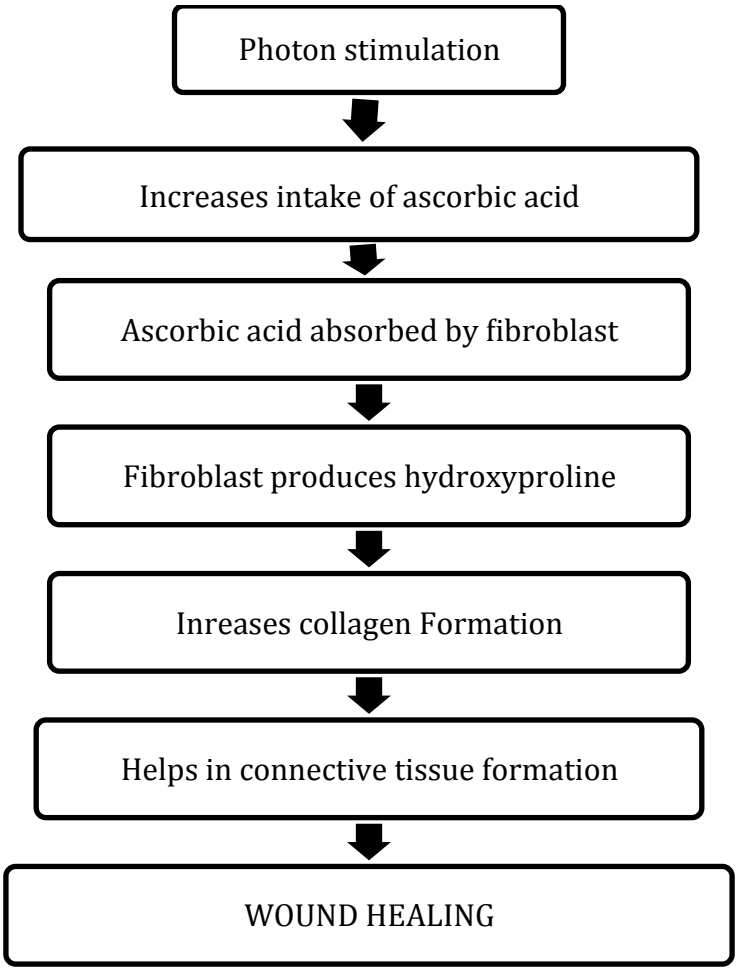

Figure 2.3 Photonic bio-stimulation processes.

Photonic bio-stimulation increases the ascorbic acid intake and optimizes hydroxyproline formation. This increases collagen formation resulting in an enormous transformation of fibroblasts into myofibroblasts, which increases the rate of wound healing [10]. Diabetic patients, for example, suffer from impaired wound healing due to the absence of carbohydrates in cells for normal aerobic metabolism. To overcome this, the body oxidizes the amino acid resulting in the depletion of amino acids and proteins further impairing wounds [11]. Photonic bio-stimulation overcomes this shortage by increasing the fibroblast production, which increases collagen production and accelerates

the rate of wound healing. Arterial disease and old age also impede the wound-healing process and it could be similarly overcome by photonic bio-stimulation [12].

There are elements in the mitochondria like cytochrome system and endogenous porphyrins that are photo receptive to monochromatic light. Cytochrome generates energy through photonic absorption, while porphyrins transfer the generated energy. Mitochondria are the "energy plants" of the cell, and it produces adenosine triphosphate (ATP), which provides energy for all physiological mechanism and is present in the cytoplasm and nucleoplasm. Its functionally is similar to chloroplasts that supply energy to plants. [A normal animal cell will have in the order of 1000 to 2000 mitochondria.] ATP, the high-energy molecule, has a carbon compound as a backbone, but the part that is actually important is the phosphorous part (i.e. the triphosphate). Here, oxygen atoms connect three phosphorous groups to each other. In addition, there are oxygen atoms that are connected to the sides of phosphorus. Under normal conditions, each oxygen atom has a negative charge that repels the other oxygen atoms creating built-in potential. The removal of one phosphate group can releases 7.3 kilocalories per mole, so conversion of ATP to ADP is an extremely crucial reaction for supplying energy for life process. The newly created ADP is transformed back to ATP with the help of the mitochondria [15]. This reaction is facilitated by photonic bio-stimulation, thus making living things use ATP like a battery. The increased ATP production produces a redox reaction, a chemical reaction in which sugar is oxidized to glucose thus producing energy to the body [10]. Therefore, via collagen formation and ATP synthesis, photonic bio-stimulation can assist the wound healing process.

2.4 Factors influencing photonic skin transmission:

There are a number of factors that influence photonic transmission through skin. The main factors are: dispersion, scattering and absorption. Each of these factors is interrelated and is described in the following section.

I. Dispersion

When light travels from one medium to another, its path is bent as it undergoes refraction. The angle at which light is refracted varies based on the refractive index of the medium and the frequency of the incident beam. The refraction is greater for electromagnetic waves of shorter wavelength than for waves of longer wavelength and for medium of higher refractive index. Hence, the transmission characteristic can differ based on the wavelength of the source. Theoretically, infrared sources of longer wavelengths should minimize dispersion in comparison to shorter wavelength near-infrared sources. However, it is difficult to calculate the dispersion that takes place in the skin due to its complex structure. If the skin thickness was less than 10μm and coherent, the refractive index could have been easily calculated from Maxwell's equation. However, the thickness is greater than 1-mm and as skin consists of many layers, it is incoherent. In addition, each layer has its own Fresnel reflection, which cannot be accurately determined. Thus, refractive index of skin is difficult to calculate and is always approximated based on the refractive indices of the different layers. Therefore, it is challenging to accurately calculate its influence on photonic transmission.

II. Scattering

The physical process that occurs when light interacts with matter is scattering. The electric field of the incident wave causes the charged particles in the medium to oscillate, and they re-emit light with the same frequency as the incident wave. Hence, the change in distribution, polarization, and reflection of incident light in the medium is attributed to this scattering effect. When light travels from one medium to another, there is a change in velocity of incident light wave in proportion to the refractive index of the medium it passes through. The scattering effect is not constant for all particles. It actually changes based on the molecular weight, size, shape, and concentration of the associated particle. If the particle is of regular shape and size, the scattering can be calculated using Maxwell's equation and Rayleigh's scattering. However, the skin structure, which has thickness of greater than 1-mm has amorphous shape and size, leading to complexities in calculating the scattering effect. In addition, the skin is not coherent as it has multiple layers each having its own refractive index, leading to multiple refraction and velocity changes. Thus, skin has multiple scattering mechanisms that are highly anisotropic.

Scattering occurs generally at non-resonance frequencies, and, the intensity is weak due to the intermolecular absorption of generated energy. Since the skin is a dense medium with different layers each having its own refractive index, the waves are scattered in all direction based on the frequency of the incident wave. The new scattered wavelets have its own phase and velocity due to dispersion; hence, the overall scattering is a sum of the interface of the scattered wavelets with the phase and decreased velocity of the incident wave. The absorption effects of the skin tissues also affect the refraction and the speed of the scattered wave.

Previous studies have shown different cell components also contribute to the scattering process. Cells have different internal components and size, but the three main constituents of all cells are cytoplasm, nucleus and mitochondria. The cytoplasm contributes the least, while the nucleus contributes the most to cell scattering. The mitochondrion also contributes to the scattering based on its concentration. The other constituents that contribute to the scattering effects are RBC and adipose tissue. Thus, scattering effects have to be well understood to increase transmission.

III. Absorption

When radiation is incident on matter consisting of discrete charged particles, the particles vibrate with frequency of incident light. The natural vibrational frequencies of most atoms and molecule coincide with frequency of infrared radiation. So, when infrared irradiation is incident on atoms or molecules, energy is transferred from the incident wave to the atoms and molecules, and its amplitude of vibration increases. Typically the lifetime of the excited atom is 10^{-7} to 10^{-8} seconds but since the excited atom collides with the neighboring atom, its lifetime is reduced to 10^{-12} seconds [29]. The collision raises the kinetic energy of neighboring atoms, resulting in energy being dissipated in the form of heat within the medium. This effect is known as absorption and it decreases the intensity of the incident light.

Due to the varying skin thickness, absorption is one of the main parameters that influence skin transmission. The absorption varies as a function of skin thickness, which can be approximated by Beer-Lambert's law

$$I = I_o\, e^{-uL} \qquad (1)$$

where L is the skin thickness, I the transmitted intensity, I_o is the incident intensity and u is the absorption coefficient (i.e. probability that a photon will be absorbed by the medium per unit length). The inverse of the absorption coefficient is the absorption length. The Beer-Lambert approximated is valid under certain conditions, i.e. the light should be monochromatic and perfectly collimated, and the medium should be pure and uniformly absorbing. The biological tissues have many components called chromophores, which absorb light differently based on its concentration and type. Hence, the Beer-Lambert law cannot be directly applied to biological tissue, as the total absorption coefficient is the sum of absorption coefficient of different individual chromophores. Some examples of chromophores present in the biological tissues are water, lipids, hemoglobin, cytochrome, melanin and myoglobin.

It is apparent that infrared irradiation is highly beneficial for photonic bio-stimulation. However, to overcome the obstacles and achieve efficient transmission, we investigated new techniques that could improve photonic transmission.

CHAPTER 3

EXPERIMENTAL EQUIPMENT AND SETUP

It is very clear that numerous obstacles have to be overcome in order to achieve optimal infrared transmission through the skin layers. It is beyond the scope of this study to solve all of them. It is, however, possible to investigate techniques to increase transmission. Hence, an optical setup was constructed to study and investigate the temperature and temporal characteristics of irradiated skin and in its influence on transmission. The optical setup used in this photonic study has two sections, i.e. transmitter and receiver. A short description of the equipment used in each of the following section and their uses are provided below.

3.1 Optical transmitter

The optical transmitter comprised of three devices: arbitrary wave function generator, laser diode controller and infrared laser diode. Each of these components is described below.

I. Function Generator

Function generator is a device used to generate various electrical waveforms of changeable frequency and amplitude (most commonly used to check the response of a circuit to input signal). The function generator can produce a single or a series of repetitive pulse trains, which are generated by cyclic charging and discharging of the

capacitor connected to a constant energy source. Depending on the experimental need, the function generator can produce the required waveform by shifting the capacitor and current values. The commonly used waveforms are square, sine, triangular, sawtooth, and pulse waves. In addition to generating the waveforms, the rate at which it is generated can also be controlled by a frequency controller. An important feature of function generator is its ability to phase lock with another external source. Once phase locked, the output of the source can be controlled. In this study, the function generator is phase locked with the laser diode controller to produce a pulsed wave. The function generator used in this experiment is model AFG 3021 B by Tektronix (Figure 3.1)

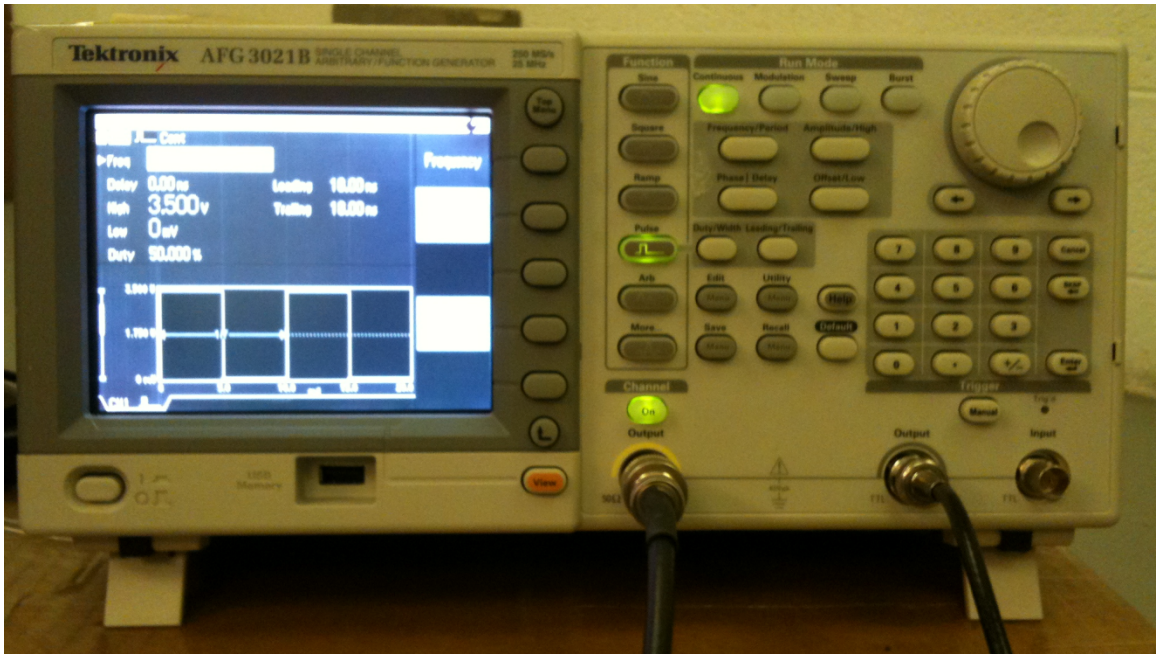

Figure 3.1 Tektronix Function generator.

II. Infrared laser diode

Laser is an acronym for light amplification by stimulated emission of radiation (LASER). The emission from the laser source has two important properties that differentiate it from ambient radiation i.e. temporal and spatial coherence. Temporal coherence is associated with the light having a single wavelength over a period of time or at various distances from the source, and spatial coherence is related to the light have very less divergence or having a narrow beam. Very high irradiance can be achieved by focusing the beam through a series of lenses. The laser used in this study is a Fabry Perot laser diode, which is the simplest type of semiconductor laser diode comprises of large group of binary, ternary and quaternary elements from Groups II-VI of the periodic table.

Semiconductor lasers in general have a low operating current, low operating cost, small size, high efficiency and have an emission ranging from blue (400 nm) to the infrared spectrum making them the most widely used laser today. The wavelength and output power of infrared laser diodes are tunable by varying the temperature and current. Fabry Perot lasers are generally made for operation in the 980 nm -1.8μm ranges. However, for advanced research in bio-photonics, wavelengths in the higher short infrared, mid-infrared and long infrared are desirable. These wavelengths cover the spectrum of the human body natural frequency, and irradiating in this spectrum could possibly lead to attaining resonance of cells and organelles. The laser diode used in this study is a 1440 nm single mode fiber coupled Fabry perot laser diode (Figure 3.2) with a low threshold current of 44 mA and an operating temperature range of -40 to +50° C. It has built-in thermistor and photodiode, with an operating current of 678 mA and spectral width of 5.97 nm producing a maximum output power of 200 mW.

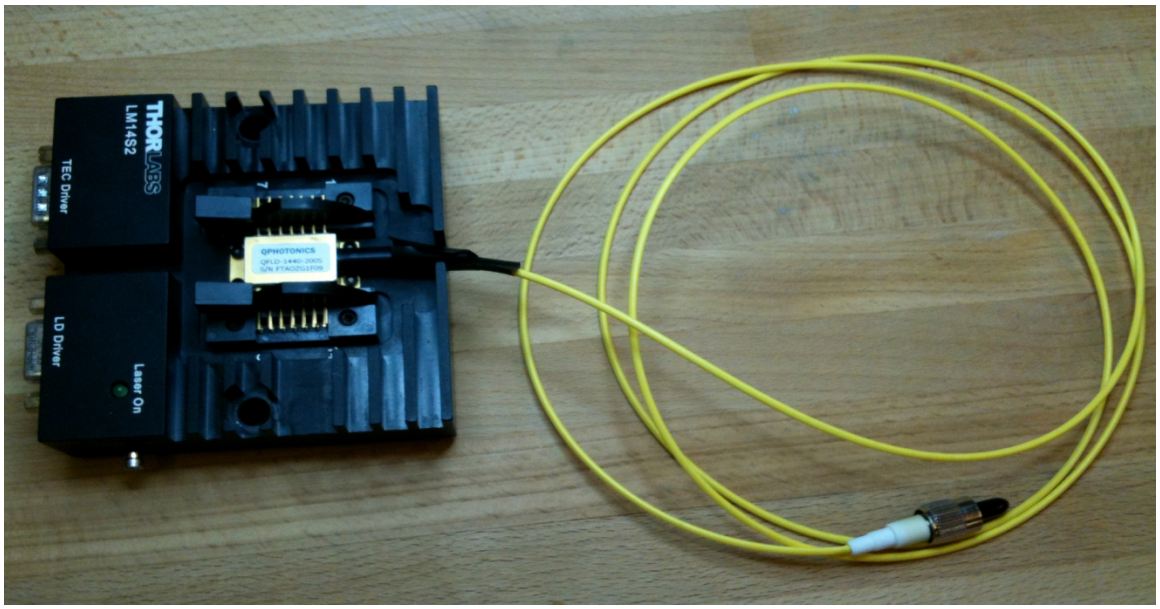

Figure 3.2 Laser diode package with attached optical fiber.

III. Laser diode controller

Laser diode controller is a device used to supply input power to the laser while controlling the temperature of the laser die. Its basic qualities are high stability, low noise and high power efficiency. The laser diode controller can generate both continuous and discrete time signals as well as respond to discrete time signals that are generated by the function generator. The laser diode controller uses a built-in temperature controller, and the maximum input current that can be supplied to the laser can be maintained using the controller, thus preventing the laser from spontaneous emission and failure. The controller used in this study is ITC 510 (Figure 3.3) from Thorlabs.

Figure 3.3 Laser diode controller.

3.2 Optical sensor

The optical sensor section comprises an infrared photodetector and an infrared camera, which are used to detect the transmitted infrared irradiation and study the temperature characteristics of the skin. A short description is given below.

I. Photodetector

A photodetector converts light energy into electrical energy and is used to measure optical signals. There are different kinds of photodetectors each having its own advantage and limitations. Photodetectors are categorized based on their principle of operation. A few examples are: photoresistors, photovoltaic cells, photomultiplier, phototubes, phototransistors, and photodiodes. The photodetector used in this study is a doped PN junction semiconductor that operates in reverse bias condition, allowing current in the junction only in the presence of light. The vital parameters that measure the

performance of the photodiode are responsivity, noise equivalent power, and dark current. The sensor used in this study is a germanium optical sensor S122B (Figure 3.4) with a spectral range of 700-1800 nm and power range of 35 nW-35 mW. The detected power is calculated by transmitting the generated electrical impulse to an analog optical power meter.

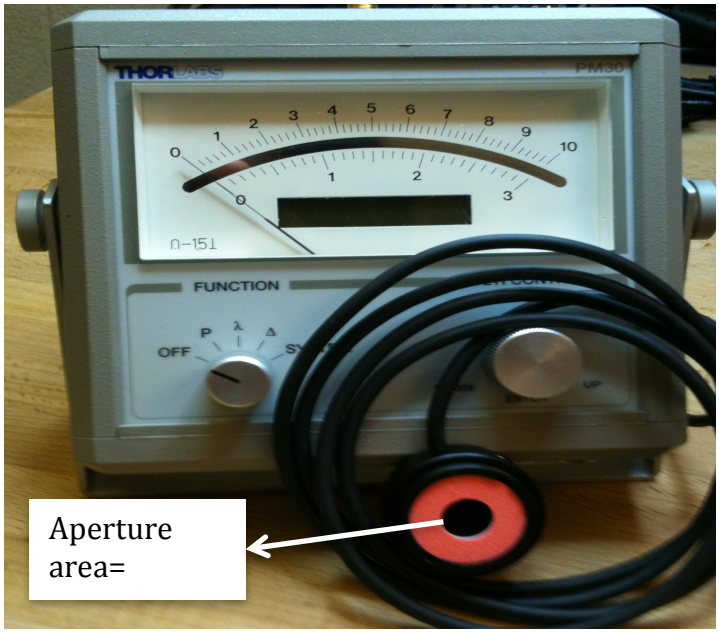

Figure 3.4 Optical sensor and power meter from Thorlabs.

II. Infrared camera

The infrared camera is a thermal detector array and is used to study the thermal signature of objects. All materials that have a temperature of greater than 0°K emit infrared irradiation. The energy irradiated depends on temperature and surface of object. Based on the objects, energy emitted has a corresponding peak wavelength, which increases to longer wavelength with increasing energy or temperature of object. Therefore, long wavelength infrared is a very important atmospheric window since room

temperature objects have their peak at 10 μm [29]. The capability of all objects to emit infrared irradiation even at room temperature makes infrared cameras useful for numerous applications. The thermal imaging camera used in this study uses a focal plane array, uncooled microbolometer detector (Figure 3.5). It has a spectral range of 7.5-13 μm, sensitivity of 0.12 ºC, accuracy of $\pm$2 ºC and temperature range of -20 ºC-250 ºC. The principle of operation of microbolometer detector begins when infrared irradiation strikes the detector causing a proportional change in electrical resistance. This is processed into temperature readings to produce a thermal image. The microbolometer detector used has a wide spectral range, and is ideal for bio-photonic study.

Figure 3.5 Infrared camera from FLIR.

3.3 Sample preparation

Skin varies in thickness throughout the body, the epidermis in particular varies from 0.1 mm-1.5 mm. Since, the absorption is a function of skin thickness, even a small change of 0.1 mm can significantly influence the infrared transmission. It is tedious to

find skin samples of identical thickness; however, all samples can be similarly prepared to minimize the anomalies encountered in these experiments.

Pigskin is used in this study for investigating transmission characteristics. Even though pigskin is 5-8 times the thickness of human skin, it most closely emulates its structure. Hence, it can be assumed that if such fleshy skin can be penetrated using infrared irradiation, the same goes for human skin. Skin of variying thicknesses from different region of the pig's anatomy (armpit, underbelly, and thigh) are employed in this study.

To ensure that the natural condition of skin is preserved, certain steps are carried out on the skin sample within an hour of pigs demise. The hair on the pigskin and the densely thick fat in the underlying layer are removed using a razor blade. Finally, to preserve its moisture content and freshness, the processed skin sample is vacuum-sealed and refrigerated.

One of the primary factors that influence infrared transmission through skin is the skin surface and internal temperature. Since the skin is refrigerated, the skin has to be brought to room temperature before irradiation. The refrigerated skin sample is placed at room temperature twenty-four hours before the start of irradiation, to guarantee that the skin is brought to room temperature. The vacuum is not removed to preserve skin moisture and is only removed before the skin is irradiated. However, the moisture content of each skin sample varies and it cannot be controlled. A picture of processed skin placed on a holder before irradiation is shown in Figure 3.6.

Figure 3.6 Pigskin sample attached to an optical mount.

3.4 Experimental Plan, Design and Setup

Although continuous wave beam signals can transmit power through the skin, it cannot limit the irradiated skin temperature. Hence, a pulsed wave is used for photonic transmission. The power source position is maintained constant for comparative analysis. The laser diode is powered by the controller and phase locked to a function generator. The beam waist influences the power transmitted through skin, thus for consistency in measurement, the beam waist is tailored to be approximately the same diameter for all experiments. Also, to avoid complications and irregularities that could possibly arise due to the above effect, the skin is irradiated at fixed distances so that the beam width is constant for all irradiation.

During irradiation, the infrared energy transmitted to the skin increases the skins energy state and an infrared camera is used to observe the resulting increase in thermal energy. The temperature distribution and spotsize are analyzed and correlated with the transmission characteristics. The transmitted power is measured using an optical sensor. The detector is positioned behind the skin sample and the power transmitted through the skin is recorded every minute for 60 minutes time duration. Care is taken to avoid contact with skin, as it could possibly introduce variations in skin temperature and transmitted power.

Figure 3.7 shows the optical setup. The pigskin is placed at approximately 3 cm from the laser source. The infrared radiation passes through skin and is detected using an optical sensor (not shown) and infrared camera, which is placed at approximately 20 cm from the skin sample.

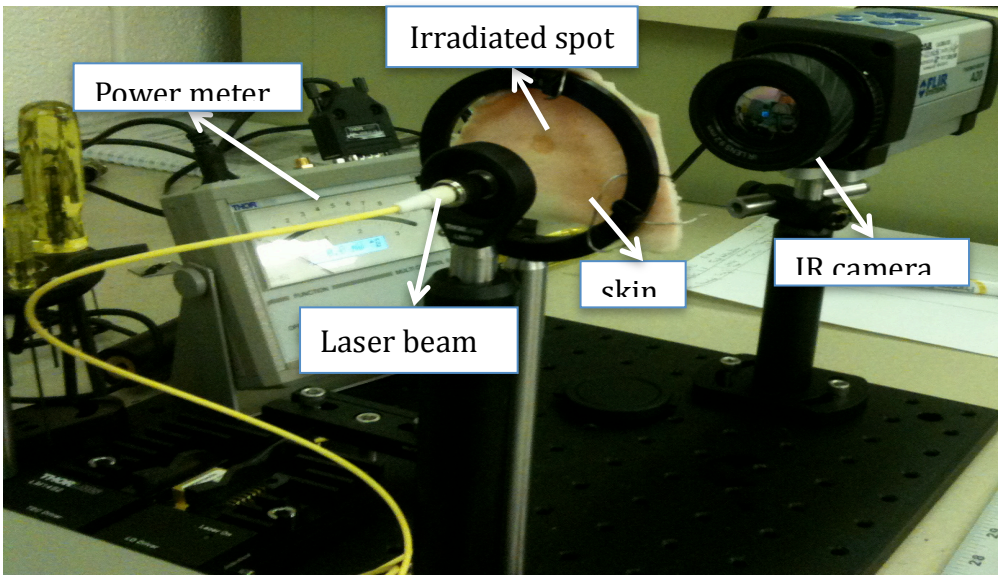

Figure 3.7 Experimental set up with laser, camera, skin & power meter.

Figure 3.8 shows the infrared view of the irradiated pigskin; the orange spot represents the irradiated spot in thermal vision. Thermal spreading varies as a function of distance at the point of irradiation; this can be noticed in the infrared view by a resulting change in color at the irradiated spot.

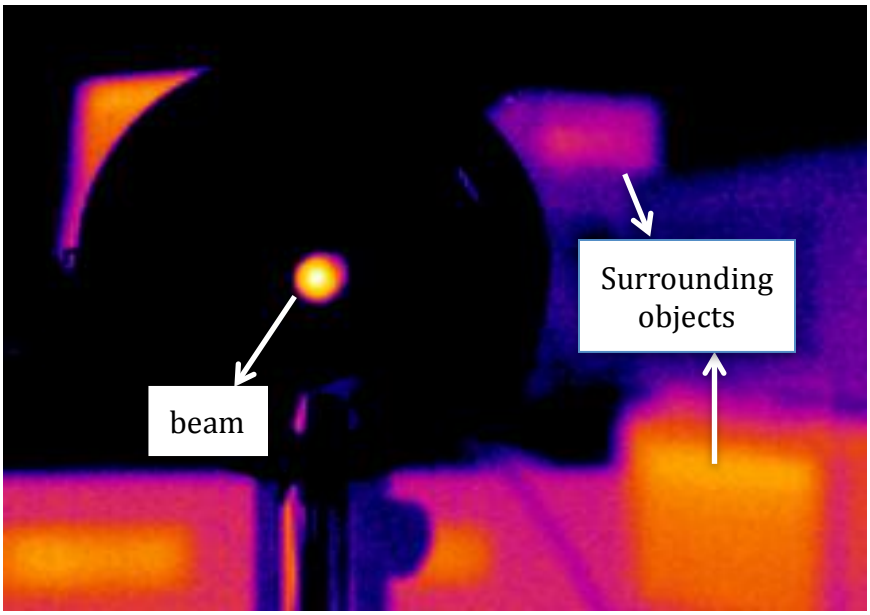

Figure 3.8 Infrared view of irradiated pigskin.

The influence of pulsed beam on the skin is investigated by varying the frequency, duty cycle and pulse width of the beam. The principal goal of the study is to explore ways to maximize transmission while keeping skin temperature under control.

CHAPTER 4

EXPERIMENTAL RESULTS AND PRELIMINARY ANALYSIS

4.1 Distribution of Temperature

Figures 4.1.1 - 4.1.4 represent the temperature variance along the x-axis and y-axis of the irradiated spot. From the figures, it can be seen that the temperature of the irradiated spot is maximum at the center (point of irradiation) and decreases as the distance from center increases. When skin is irradiated, its thermal state changes resulting in an increase in temperature at the point of irradiation. However, the surrounding skin is at a lower temperature resulting in a temperature gradient, which causes heat to be transferred to the surrounding layers. This transfer of heat signifies absorption and dissipation losses. Hence, to improve beam transmission, the dissipation and absorption losses have to be minimized. (Refer to appendix Data table A1)

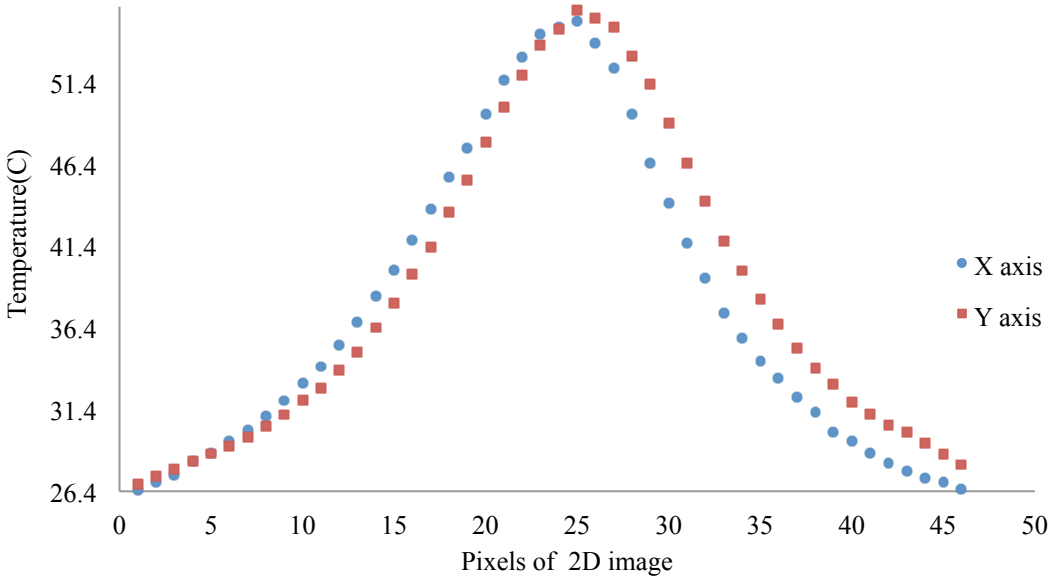

Figure 4.1.1 Thermal variance along X & Y axis for 10 kHz pulsed wave at 1% Duty cycle.

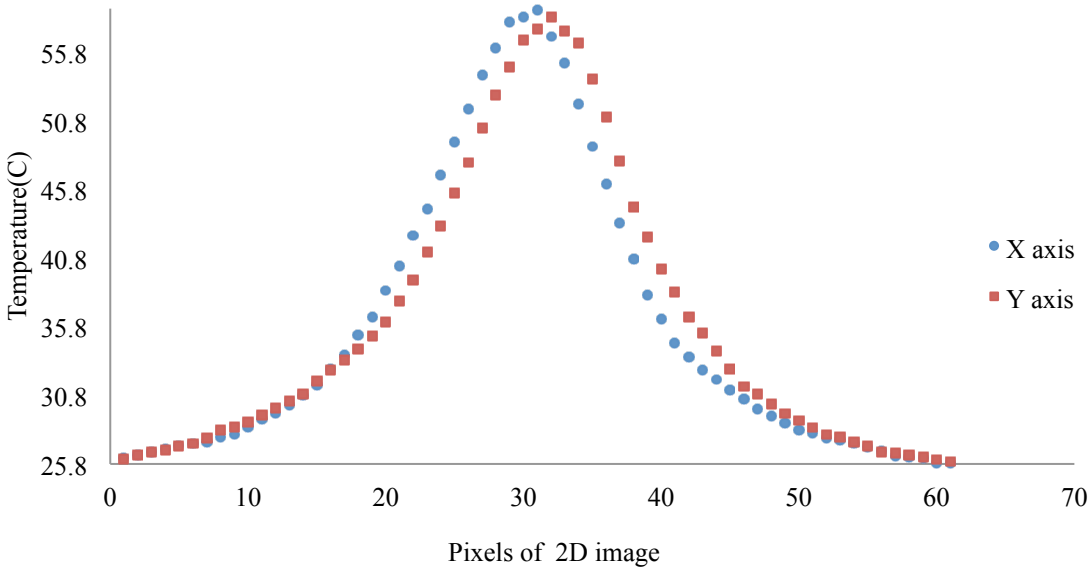

Figure 4.1.2 Thermal variance along X & Y axis for 100 kHz pulsed wave at 1% Duty cycle.

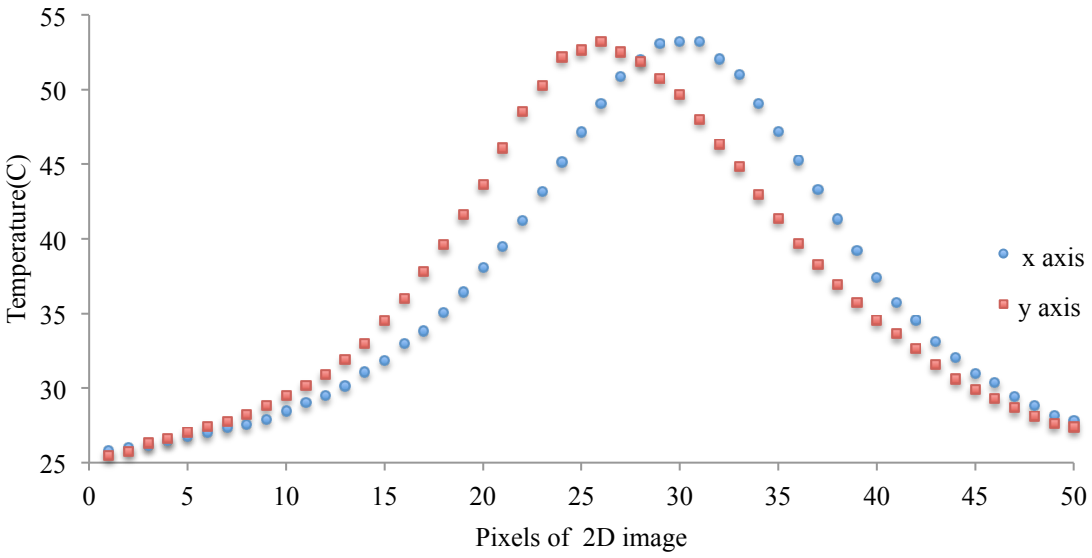

Figure 4.1.3 Thermal variance along X & Y axis for 500 kHz pulsed wave at 1% Duty cycle.

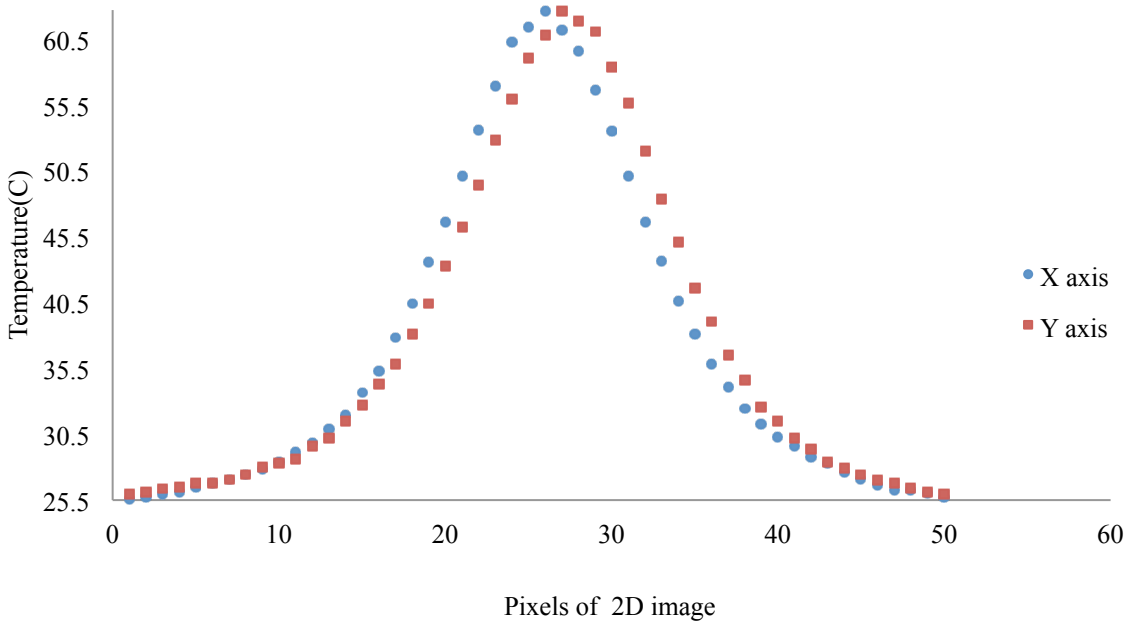

Figure 4.1.4 Thermal variance along X & Y axis for 1 MHz pulsed wave at 1% Duty cycle.

4.2 Frequency study

From Figures 4.2.1 and 4.2.2, it can be seen that power transmitted through skin increases exponentially with skin temperature and this resultant exponential rise is a function of pulsed beam frequency. Figure 4.2.1 shows that higher frequency pulsed beam transmits more power than lower frequency when evaluated at equal temperature. This is because at higher frequencies, there is a comparative decrease in the pulse width of the beam resulting in shorter interpulse duration. When interpulse duration decreases, the thermal energy builds more efficiently, thus increasing the transmission. Therefore, to transmit equal power using a low frequency pulsed wave (in this case 1 kHz), the skin needs to be irradiated for extended times. (Refer to appendix Data Table A2 & A3)

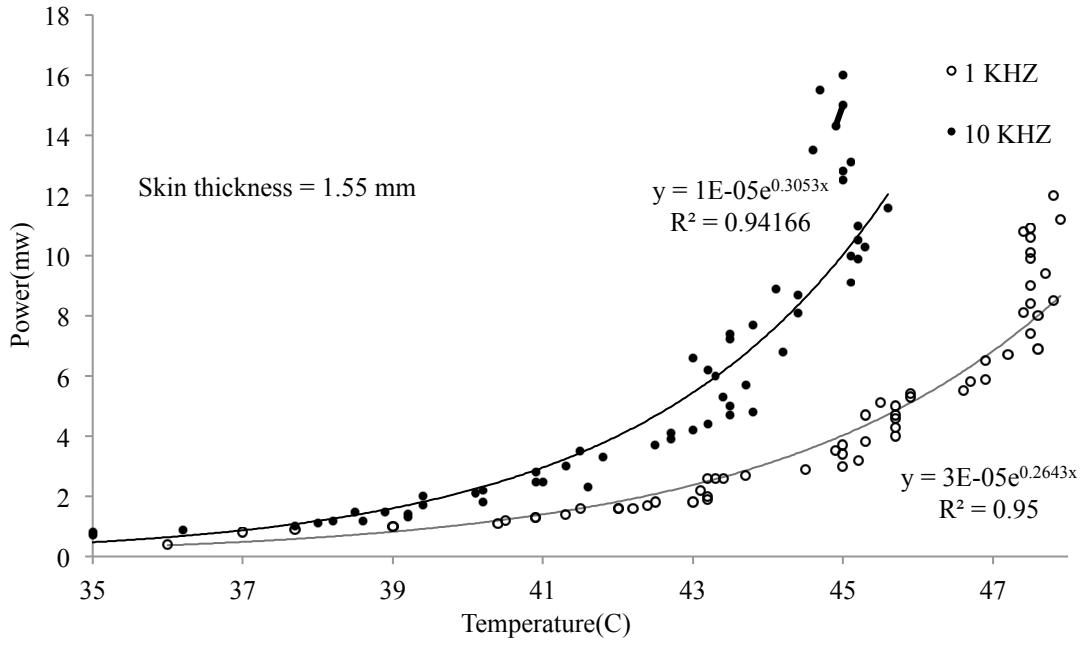

Figure 4.2.1 Transmission characteristic of 1 kHz vs. 10 kHz pulsed wave.

Similarly from Figure 4.2.2, it is evident that at the same temperature, the higher frequency (100 kHz) transmits more beam power than lower frequency (10 kHz) due to the comparatively shorter inter pulse duration of 100 kHz pulsed wave.

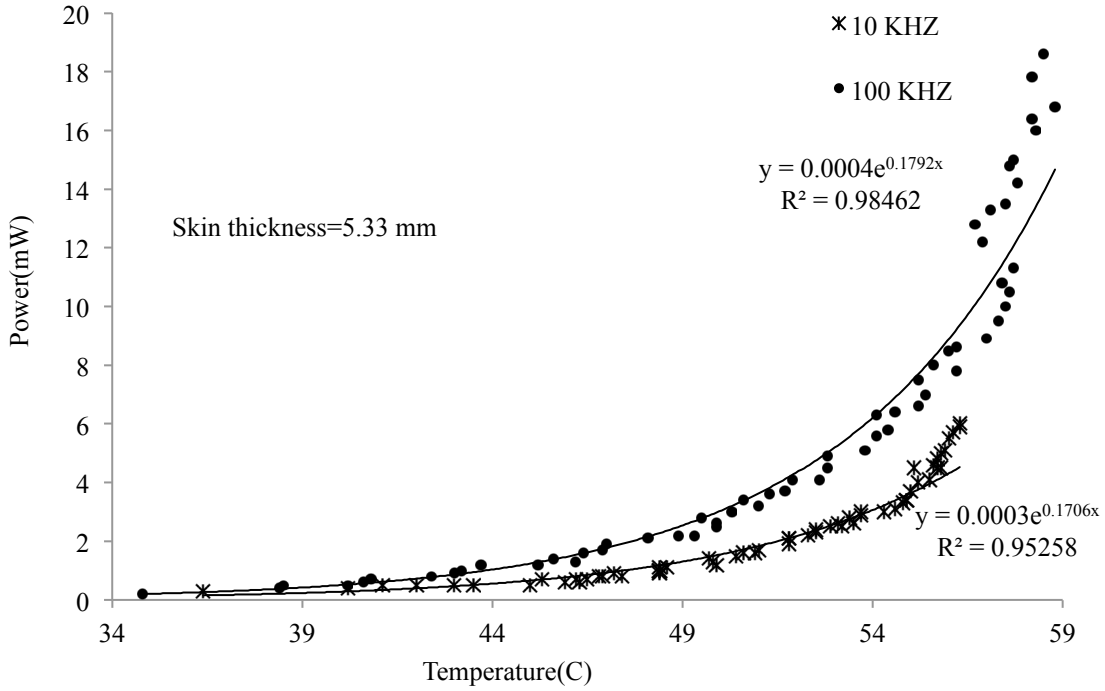

Figure 4.2.2 Transmission characteristic of 10 kHz vs. 100 kHz pulsed wave.

The skin has to attain a certain thermal state to be conducive to infrared transmission. This thermal state varies based on the skin thickness, its moisture content, and transmission parameters. It is also important to understand that the transmission is not just dependent on the skin's thermal state, but also on the variance of temperature around the irradiation spot. By altering the frequency of the irradiating pulsed beam, the thermal variance around the irradiation spot is varied efficiently. Thus, minimizing the spot size and causing an increase in transmission.

Figures 4.2.3 (1 kHz) and 4.2.5 (10 kHz) represents the pixel map of the irradiated skin recorded at 50 minutes of radiation. The temperature distribution around the irradiated spot varies with frequency and this can be observed from the figures. By analyzing the temperature distribution using pixel analysis, it is evident that 1 kHz has higher percentage of pixels in 30-50ºC-temperature range (in comparison to 10 kHz) signifying that more optical energy is lost thermally, thus resulting in lower transmission. Also, the 1 kHz and 10 kHz temperature distributions were recorded at equal temperature (Figure 4.2.4 and 4.2.5) and as expected they were different. The 1 kHz had a larger spotsize and more percentage of temperature in the 30-50º C-range signifying it experienced more loss than 10 kHz.

The diameter of the irradiated spot varies as a function of thermal loss and increases when losses increase. Since 1 kHz has greater loss, it has a bigger spot size. From Figures 4.2.3 and 4.2.4, it is evident that irradiation time influences the temperature gradient and therefore, the transmission.

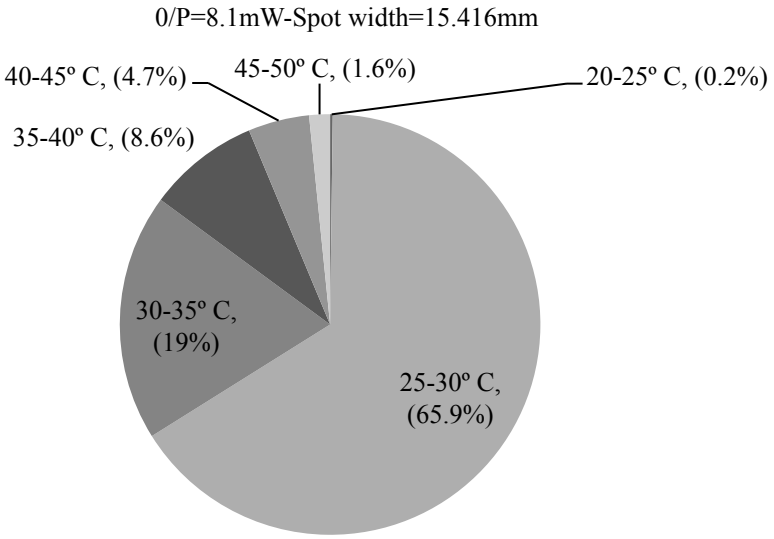

Figure 4.2.3 Temperature distribution of 1 kHz pulsed wave (50 minutes).

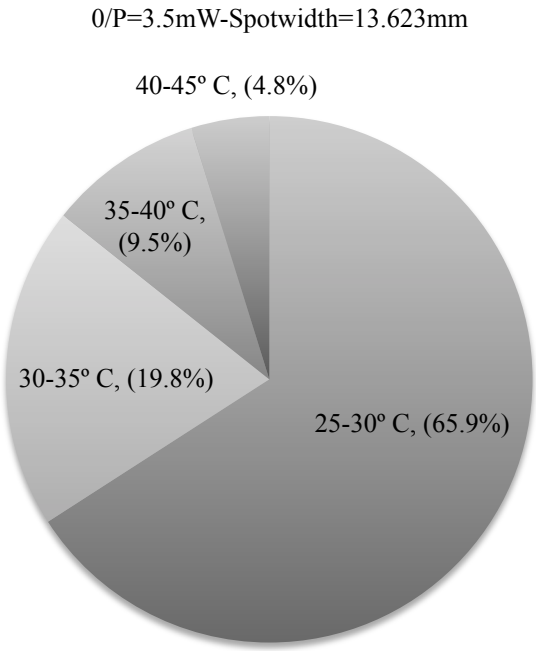

Figure 4.2.4 Temperature distribution of 1 kHz pulsed wave (30 minutes).

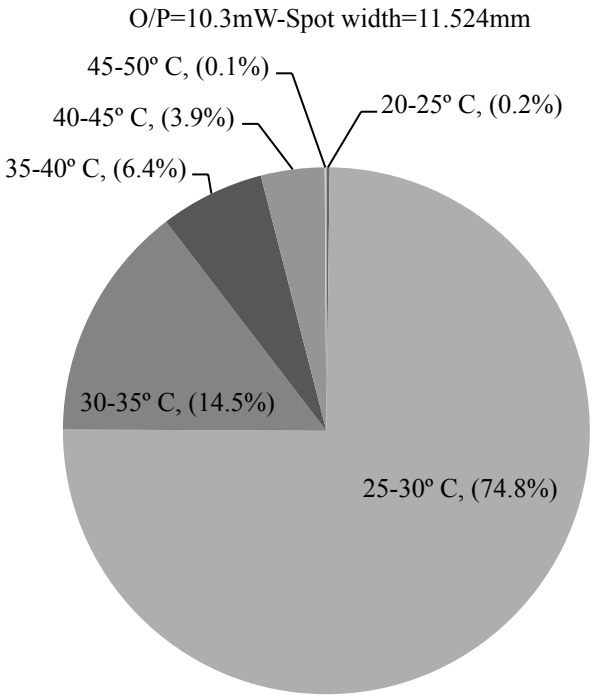

Figure 4.2.5 Temperature distribution of 10 kHz pulsed wave (50 minutes).

Figures 4.2.6, 4.2.7 and 4.2.8 represent the temperature distribution of 10 kHz and 100 kHz. From these Figures, it can be seen that 100 kHz has a smaller spot width in comparison to 10-kHz pulsed wave, resulting in 100 kHz having better transmission. In addition, from Figures 4.2.6 and 4.2.7, it can be seen that even after increasing the irradiation time of 10 kHz, it transmits less optical power than 100 kHz owing to its longer pulse duration and losses, which results in less transmission.

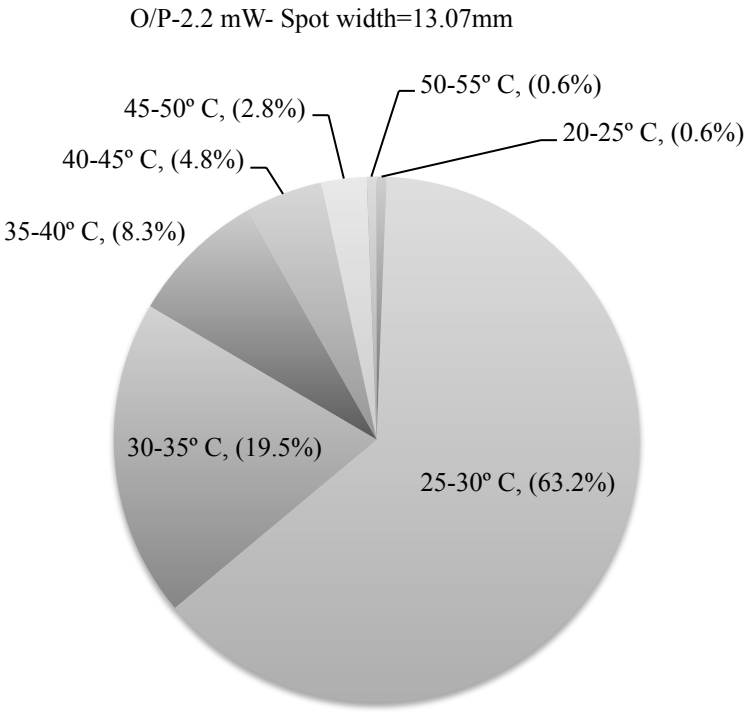

Figure 4.2.6 Temperature distribution of 10 kHz pulsed wave (30 minutes).

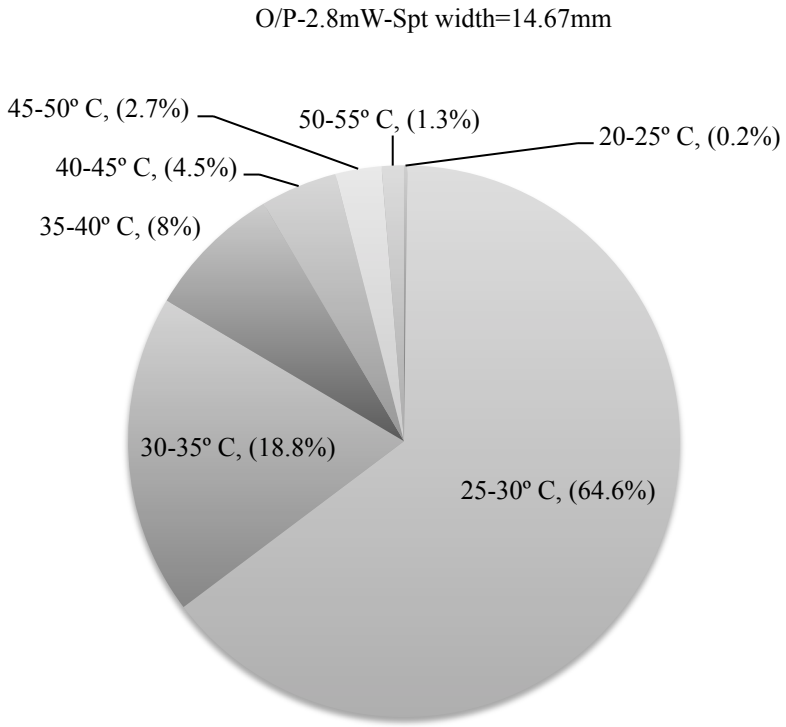

Figure 4.2.7 Temperature distribution of 10 kHz pulsed wave (40 minutes).

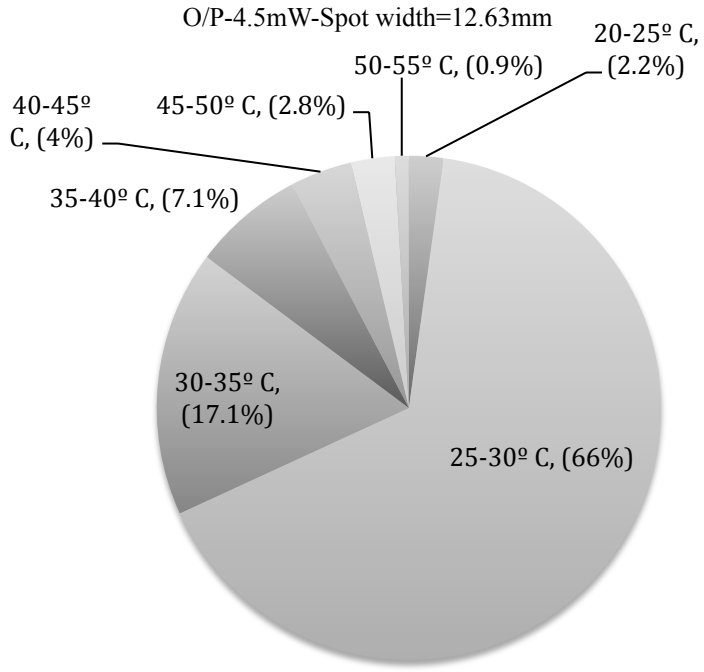

Figure 4.2.8 Temperature distribution of 100 kHz pulsed wave (30 minutes).

Upon radiation, skin temperature gradually increases indicating that it absorbs thermal energy. From Figures 4.2.9 and 4.2.10, the absorption decreases linearly with increase in temperature. This is comparable to water whose absorption coefficient is inversely proportional with temperature [27]. Since skin constitutes 80% water, absorption should decrease with temperature and these results prove the same. The primary reason for decrease in absorption with temperature is due to the skins moisture content, which decreases when temperature increases. This decrease in moisture causes an increase in transmission and dryness. Therefore, to prevent dryness long radiation exposure needs to be avoided. The absorption coefficient was extracted for each data point is plotted in Figures 4.2.9 and 4.2.10.

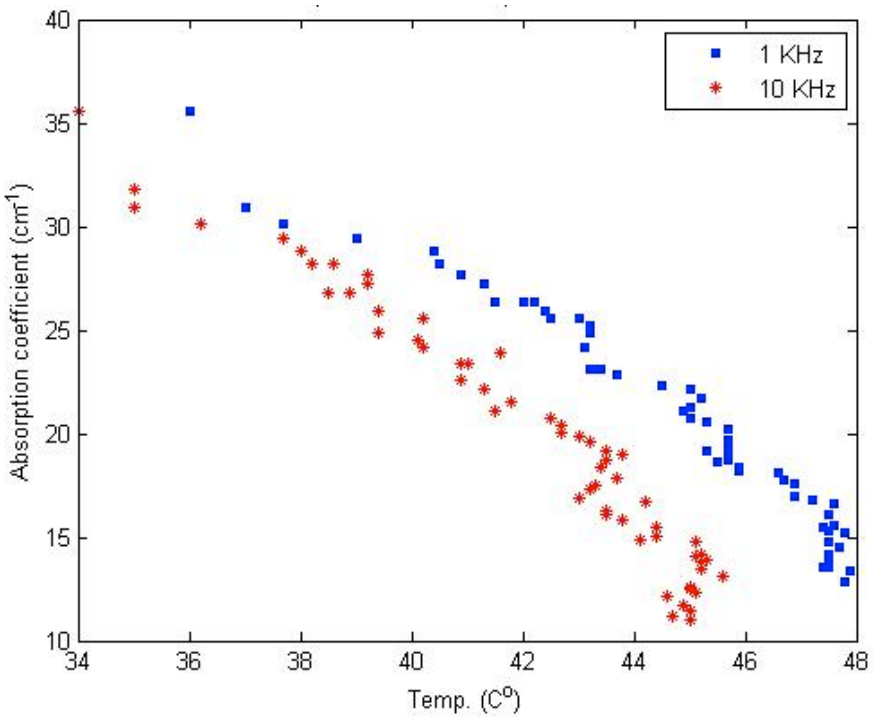

Figure 4.2.9 Absorption of 1 kHz vs. 10 kHz pulsed wave.

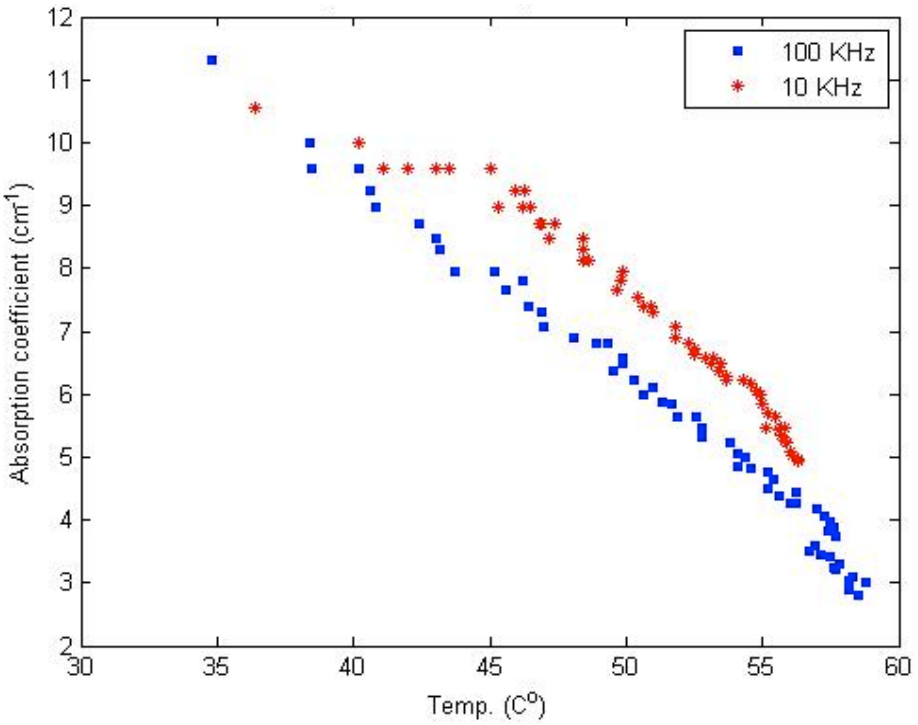

Figure 4.2.10 Absorption of 10 kHz vs. 100 kHz pulsed wave.

From the above figures, it is clear that drop in temperature is steeper at higher frequencies. Since higher frequencies have shorter pulse width, heat buildup is more efficient at higher frequencies. Therefore, drop in absorption is steeper for higher frequency pulsed wave.

4.3 Duty cycle study

Figure 4.3.1 represents the transmission characteristics of 3% vs. 5% duty cycle study. From the figure, 5% duty cycle transmits more power than 3% duty cycle for equal exposure period. When the duty cycle increases and frequency is constant, the pulse width increases and inter-pulse duration decreases, thus giving the skin less time to return to equilibrium before the next pulse arrives, thus resulting in more efficient energy transfer. Also, when the duty cycle increases the power delivered to the skin increases.

Thus, at high duty cycle, skin transmits power sooner. Similarly, from Figure 4.3.2 it can also be seen that 7.5% duty cycle transmits power sooner than 5% duty cycle. (Refer to appendix Data Table A4, A5 & A6)

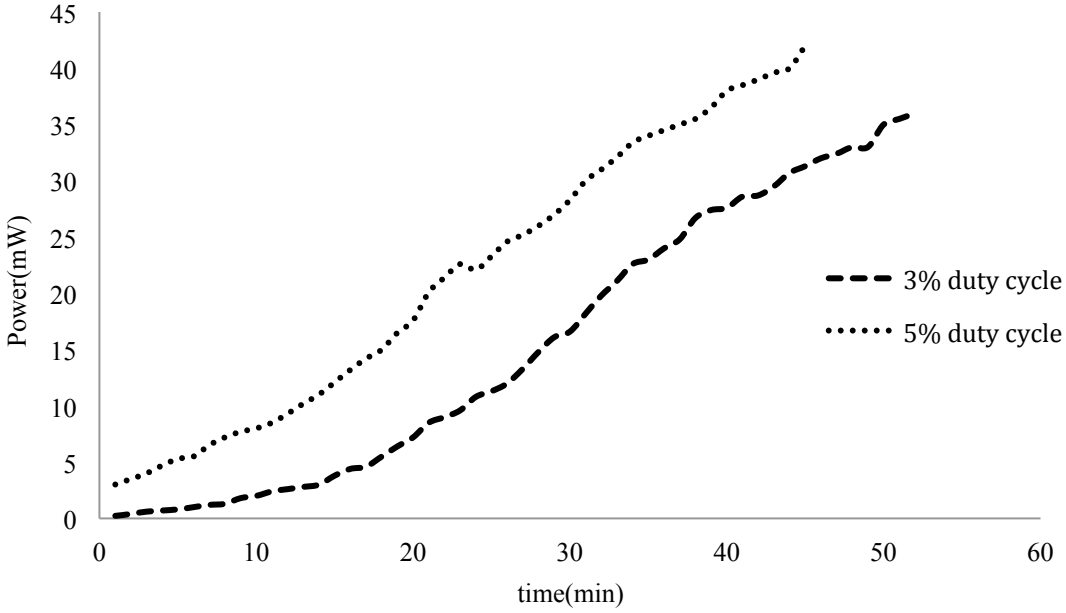

Fig 4.3.1 Time characteristic of 3% vs. 5% duty cycle pulsed wave.

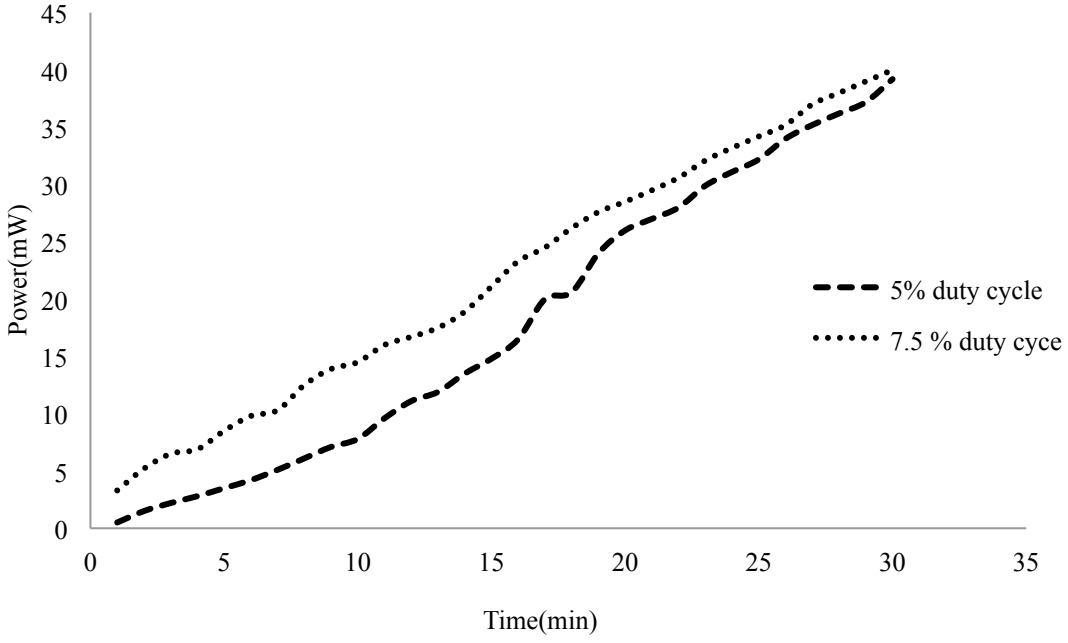

Figure 4.3.2 Time characteristic of 5% vs. 7.5% duty cycle pulsed wave.

The inter-pulse duration can be made shorter by increasing the frequency or duty cycle of the pulsed beam; however frequency varied inter-pulse width and duty cycle varied inter-pulse width both have a difference influence on transmission characteristic. Increasing frequency not only makes the inter-pulse duration shorter, it also makes the pulse width shorter. Thus, it facilitates in the gradual build-up of skin entropy, which is better suited for facilitating transmission because it prevents over heating of skin. However, when duty cycle is increased, the inter-pulse duration becomes smaller but the pulse duration becomes larger, this results in overheating of skin. Figure 4.3.3 represents the duty cycle schematic.

Figure 4.3.3 Duty cycle Schematic.

Figure 4.3.4 shows the transmission characteristic of 5% vs. 7.5% duty cycle pulsed wave, radiated continuously for 30 minutes time duration. From the Figure, it can be seen that 5% duty cycle can transmit more power than 7.5% duty cycle at equivalent temperature.

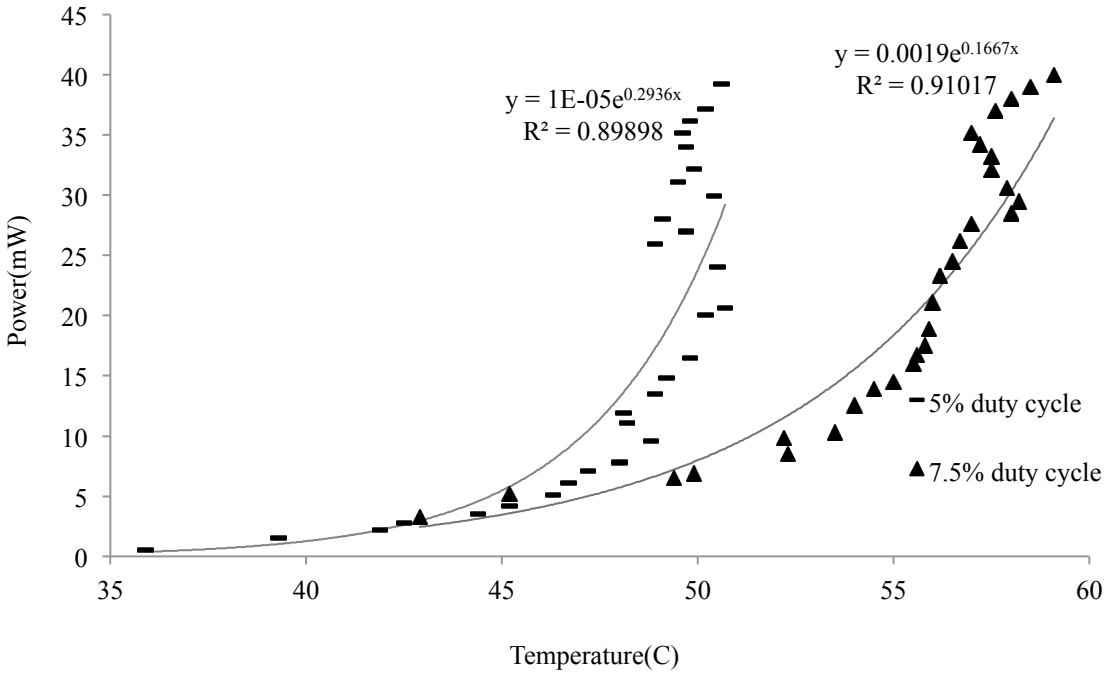

Figure 4.3.4 Transmission characteristic of 5% vs. 7.5% duty cycle pulsed wave.

Similarly, from Figure 4.3.5, it can be seen that 15% duty cycle transmits more power than 20% duty cycle at equal temperature.

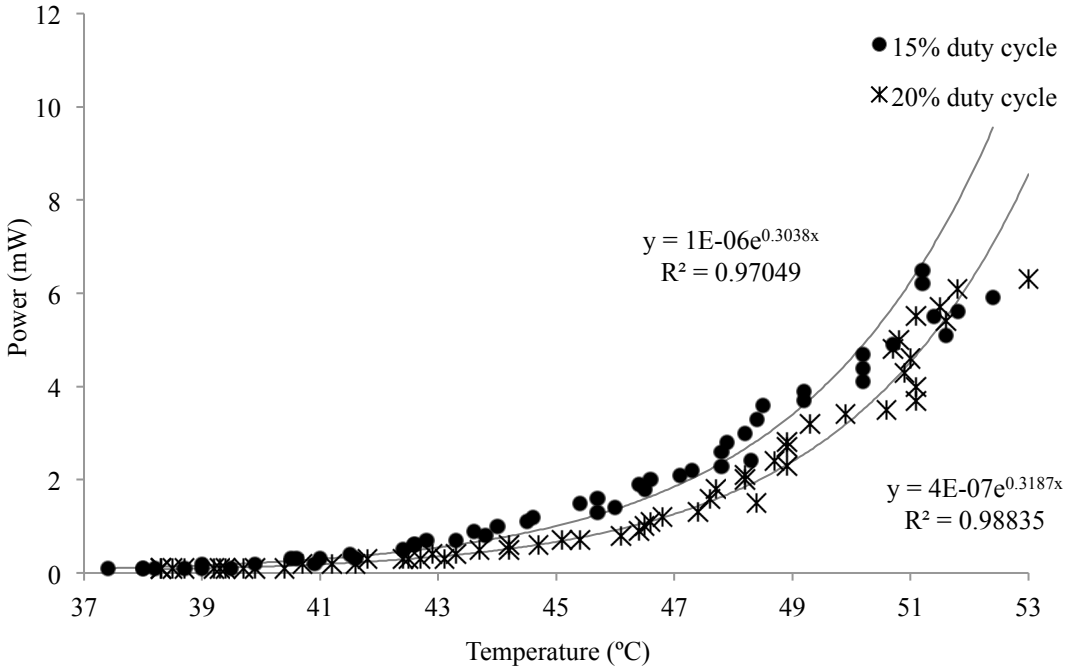

Figure 4.3.5 Transmission characteristic 15% vs. 20% duty cycle pulsed wave.

Increasing the duty cycle also increases the spot size of the skin, as verified with infrared thermography. From Figures 4.3.6 & 4.3.7, it can also be seen that higher duty cycle has a larger percentage of pixels in the 30-55 ºC-temperature range, demonstrating the influence of pulse width, which increases dissipation, thus decreasing transmission.

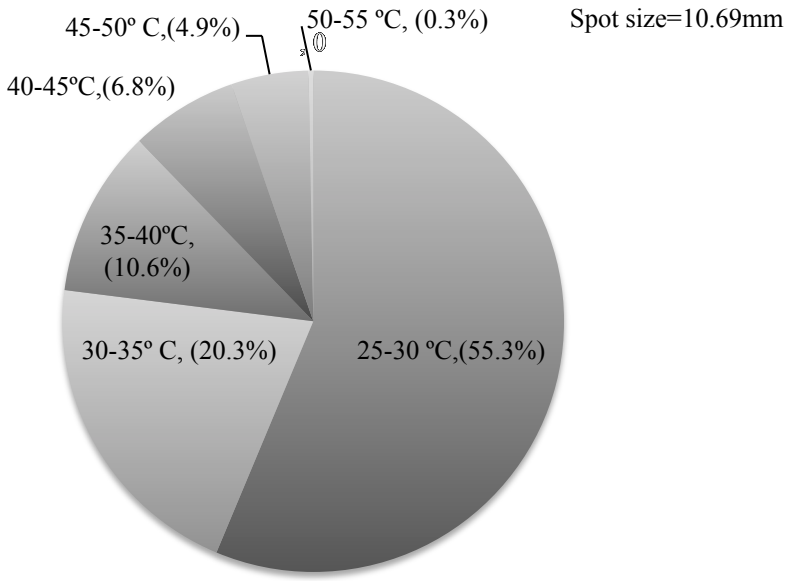

Figure 4.3.6 Temperature distribution of 5% duty cycle experiments.

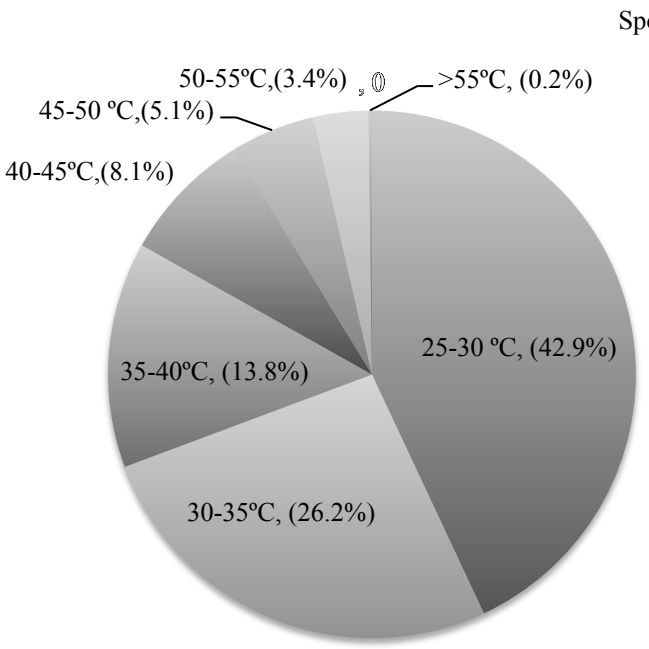

Fig 4.3.7 Temperature distribution of 7.5% duty cycle experiments.

Figures 4.3.8 and 4.3.9 show the 20% duty cycle has greater percentage of pixels in the 30-55º C range, which signifies 20% duty cycle, has greater dissipation losses than 15% duty cycle; hence 20% has a bigger spot size and reduced transmission. Therefore, from this analysis we can summarize that when duty cycle increases, a reduction in transmission follows.

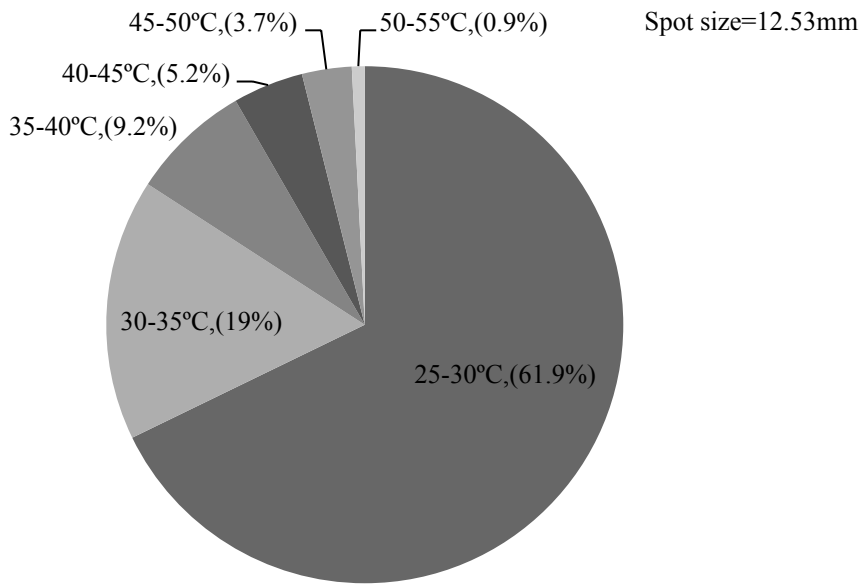

Figure 4.3.8 Temperature distribution of 15% duty cycle experiments.

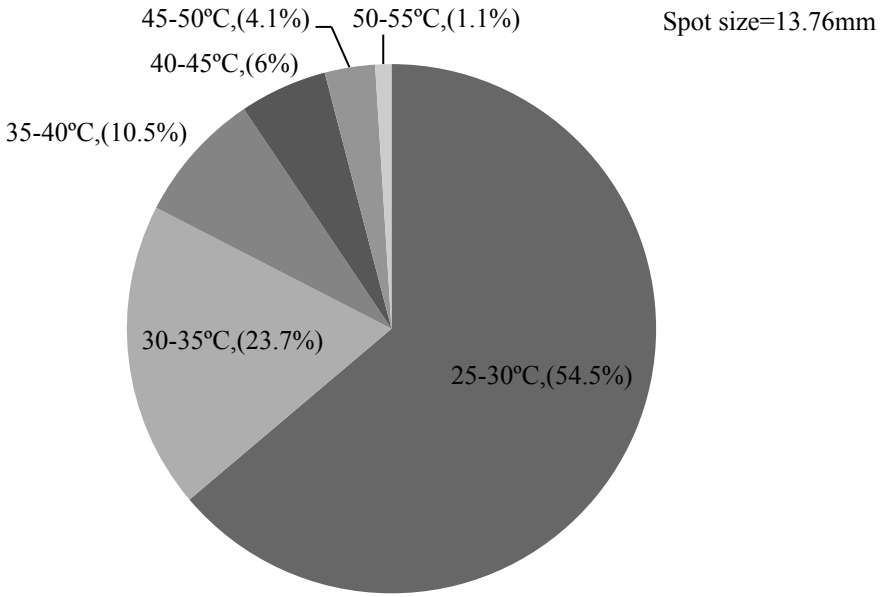

Figure 4.3.9 Temperature distribution of 20% duty cycle experiments.

4.4 Skin thickness study

From Figure 4.4.1, it is evident that at equal exposure times, 2.8 mm thick skin transmits approximately 10 times more optical power than 3.5 mm thick skin. Since thicker skin experience more absorption and dissipation, it requires additional optical energy to overcome these losses resulting in longer exposures for transmitting equivalent levels of optical power. Regardless of the thickness, all skin samples can transmit equivalent power; however, the necessary exposure varies based on the thickness. In this case, 2.8 mm skin transmits power at a faster rate than 3.5 mm skin. (Refer to appendix Data Table A7)

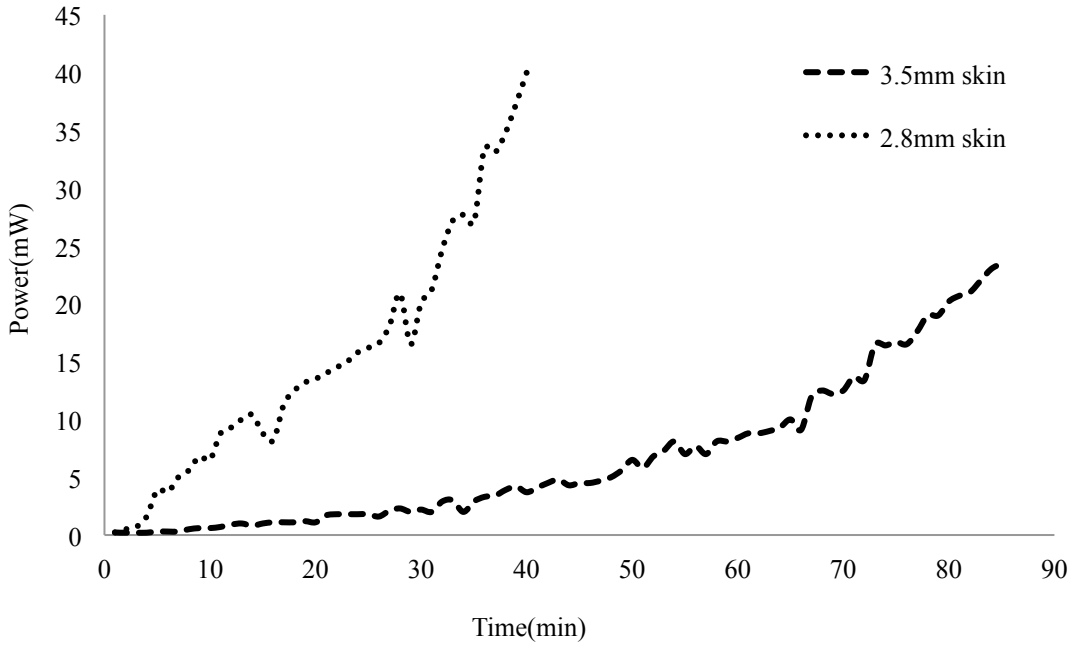

Figure 4.4.1 Temporal characteristics of 2.81mm vs. 3.5 mm skin thicknesses.

Figure 4.4.2 represents the transmission characteristic of 2.8 mm vs. 3.5 mm. The 3.5 mm skin can transmit equal power as 2.8 mm skin but with much higher skin

temperature because thicker skin has significantly more absorption and dissipation to overcome, thus increasing its temperature.

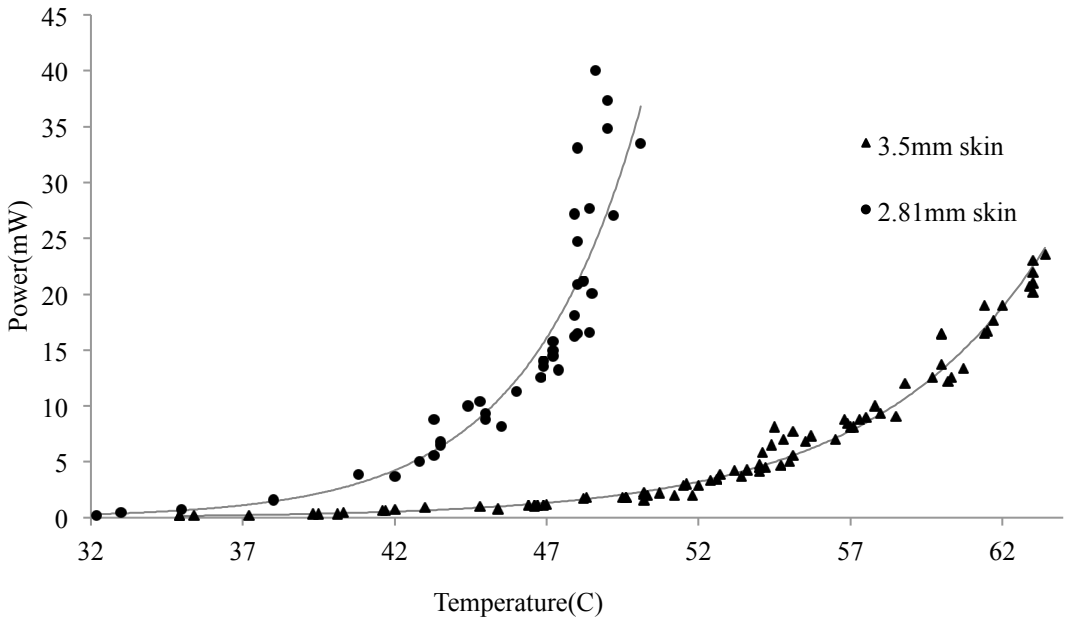

Figure 4.4.2 Transmission characteristic of 2.81mm vs. 3.5mm skin thicknesses.

From Figures 4.4.3 and Fig 4.4.4, it is evident that 3.5 mm skin has greater percentage of pixels in the 30-50 ºC-temperature range, signifying it has higher absorption. Also, the bigger spot size suggest it experiences more dissipation due to its thickness.

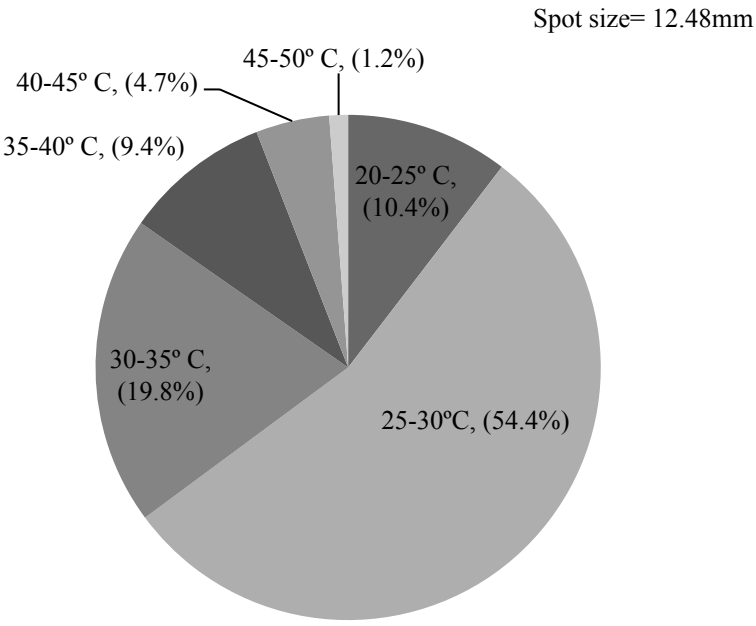

Figure 4.4.3 Temperature distribution of 2.8 mm thick skin.

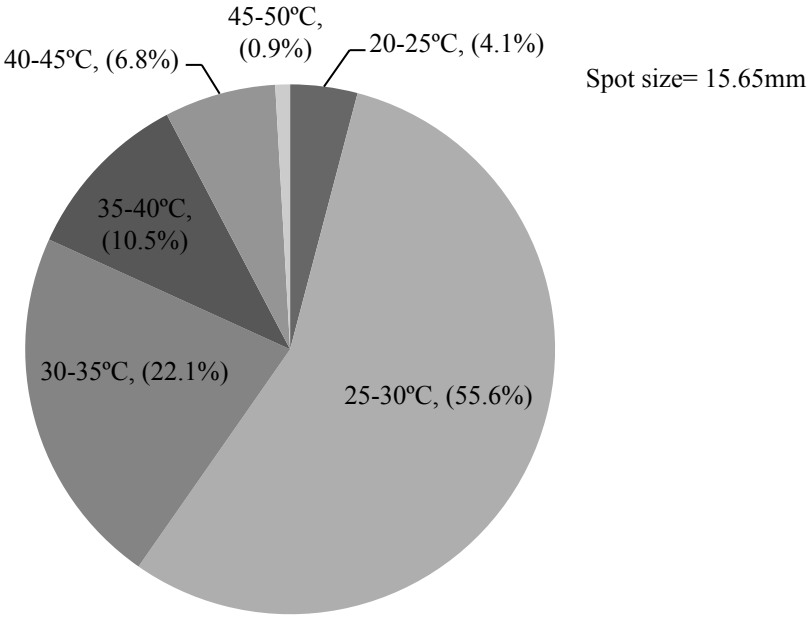

Figure 4.4.4 Temperature distribution of 3.5 mm thick skin.

4.5 Efficiency study

For extended exposure time, the increased thermal state of the skin combined with resulting dryness that arises due to the prolonged irradiation of skin can result in transmission of high optical power. The input power was kept constant at 83 mW and a maximum output power of 71mW was recorded for 100 kHz wave. The aim of this study was to determine if 1-10 J/cm^2 could be transmitted through skin, as this power window could help in photonic bio-stimulation [11]. The area of beam spotsize is essential for optimizing the power density and this was approximated using an infrared sensor and camera; the calculated area of beam spot size was 0.59382 mm^2. Thus, knowing the transmitted power and beam area, the power density of the transmitted optical infrared wave was calculated for different frequencies. (Table 4.5.1)

The efficiency was calculated for the measured power density. 11.956 W/cm^2 was the maximum measured power density and it was achieved through irradiation with a 100 kHz wave. (Input power was constant=13.97 W/cm^2) Thus, the maximum achieved efficiency is calculated as follows:

$$\eta(maximum) = \frac{Output\ power\ density}{Input\ power\ density} * 100 = 85.54\%$$

Figure 4.5.1 represents the power density calculated for different frequencies, and from the figure it can be seen that maximum power was transmitted using 100 kHz wave.

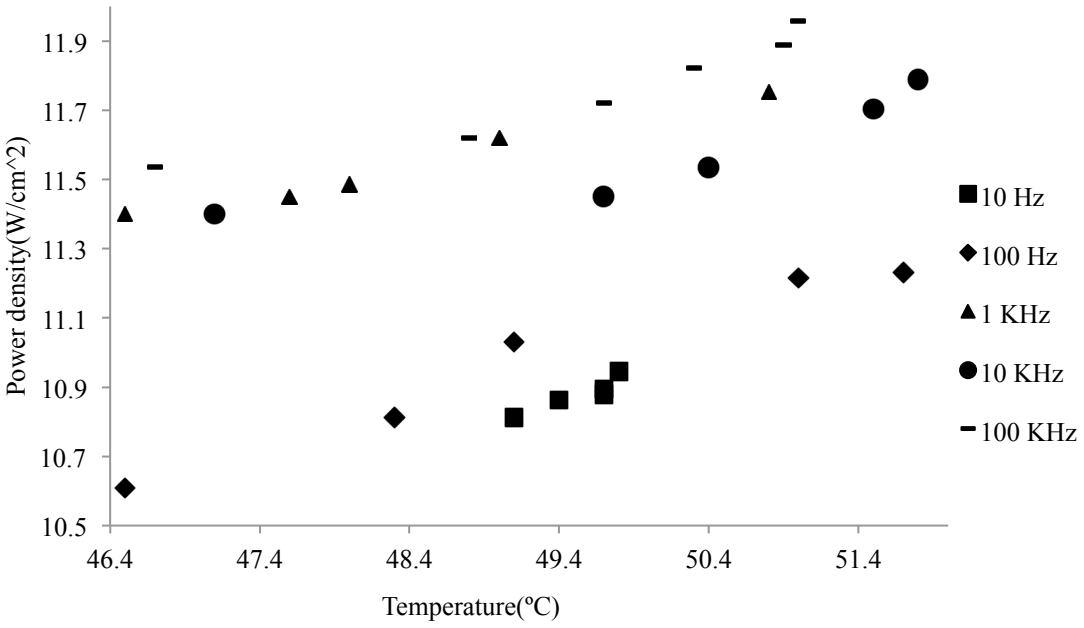

Figure 4.5.1 Power density study of different frequency pulsed waves.

Higher transmission efficiency can be achieved by using infrared irradiation. However, prolonged infrared irradiation should be avoided, since high skin temperature could cause dryness and burns. The measured power density was found to be at a maximum of 11.97 J/cm^2. Research shows that power in the 1-10 J/cm^2 can induce laser bio-stimulation [11] and this can be achieved by controlling the radiation parameters.

Table 4.5.1 Power densities for varying frequencies

	10 Hz				100 Hz			
Time (Min)	Temp (ºC)	Power (mW)	Power density W/cm^2	Power density J/cm^2	Temp (ºC)	Power (mW)	Power density W/cm^2	Power density J/cm^2
1	49.1	64.2	10.81	10.81	46.5	63	10.60	10.60
2	49.4	64.5	10.86	10.86	48.3	64.2	10.81	10.81
3	49.7	64.6	10.87	10.87	49.1	65.5	11.03	11.03
4	49.7	64.7	10.89	10.89	51	66.6	11.21	11.21
5	49.8	65	10.94	10.94	51.7	66.7	11.23	11.23

	1 kHz				10 kHz			
Time (Min)	Temp (ºC)	Power (mW)	Power density W/cm^2	Power density J/cm^2	Temp (ºC)	Power (mW)	Power density W/cm^2	Power density J/cm^2
1	46.5	67.7	11.40	11.40	47.1	67.7	11.40	11.40
2	47.6	68	11.45	11.45	49.7	68	11.45	11.45
3	48	68.2	11.48	11.48	50.4	68.5	11.53	11.53
4	49	69	11.61	11.61	51.5	69.5	11.70	11.70
5	50.8	69.8	11.75	11.75	51.8	70	11.78	11.78

	100 kHz			
Time (Min)	Temp (ºC)	Power (mW)	Power density W/cm^2	Power density J/cm^2
1	46.7	68.5	11.53	11.53
2	48.8	69	11.61	11.61
3	49.7	69.6	11.72	11.72
4	50.3	70.2	11.82	11.82
5	50.9	70.6	11.88	11.88
6	51	71	11.95	11.95

CHAPTER 5

COMPREHENSIVE ANALYSIS

The previous chapter explained in detail the influence of duty cycle, frequency, and skin thickness on transmission. However, an in-depth analysis of the inter-relationships between the parameters and its influence on transmission are told in this chapter. The goal of this chapter is to analyze the relationships between the influencing variables and also include the parameters of lesser significance. The need for advanced multi-variable statistical tool is important and utilized in this study.

Principal Component Analysis (PCA) is a useful statistical tool that reveals patterns in high dimension, multi-variable data. It also reduces the dimensionality of data by introducing artificial variable without loss of any significant information. In some cases, PCA variables provide redundant information. So, PCA introduces principal component, along each dimension each component accounts for the corresponding variable correlation and is absolutely uncorrelated and orthogonal to one another. In reality, the number of components is equal to the number of variables. Here, a few components are sufficient for enclosing most of the data. The reduced components can be used to create predictor variable for the successive analysis.

The first (building of the correlation and covariance matrix) denotes the relationships between variables. The correlation matrix is simply a scaled version of the covariance matrix and the resulting relationships between the variables have the same sign

(i.e. positive, negative or zero). If the correlations between variables have a positive sign, the variables are directly related; if the sign is negative the variables are inversely related; and a zero indicate the variable are uncorrelated, hence indicating the relationship between the variables. As the variables are interdependent, this study is very complicated. Thus, a threshold value of 0.25 is randomly chosen. The purpose of this study is to understand the variable interdependency and not to obtain absolute correlation values.

The next step generates the eigenvectors and eigenvalues from the covariance matrix, as these indicates the significance of the components. Based on the strength of the resulting eigenvalues, the significance of components are determined. The components can then be plotted using loading matrix, which is created according to the covariance matrix, eigenvalues and eigenvector. Usually, components that account for 97% are sufficient for data compression.

Finally, the extracted components are tested using a chi-square test and probability test. In addition, the eigenvalues can be plotted using a scree plot. If the gap between successive eigenvalues is small, then the component related to the eigenvalue is significant. PCA is implemented in this study to highlight the impact of two principal parameters: frequency and duty cycle. Appropriately, the analysis is split into two sections. In each, the other parameter is held constant.

5.1. Impact of Frequency on Infrared transmission

As explained, the first step in the analysis is to create correlation matrix (Table 5.1.1) that reveals the relationship between inter-related variables. Each row of the correlation matrix represents the influence of an individual factor on the other variables.

Table 5.1.1 demonstrates that irradiation time correlates with temperature and power. When irradiation exposure time increases, the skin temperature gradually increases, resulting in an increase in transmitted power. The irradiation time has a slightly weaker correlation with transmitted power, indicating that some optical power is lost due to dissipation and absorption.

Table 5.1.1 also illustrates that skin temperature is positively correlated with time, power, frequency, spot size and thickness. The skin temperature increases with frequency, as when frequency increases, the pulses become shorter; the shorter pulse minimizes the dissipation losses, thus improving transmission. The skin temperature also increases with skin thickness, as more optical energy is required to transmit through thicker skin, thus increasing the necessary temperature conditions to transmit equal power. The thermal spot size increases with skin temperature, since skin is more thermally conductive. This can be observed via infrared thermography.

Table 5.1.1 shows that transmitted power has a positive correlation with time, temperature and frequency; conversely, it is negative with respect to spot size and thickness. The high correlation between power and temperature signifies that the skin temperature must be increased for transmitting high power because skin is more transmissive to optical radiation at high temperature. The transmitted power increases with frequency, because shorter on and off pulses decreases absorption and dissipation and improves transmission. Also, the power transmitted increases when the thermal spot size decreases because smaller spot size signifies less absorption and dissipation. Finally, the power transmitted decreases when thickness increases, as thicker skins requires more incident optical energy for transmission.

Table 5.1.1 also denotes that frequency is negatively correlated with thickness, as when frequency increases, the thicker skin transmits more efficiently due to the reduced absorption, thus minimizing the influence of thick skin. However, the spot size has a positive correlation with thickness, since thicker skin experiences more absorption, thus increasing the thermal spot size, which is clearly seen using IR thermography. This increase in spot size reveals decrease in power transmitted.

Table 5.1.1 Correlations of the independent variables

	Time	Temp	Power	Frequency	Spot size	Thickness
Time	1.0000	0.5716	0.4171	0.0000	-0.0000	-0.0000
Temp	0.5716	1.0000	0.7305	0.3993	0.0116	0.0559
Power	0.4171	0.7305	1.0000	0.3490	-0.1528	-0.2430
Frequency	0.0000	0.3993	0.3490	1.0000	0.1513	-0.2956
Spot size	-0.0000	0.0116	-0.1528	0.1513	1.0000	0.0739
Thickness	-0.0000	0.0559	-0.2430	-0.2956	0.0739	1.0000

Using the correlation matrix, a covariance matrix (Table 5.1.2), eigenvectors (Table 5.1.3), eigenvalues (Table 5.1.4) and loading matrix (Table 5.1.5) is generated. Six principle components are generated, and are tested using chi-square and probability tests (Table 5.1.4). It can be seen that at least five components are required for displaying greater than 95% information; hence a 5-dimensional analysis is required to model the output.

Table 5.1.2 Covariance Matrix of the independent variables

	Time	Temp	Power	Frequency	Spot size	Thickness
Time	96.60517	40.35111	39.26993	0.00000	-0.00000	-0.00000
Temp	40.35111	51.59160	50.26559	965.74617	0.22417	0.59671
Power	39.26993	50.26559	91.76640	1125.6051	-3.93223	-3.46006
Frequency	0.00000	965.74617	1125.60	113366.27	136.85696	147.9417
Spot size	-0.00000	0.22417	-3.93223	136.85696	7.22007	0.29526
Thickness	-0.00000	0.59671	-3.46006	-147.9417	0.29526	2.20984

Table 5.1.3 Eigenvectors for covariance matrix

	PC1	PC2	PC3	PC3	PC5	PC6
Time	0.42470	0.43640	0.00778	-0.55216	0.51133	0.25057
Temperature	0.58633	0.20721	0.12956	0.20224	-0.08452	-0.74057
Power	0.57113	-0.01877	-0.17557	0.08563	-0.61291	0.50955
Frequency	0.35229	-0.54961	0.27412	0.42311	0.51663	0.22967
Spot size	-0.02872	-0.11117	0.88028	-0.35253	-0.29366	0.03740
Thickness	-0.15723	0.67219	0.31983	0.58617	0.05083	0.27382

Table 5.1.4 Eigenvalues of the corresponding vectors used to find the significance of components

Number	Eigenvalue	Percent	Total	ChiSquare	DF	Prob>ChiSq
1	2.3500	39.166	39.166	509.784	20.000	<.0001*
2	1.2535	20.891	60.057	314.906	14.000	<.0001*
3	1.1061	18.436	78.493	247.264	9.000	<.0001*
4	0.7260	12.100	90.592	144.012	5.000	<.0001*
5	0.4056	6.760	97.352	57.451	2.000	<.0001*
6	0.1589	2.648	100.000	0.000	0.000	.

Table 5.1.5 Loading Matrix for plotting the principal components

	Prin1	Prin2	Prin3	Prin4	Prin5	Prin6
Time	0.65105	0.48858	0.00818	-0.47046	0.32564	0.09988
Temperature	0.8988	0.23199	0.13626	0.17231	-0.05383	-0.29518
Power	0.87552	-0.02101	-0.18465	0.07296	-0.39034	0.20310
FREQUENCY	0.54005	-0.61533	0.28830	0.36051	0.32902	0.09155
Spot size	0.04402	-0.12447	0.92582	-0.30037	-0.18702	0.01491
Thickness	0.24103	0.75257	0.33637	0.49944	0.03237	0.10914

The resultant eigenvalues are plotted using a Scree plot (Fig 5.1.1). The plot shows that components 2 to 5 are equally spaced and hence all components contain significant information that cannot be ignored.

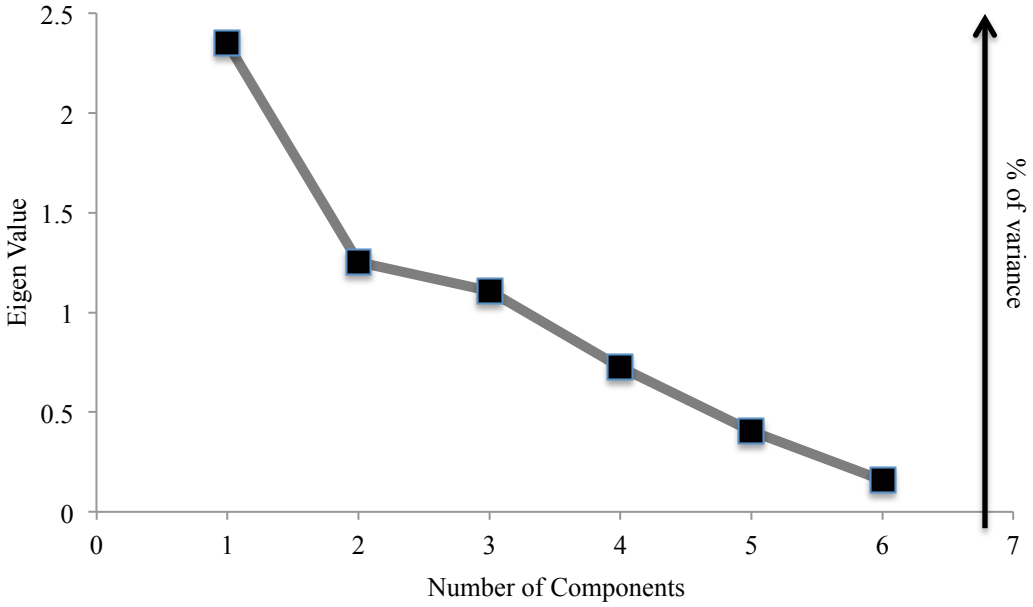

Figure 5.1.1 Scree plot-representing significance of components for pulse frequency.

In general, two components are sufficient to compress majority of the data, but the loading plot (Fig 5.1.2) in this study indicates that when two components are used only 60% of data is retained.

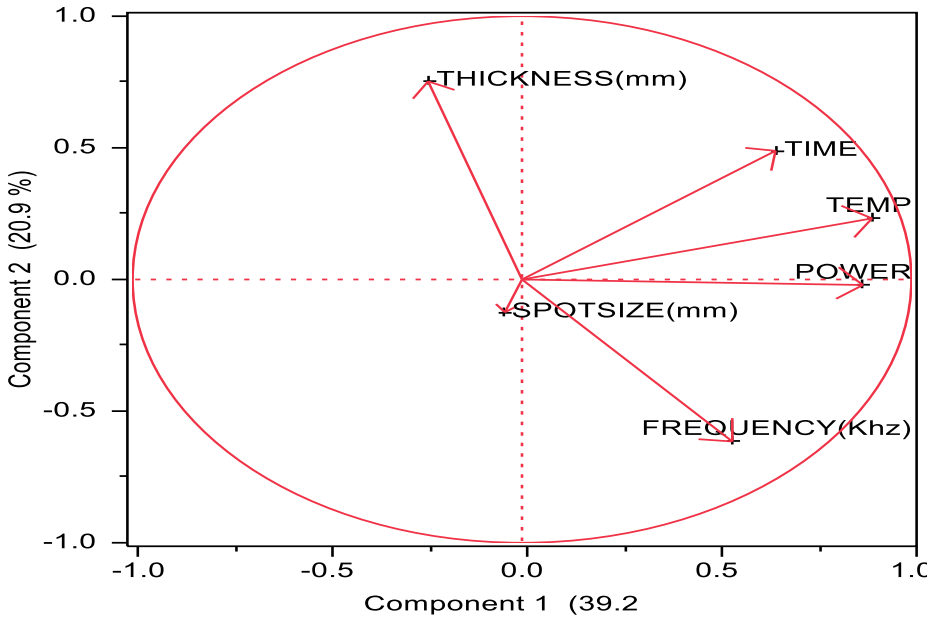

Figure 5.1.2 Loading plot-representing components 1 & 2, only.

Therefore, a minimum of 5 components is required to compress at least 95% of significant data.

5.2. Impact of Duty cycle on Infrared transmission

`Table 5.2.2 demonstrates that temperature has a negative correlation with duty cycle, spot size and thickness. When duty cycle increases, the pulse width increases and the inter-pulse duration decreases. Thus, more energy is delivered, and less time is provided for skin to recover. This inefficient optical transmission results in the dissipation of the incident optical power to the surrounding skin, thus causing temperature to drop. This temperature decrease is due to the transfer of thermal energy to the sub-layers of skin, thus causing the thermal spot size to increase. The change in temperature increases with thickness, as thicker skin has more absorption.

Table 5.2.1 shows that power has a negative correlation with duty cycle. When duty cycle increases, the transmission is inefficient due to dissipation and absorption, thus decreasing transmitted power. Also, the duty cycle has negative correlation with thickness and spot size. The absorption increases when duty cycle increases, resulting in thermal energy lost to the sub-layers of skin, thus, causing an increase in thermal spot size and this effect is enhanced when skin thickness increases (since thicker skin has more absorption).

Table 5.2.1 also shows spot size has a negative correlation with temperature and power, and a positive correlation with duty cycle and thickness. When the thermal spot size spreads, the temperature drops due to the increased dissipation. Since thermal losses

and dissipation rise as duty cycle and thickness increase, the thermal spot size also increases.

Table 5.2.1 Correlations of the independent variables

	Time	Temp	Power	Duty cycle	Spot size	Thickness
Time	1.0000	0.4238	0.3375	-0.0000	-0.0000	-0.0000
Temp	0.4238	1.0000	0.7631	-0.5033	-0.2802	-0.4478
Power	0.3375	0.7631	1.0000	-0.3098	-0.3703	-0.4809
Duty cycle	0.0000	-0.5033	0.3098	1.0000	0.1879	0.6071
Spot size	0.0000	-0.2802	0.3703	0.1879	1.0000	0.4232
Thickness	0.0000	-0.4478	0.4809	0.6071	0.4232	1.0000

As in the frequency study, using the correlation matrix, the covariance matrix (Table 5.2.2), eigenvectors (Table 5.2.3), eigenvalues (Table 5.2.4) and loading matrix (Table 5.2.5) were generated. From the generated eigenvalues, it is evident that at least 5 principle components are required to retrieve 97% data. Also, the chi-square test and probability test (Table 5.2.4) indicate that five components are required to model the collected data.

Table 5.2.2 Covariance Matrix of the independent variables

	Time	Temp	Power	Duty cycle	Spot size	Thickness
Time	75.0954	26.63294	26.8856	-0.00000	-0.00000	-0.00000
Temp	26.6329	52.58962	50.8678	-0.28759	-5.07928	-3.85692
Power	26.8856	50.86786	84.4998	-0.22441	-8.50830	-5.24987
Duty cycle	-0.00000	-0.28759	0.22441	0.00621	0.03700	0.05682
Spot size	-0.00000	-5.07928	8.50830	0.03700	6.24689	1.25624
Thickness	-0.00000	-3.85692	5.24987	0.05682	1.25624	1.41060

Table 5.2.3 Eigenvectors for covariance matrix

	PC1	PC2	PC3	PC3	PC5	PC6
Time	0.20434	0.73833	0.01130	-0.61784	-0.13474	-0.11445
Temperature	0.50922	0.26012	0.12712	0.28183	0.33781	0.68068
Power	0.48977	0.22436	-0.16458	0.57070	-0.17266	-0.57200
Duty cycle	-0.39685	0.33607	-0.56777	0.28571	-0.43331	0.37124
Spot size	-0.31569	0.27656	0.79185	0.30767	-0.31934	0.01370
Thickness	-0.44935	0.38397	-0.08507	0.19197	0.74040	-0.24161

Table 5.2.4 Eigenvalues of the corresponding vectors used to find the significance of components for duty cycle

Number	Eigenvalue	Percent	Total	ChiSquare	DF	Prob>ChiSq
1	2.8651	47.752	47.752	995.000	20.0	<.0001*
2	1.2519	20.865	68.617	458.000	14.0	<.0001*
3	0.8518	14.197	82.813	267.431	9.0	<.0001*
4	0.4949	8.249	91.062	120.638	5.0	<.0001*
5	0.3700	6.166	97.228	65.253	2.0	<.0001*
6	0.1663	2.772	100.000	0.000	0.0	.

Table 5.2.5 Loading Matrix for plotting the principal components for duty cycle

	Prin1	Prin2	Prin3	Prin4	Prin5	Prin6
Time	0.34587	0.82610	0.01043	-0.4346	-0.0819	-0.0466
Temperature	0.86194	0.29104	0.11732	0.19827	0.20547	0.27759
Power	0.82902	0.25103	-0.1519	0.40149	-0.1050	-0.2332
Duty cycle	-0.6717	0.37602	-0.5240	0.20100	-0.2635	0.15140
Spot size	-0.5343	0.30943	0.73082	0.21645	-0.1942	0.00559
Thickness	-0.7606	0.42961	-0.0785	0.13506	0.45035	-0.0985

The eigenvalues are plotted using a scree plot (Figure 5.2.1). All components 2 to 5 are close and approximately equidistance and therefore cannot be ignored.

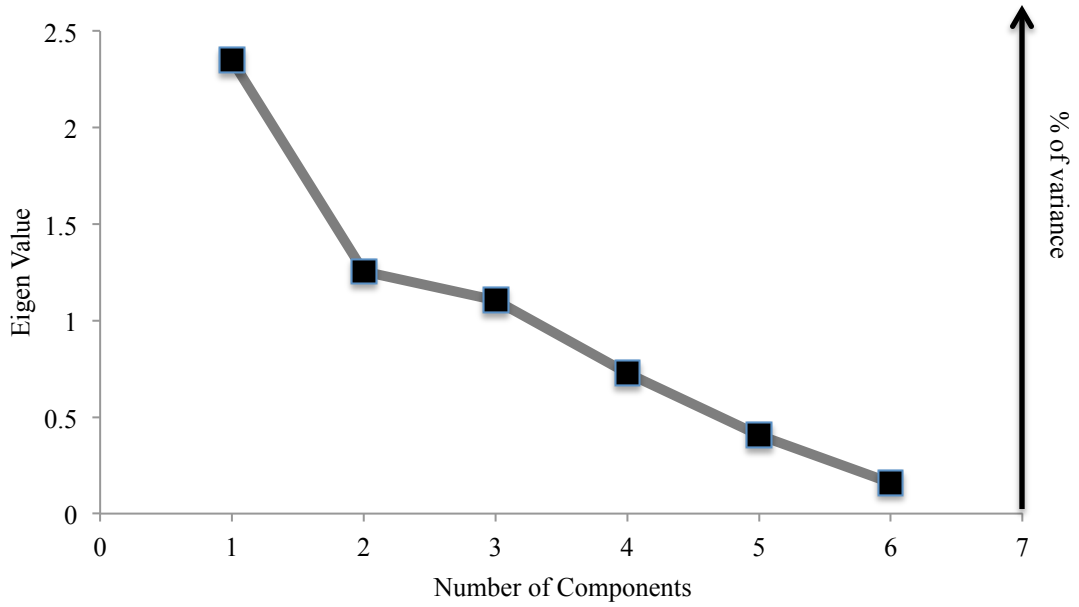

Figure 5.2.1 Scree plot (duty cycle) representing significance of components on duty cycle.

According to the loading plot (Figure 5.2.2), it is clear that more than 30% of data is lost for 2 PC's only (PC1 is x-axis & PC2 is y-axis).

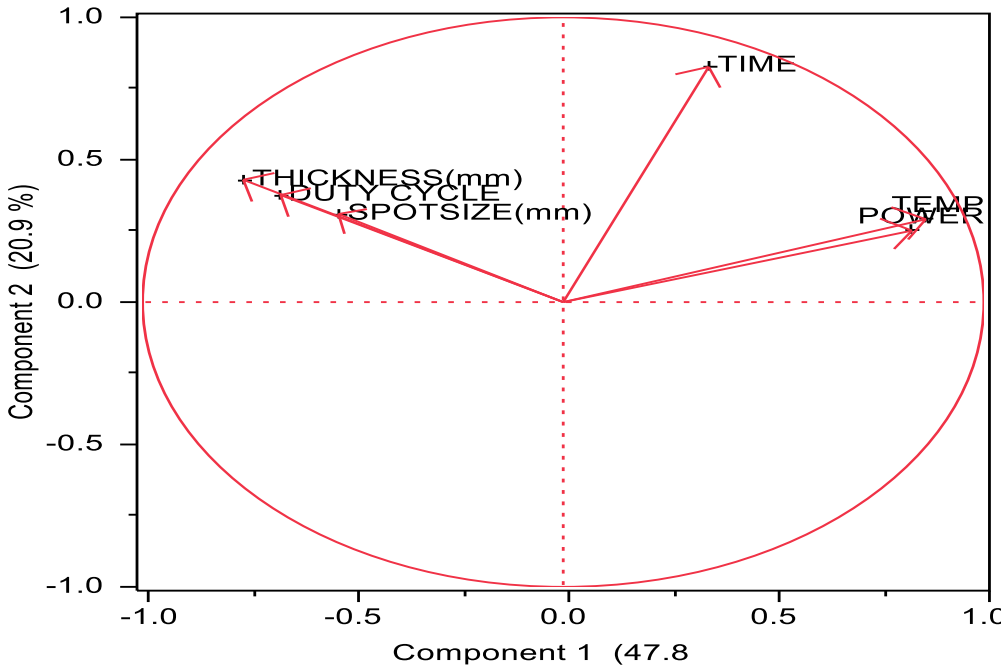

Figure 5.2.2 Loading plot (Duty cycle) representing components.

Therefore, a minimum of 5 components is required to compress at least 95% of significant data.

5.3. Future proposed work

The results obtained in this study highlight the correlation between the different parameters and how each parameter influences the transmission. It must be remembered that all the studies were carried out under constant power. Since the skin was directly exposed to a constant optical power source, there were losses and dissipation at the commencement of irradiation mainly due to initial conditions of skin. One possible approach, which could minimize the losses, is slow elevation of power delivered to the

skin. Also, the skin can be irradiated for different input power levels; this could possibly minimize losses and improve transmission. For example, in this study, the skin was irradiated constantly at 84 mW for all experiments. Maintaining the parameters studied while varying input power could provide another set of experiments.

One of the factors that caused complications during the study was the varying skin thickness. Though its effects were greatly reduced, it introduced variance and most of the experiments were conducted on thick fleshy skins (approx. 5-8 times thick as human skin). Since the research is projected for human use in the future, human trials are proposed.

The study was carried out using an l440 nm laser; so it cannot be established from this study if the pulsed wave approach should work for other (higher/lower) wavelengths as skin chromophores can possibly behave differently depending on wavelength. Hence a similar study needs to be carried out for sources of different wavelengths preferably in the 1.5-3 μm spectrum as they have less energy per photon and longer wavelength.

From the study, it is clear that IR irradiation increases the skin temperature and subsequently power transmitted. Though the parameters that influence the temperature and power output were found in this study, techniques to accurately control the temperature in the desired temperature range are unresolved. In the conducted study, the temperature fluctuated between 45-55ºC. However, it would be more ideal if the temperature were maintained between 47-50º C. Therefore, by carefully designing a study where frequency, duty cycle, input power and wavelength are varied by controlling two parameters at a time, the skin temperature could be maintained in the desired range.

Finally, an essential study must be the analysis of whether pulsed approach is practically viable. For this, a detailed study on the power requirements of different bio-cells must be determined. For example, the cells regenerate if power is delivered within a specific window. If power delivered is more than this specified window it could lead to adversarial effects and if lesser than this window, the irradiation has essentially no effect. Therefore, a detailed study is in order to resolve the power specification and requirement for different cell categories.

CHAPTER 6

CONCLUSION

This thesis investigates the influence of pulsed infrared irradiation on pigskin, at atmospheric conditions. Pigskin and infrared irradiation were selected because pigskin is the closest to human skin in terms of structure, and infrared irradiation has low power and long wavelength. Therefore, it offers great penetrative and thermal abilities, which could produce positive effects on the body, if applied efficiently. The irradiation was pulsed as it provided control on skin temperature.

The skin was pulsed using infrared irradiation and studies were conducted to explore the influence of frequency and duty cycle. Both studies exhibited variations in transmission when the parameters were changed, proving that both influence transmission. The frequency study demonstrated that higher frequency transmitted more optical power at a lower skin temperature while the duty cycle study revealed that higher duty cycle transmitted higher power at reduced exposure times but at a faster rate was observed at the expense of skin temperature.

The skin temperature recorded during the study covered a wide range of temperature. For instance, in one experiment the maximum temperature recorded was 65 ºC. In general, the temperature of the irradiated spot was between 25-50 ºC. Temperature was observed for all samples, but greater for thicker samples. The study also demonstrates that when spot size increases, the power transmitted decreases. Also, the spot increases when duty cycle increases.

The transmission characteristics of pigskin reveal that optical power transmitted through skin increases exponentially with skin temperature, while the absorption

characteristics show that absorption decreases linearly with increase in temperature, which is similar to the absorption characteristic of water. A maximum efficiency of 86% was achieved during the studies.

Based on the bio-photonic application, the two pulsing parameters i.e. frequency and duty cycle can be varied to enhance stimulation. For example in an application related to cell regeneration, frequency modulation would be beneficial as it aids in transmitting power at lower temperature. Where heating is more significant, duty cycle would be beneficial. For example, a new study has revealed that cancer cells and tumors at initial stages can be killed by irradiating with infrared lasers, as it can produces a temperature of 60-65 ºC on skin. For such applications, duty cycle modulation would be beneficial as it increases skin temperature in smaller time duration. Hence, this research has a wide range of medical and cosmetic applications.

APPENDIX.

Table A1: Temperature distribution along X and Y axis of 10 KHz, 100 KHz, 500 & 1 MHz pulsed wave (**Temperature distribution study**)

	10 KHz		100 KHz		100 KHz		1 MHz	
Pixel	X	Y	X	Y	X	Y	X	Y
1	26.48	26.85	26.28	26.17	25.6	25.96	25.82	25.52
2	26.94	27.33	26.46	26.44	25.74	26.09	26	25.76
3	27.42	27.74	26.7	26.7	25.96	26.35	26.17	26.31
4	28.24	28.28	26.85	26.83	26.15	26.48	26.48	26.63
5	28.75	28.71	27.13	27.09	26.46	26.81	26.77	27.03
6	29.43	29.16	27.27	27.29	26.77	26.81	27	27.44
7	30.13	29.73	27.42	27.7	27.03	27.07	27.33	27.78
8	31.02	30.39	27.76	28.28	27.42	27.44	27.57	28.24
9	31.93	31.08	27.94	28.52	27.89	27.96	27.91	28.79
10	33.01	32	28.49	28.82	28.43	28.32	28.47	29.5
11	34.01	32.74	29.05	29.39	29.16	28.6	29.01	30.18
12	35.33	33.83	29.5	29.9	29.88	29.56	29.5	30.91
13	36.73	34.9	30.11	30.43	30.89	30.22	30.15	31.89
14	38.31	36.41	30.79	30.93	31.98	31.48	31.08	32.99
15	39.93	37.9	31.54	31.83	33.66	32.68	31.87	34.52
16	41.77	39.64	32.68	32.66	35.33	34.3	32.99	36.01
17	43.62	41.31	33.75	33.38	37.84	35.79	33.81	37.82
18	45.58	43.45	35.19	34.15	40.39	38.15	35.09	39.6
19	47.37	45.41	36.53	35.15	43.59	40.43	36.43	41.64
20	49.41	47.72	38.45	36.17	46.57	43.27	38.06	43.64
21	51.52	49.89	40.24	37.7	50.09	46.18	39.5	46.11
22	52.91	51.84	42.45	39.23	53.57	49.41	41.24	48.53
23	54.34	53.65	44.37	41.24	56.95	52.8	43.17	50.3
24	54.74	54.67	46.84	43.17	60.27	55.95	45.15	52.19
25	55.13	55.77	49.29	45.58	61.42	59.05	47.15	52.66
26	53.81	55.29	51.7	47.77	62.64	60.83	49.07	53.2
27	52.26	54.74	54.17	50.29	61.14	62.64	50.91	52.54
28	49.43	52.98	56.11	52.73	59.6	61.88	52.02	51.88
29	46.46	51.26	57.98	54.72	56.58	61.05	53.1	50.75
30	43.98	48.89	58.41	56.67	53.55	58.38	53.22	49.7
31	41.56	46.44	58.95	57.49	50.09	55.63	53.2	48.04
32	39.4	44.09	56.95	58.41	46.61	52.02	52.05	46.35
33	37.29	41.66	55.05	57.41	43.62	48.35	51.03	44.84
34	35.75	39.89	52.07	56.48	40.62	45.08	49.09	42.98
35	34.34	38.13	48.93	53.88	38.13	41.56	47.19	41.39
36	33.3	36.65	46.24	51.08	35.81	39.03	45.26	39.71

	10 KHz		100 KHz		100 KHz		1 MHz	
37	32.12	35.15	43.32	47.86	34.09	36.51	43.32	38.29
38	31.23	33.95	40.74	44.56	32.43	34.56	41.33	36.95
39	30.03	32.95	38.13	42.36	31.29	32.56	39.25	35.75
40	29.43	31.87	36.37	40.01	30.26	31.46	37.44	34.56
41	28.75	31.12	34.6	38.35	29.56	30.2	35.73	33.64
42	28.11	30.47	33.6	36.55	28.73	29.39	34.54	32.68
43	27.65	30.01	32.64	35.33	28.26	28.37	33.13	31.6
44	27.2	29.37	31.95	34.01	27.61	27.91	32.06	30.62
45	26.94	28.64	31.18	32.76	27.09	27.46	31	29.94
46	26.5	28.04	30.51	31.46	26.68	27	30.36	29.28
47	-	-	-	-	26.28	26.83	29.46	28.67
48	-	-	-	-	26.26	26.44	28.79	28.13
49	-	-	-	-	26.04	26.15	28.17	27.63
50	-	-	-	-	25.71	25.98	27.81	27.37

Table A2: Power & Temperature of 1-kHz, 10-kHz and 100-kHz pulsed wave for varying thickness **(Frequency study**)

	1 kHz (1.55mm)		10kHz (1.55mm)		10 kHz (5.3mm)		100kHz(5.3mm)	
Time (Min)	Temp (C)	Power (mW)	Temp (C)	Power (mW)	Temp (C)	Power (mW)	Temp (C)	Power (mW)
1	36	0.4	34	0.4	36.4	0.3	34.8	0.2
2	37	0.8	35	0.7	40.2	0.4	38.4	0.4
3	37.7	0.9	35	0.8	41.1	0.5	38.5	0.5
4	39	1	36.2	0.9	42	0.5	40.2	0.5
5	39	1	37.7	1	43	0.5	40.6	0.6
6	40.4	1.1	38	1.1	43.5	0.5	40.8	0.7
7	40.5	1.2	38.2	1.2	45	0.5	42.4	0.8
8	40.9	1.3	38.6	1.2	45.3	0.7	43	0.9
9	40.9	1.3	39.2	1.3	45.9	0.6	43.2	1
10	41.3	1.4	39.2	1.4	46.3	0.6	43.7	1.2
11	41.5	1.6	38.9	1.5	46.2	0.7	45.2	1.2
12	42	1.6	38.5	1.5	46.5	0.7	46.2	1.3
13	42	1.6	39.4	1.7	46.9	0.8	45.6	1.4
14	42.2	1.6	40.2	1.8	46.8	0.8	46.4	1.6
15	42.4	1.7	39.4	2	47.2	0.9	46.9	1.7
16	42.5	1.8	40.1	2.1	47.4	0.8	47	1.9
17	43	1.8	40.1	2.1	48.4	0.9	48.1	2.1
18	43.2	1.9	40.2	2.2	48.4	1	49.3	2.2
19	43.2	2	41.6	2.3	48.4	1	48.9	2.2
20	43.1	2.2	41	2.5	48.6	1.1	49.9	2.5
21	43.2	2.6	40.9	2.5	48.4	1.1	49.9	2.6
22	43.4	2.6	40.9	2.8	49.9	1.2	49.5	2.8
23	43.3	2.6	41.3	3	49.8	1.3	50.3	3
24	43.7	2.7	41.8	3.3	49.7	1.4	51	3.2
25	44.5	2.9	41.5	3.5	50.4	1.5	50.6	3.4
26	45	3	42.5	3.7	50.6	1.6	51.3	3.6
27	45.2	3.2	42.7	3.9	50.9	1.6	51.7	3.7
28	45	3.4	42.7	4.1	51	1.7	52.6	4.1
29	44.9	3.5	43	4.2	51.8	1.9	51.9	4.1
30	45	3.7	43.2	4.4	51.8	2.1	52.8	4.5
31	45.3	3.8	43.5	4.7	51.8	2.1	52.8	4.9
32	45.7	4	43.8	4.8	52.3	2.2	53.8	5.1
33	45.7	4.3	43.5	5	52.5	2.3	54.1	5.6
34	45.7	4.6	43.4	5.3	52.5	2.4	54.4	5.8
35	45.7	4.7	43.7	5.7	52.9	2.5	54.1	6.3
36	45.3	4.7	43.3	6	53.2	2.5	54.6	6.4
37	45.5	5.1	43.2	6.2	53.1	2.6	55.2	6.6
38	45.7	5	43	6.6	53.5	2.6	55.4	7
39	45.9	5.3	44.2	6.8	53.4	2.8	55.2	7.5
40	45.9	5.4	43.5	7.2	53.7	3	56.2	7.8

41	46.6	5.5	43.5	7.4	53.7	2.9	55.6	8
42	46.7	5.8	43.8	7.7	54.3	3	56	8.5
43	46.9	5.9	44.4	8.1	54.6	3.1	56.2	8.6
44	46.9	6.5	44.4	8.7	54.8	3.3	57	8.9
45	47.2	6.7	44.1	8.9	54.9	3.4	57.3	9.5
46	47.6	6.9	45.1	9.1	54.9	3.4	57.5	10
47	47.5	7.4	45.2	9.9	55	3.7	57.6	10.5
48	47.6	8	45.1	10	55.2	4	57.4	10.8
49	47.4	8.1	45.3	10.3	55.5	4.1	57.7	11.3
50	47.5	8.4	45.2	10.5	55.1	4.5	56.9	12.2
51	47.8	8.5	45.2	11	55.7	4.5	56.7	12.8
52	47.5	9	45.6	11.6	55.8	4.5	57.1	13.3
53	47.7	9.4	45	12.5	55.6	4.6	57.5	13.5
54	47.5	9.9	45	12.8	55.7	4.8	57.8	14.2
55	47.5	10.1	45.1	13.1	55.8	5	57.6	14.8
56	47.5	10.6	44.6	13.5	55.9	5.1	57.7	15
57	47.4	10.8	44.9	14.3	56	5.5	58.3	16
58	47.5	10.9	45	15	56.1	5.7	58.2	16.4
59	47.9	11.2	44.7	15.5	56.3	5.9	58.8	16.8
60	47.8	12	45	16	56.3	6	58.2	17.8
61	-	-	-	-	-	-	58.5	18.6

Table A3: Power and Temperature of 100 KHz, 500 KHz & 1 MHZ pulsed wave for varying thickness (**Frequency study**)

	100kHz(2.49mm)		500kHz(2.49mm)		500kHz(2.01mm)		1 MHz(2.01mm)	
Time (Min)	Temp (C)	Power (mW)	Temp (C)	Power (mW)	Temp (C)	Power (mW)	Temp (C)	Power (mW)
1	39.8	0.6	36.6	0.1	38.6	0.6	41	2
2	42	1.2	35	0.1	38.8	0.6	44	2.3
3	43.1	2.4	36	0.1	40.8	1.8	46	2.7
4	45	2.6	36.4	0.1	42	2.7	46	2.9
5	45.7	2.9	36.8	0.1	44.5	6	49	3.3
6	47.3	3	37	0.1	45	4.7	49.9	3.6
7	47.8	3.5	37.4	0.1	48	5.4	49.2	4
8	47.9	4	37.4	0.1	50.8	7.4	49.2	4.4
9	49.9	4	37.4	0.2	52	8.2	50.9	4.8
10	49.8	4.4	38	0.2	53	8.7	51	5.1
11	51	4.6	39	0.2	54	9.4	52	5.6
12	51.2	4.7	39.1	0.2	55	11.6	53	6.2
13	50	5.7	39.6	0.3	56	12	54	6.4
14	50.7	6.1	40	0.4	56.7	15	54	7
15	51.8	7	41	0.4	57	15.8	54.5	7.4
16	52.7	6.4	41	0.4	58	18.3	54.6	8.2
17	53.7	7.2	41.1	0.4	58.5	18.8	55.7	8.9
18	53.9	7.1	41.3	0.5	59	21.7	56.5	9.1
19	54	7	42.3	0.5	59.8	23.7	55.9	9.7
20	54.5	8.4	42.3	0.5	59.2	24.7	56.2	10.2
21	54.4	8.9	42.8	0.5	59.2	26.8	56.7	11.3
22	54.8	9.4	42.2	0.6	59.8	28.7	57	11.6
23	54.9	11.5	43	0.7	60	30.4	57	12.2
24	55.8	10.4	43.5	0.7	60.3	32.8	58	13.3
25	56.5	12	44.4	0.9	61	34.4	58.3	13.8
26	57.3	13.3	45	1	59.8	36.8	58.9	15.1
27	57.4	14.2	44.6	1	60	40.4	59.2	15.7
28	57.5	13.2	44.4	1.1	60	42	59.4	16.1
29	57.7	14.1	45	1.2	60.1	43.5	59.8	16.5
30	58.5	15.2	45.4	1.4	60	45.8	60.2	18.5
31	59	15.2	45.6	1.4	59.6	48.1	60.6	19.3
32	59.5	16.5	46.4	1.4	59	49.6	60.2	20.2
33	58.4	16.9	46.4	1.5	58	49.6	60.2	21
34	59.2	17.5	46.4	1.6	56	51.4	59.6	21.6
35	59.2	18.2	46.8	1.8	57.2	52.3	58.9	23
36	59.5	18.4	47.3	2.1	57.9	53.5	59.4	24.2
37	59.8	21.5	49	2.1	58.6	54	59.8	25.1
38	60.5	21.6	48.8	2.3	-	-	59.8	25.7

	100kHz(2.49mm)		500kHz(2.49mm)		500kHz(2.01mm)		1 MHz(2.01mm)	
Time (Min)	Temp (C)	Power (mW)	Temp (C)	Power (mW)	Temp (C)	Power (mW)	Temp (C)	Power (mW)
39	60.7	23	49.3	2.3	-	-	59.9	27.5
40	60.9	22.7	49.4	2.6	-	-	60.3	28.4
41	60.9	23.4	50.2	2.7	-	-	60.2	29.3
45	61.2	30.6	52	3.8	-	-	60.7	33.8
46	61.9	30.7	52	3.9	-	-	60.4	34.2
47	61.7	32.1	51	4.2	-	-	61	35.8
48	62.9	31.8	51.1	4.2	-	-	61.1	36.2
49	62.2	33.8	51.7	4.3	-	-	61	37
50	61.2	33.7	52	4.7	-	-	60.9	39
51	61.8	35	52.7	5	-	-	60.7	39.6
52	61.9	38	53	5.4	-	-	60.7	40.7
53	62.1	36.4	53.1	5.5	-	-	60.5	40.9
54	62	38.8	53	5.9	-	-	60.1	42.2
55	62.2	37.2	53.3	6.5	-	-	59.9	43.1
56	62	38.4	-	-	-	-	59.6	44
57	62.7	40.2	-	-	-	-	59.5	44.7
58	61.9	39	-	-	-	-	59.4	44.7
59	62.2	40.5	-	-	-	-	59.5	45
60	62.8	41.1	-	-	-	-	59.2	47.5

Table A4: Power & Temperature of 1%, 3% & 5% duty cycle pulsed wave for varying thickness (**Duty cycle study**)

	1%(2.75mm)		3% (2.75mm)		3% (4.33mm)		5% (4.33mm)	
Time (Min)	Power (mW)	Temp (C)	Power (mW)	Temp (C)	Power (mW)	Temp (C)	Power (mW)	Temp (C)
1	0.1	37.7	0.1	32.3	3	42	0.2	36
2	0.1	34.8	0.1	34.3	3.5	46.7	0.4	36.3
3	0.1	36	0.1	35.7	4	48	0.6	40.1
4	0.1	37	0.1	36.3	4.7	49	0.7	41.5
5	0.1	37.7	0.1	37.7	5.3	49.7	0.8	42.5
6	0.1	38.1	0.1	37.7	5.5	50.5	1	43
7	0.1	38.6	0.1	36.7	6.5	52.5	1.2	44
8	0.1	39.1	0.1	39.2	7.2	52.8	1.3	43.5
9	0.1	39.7	0.1	40.1	7.7	54	1.8	44.5
10	0.1	40.2	0.1	40.2	8	54.5	2	44.5
11	0.1	39.6	0.1	40.3	8.5	54.7	2.4	46.5
12	0.1	39.7	0.1	40.2	9.3	55	2.6	46.5
13	0.1	40.1	0.1	41	10.2	55.5	2.8	47.9
14	0.1	40.3	0.1	41.8	11	55.9	3	48.9
15	0.1	40.3	0.2	41.7	12.1	55.6	3.8	49
16	0.2	40.7	0.2	42	13.2	56.5	4.4	50.2
17	0.2	40.8	0.2	41.6	14.2	58	4.6	51.6
18	0.2	40.8	0.2	39.2	15	57.8	5.5	51.3
19	0.2	39.2	0.2	41.6	16.5	57.1	6.4	52.5
20	0.2	40.2	0.2	42.1	17.6	57	7.2	54.1
21	0.2	41.1	0.2	42.5	20.1	59	8.5	54
22	0.2	41.5	0.2	42.9	21.4	58.4	9	54
23	0.2	41.7	0.3	43.4	22.6	58.6	9.6	54.9
24	0.2	41.8	0.3	43.1	22.1	58.7	10.8	56
25	0.2	42.1	0.3	43.8	23.3	60	11.3	55.6
26	0.2	42	0.3	44.2	24.6	60.2	12	55.8
27	0.2	41.9	0.3	44.5	25.2	60.5	13.3	56.8
28	0.3	42.3	0.3	44.1	26	61	14.8	57.3
29	0.3	42.5	0.3	44.4	27	60.8	16.1	57
30	0.3	42.5	0.4	44.5	28.3	60.3	16.6	58
31	0.3	42.5	0.4	44.5	30	60.3	18.2	58.5
32	0.3	43	0.4	44.8	31	59.8	19.8	58.1
33	0.3	43	0.4	45	32.1	60	21.1	59
34	0.3	43.2	0.4	45.8	33.4	60	22.6	59.2
35	0.3	43.3	0.4	46.1	34	60	23	59.5
36	0.3	43.5	0.4	46.5	34.5	60	24	59.1
37	0.3	43.3	0.5	46.7	35	60	24.8	58.9
38	0.3	43.5	0.5	46.4	35.5	60	26.7	58.5
39	0.3	43.7	0.5	46.4	36.5	60	27.4	59.5
40	0.3	43.8	0.5	46.8	38	61.5	27.6	59.5
41	0.3	43.7	0.6	46.8	38.5	60.2	28.6	60.5

42	0.3	43.5	0.6	47.1	39	60.3	28.7	60.8
43	0.4	43.3	0.6	47.1	39.6	60.5	29.5	59.5
44	0.4	43.2	0.6	47.2	40	62	30.7	59.8
45	0.4	43.7	0.6	47.7	42	60	31.3	59.8
46	0.4	44.1	0.7	46.8	-	-	32	60.4
47	0.4	44.1	0.7	47.1	-	-	32.4	60.2
48	0.4	44.4	0.7	47.6	-	-	33	60.5
49	0.5	44.4	0.7	47.8	-	-	33	60.8
50	0.5	44.5	0.7	48.1	-	-	35	62.5
51	0.5	44.7	0.8	47.7	-	-	35.5	62.8
52	0.5	45	0.8	47.8	-	-	36	63
53	0.5	46.8	0.9	48.1	-	-	-	-
54	0.5	45.2	0.9	48.4	-	-	-	-
55	0.5	45.2	0.9	48.5	-	-	-	-
56	0.5	45.6	0.9	48.7	-	-	-	-
57	0.6	45.4	1	49	-	-	-	-
58	0.6	45.3	1	49.2	-	-	-	-
59	0.6	45.5	1	49.5	-	-	-	-
60	0.6	45.8	1.1	49.7	-	-	-	-

Table A5: Power & Temperature of 5%, 7.5%, 10% & 15% duty cycle pulsed wave for varying thickness (**Duty cycle study**)

	5%(1.89mm)		7.5% (1.89mm)		10% (5.17mm)		15% (5.17mm)	
Time (Min)	Power (mW)	Temp (C)	Power (mW)	Temp (C)	Power (mW)	Temp (C)	Power (mW)	Temp (C)
1	0.5	35.9	3.3	42.9	0	31.7	0	31.3
2	1.5	39.3	5.2	45.2	0	34	0	32.9
3	2.2	41.9	6.5	49.4	0	35	0	34.1
4	2.8	42.5	6.9	49.9	0	35.7	0	34
5	3.5	44.4	8.5	52.3	0	37	0	34.3
6	4.2	45.2	9.8	52.2	0.1	37.4	0	35.2
7	5.1	46.3	10.3	53.5	0.1	37.2	0	35.5
8	6.1	46.7	12.5	54	0.1	38	0	35.8
9	7.1	47.2	13.9	54.5	0.1	38.4	0	35.9
10	7.8	48	14.5	55	0.1	38.7	0	36
11	9.6	48.8	16	55.5	0.1	39.1	0	36.3
12	11.1	48.2	16.7	54.7	0.1	39	0	37
13	11.9	48.1	17.5	55.8	0.1	39.4	0	36.7
14	13.5	48.9	18.9	55.4	0.1	39.5	0	37
15	14.8	49.2	21.1	55.6	0.1	39.4	0	38
16	16.5	49.8	23.3	55.2	0.1	39.2	0	37.5
17	20	50.2	24.5	55.7	0.1	39.6	0	37.6
18	20.6	50.7	26.2	56.2	0.1	39.8	0	38.1
19	24	50.5	27.6	57	0.1	40	0	37.9
20	26	48.9	28.5	58	0.1	40.2	0	38.5
21	27	49.7	29.5	58.2	0.1	40.3	0	38.3
22	28	49.1	30.6	57.9	0.1	40.2	0	38
23	29.9	50.4	32.1	57.5	0.1	40.3	0.1	38.7
24	31.1	49.5	33.2	57.5	0.1	40.6	0.1	38.9
25	32.2	49.9	34.2	57.2	0.1	40.7	0.1	39.2
26	34	49.7	35.2	57	0.1	41	0.1	39
27	35.2	49.6	37	56.2	0.1	41.2	0.1	39.2
28	36.2	49.8	38	55.1	0.1	41.4	0.1	39.5
29	37.2	50.2	39	55.2	0.1	41.3	0.1	39.5
30	39.2	50.6	40	59.1	0.1	41.3	0.1	40.4
31	-	-	-	-	0.1	41.4	0.1	40.9
32	-	-	-	-	0.2	41.4	0.1	39.8
33	-	-	-	-	0.2	41.5	0.1	40.3
34	-	-	-	-	0.2	41.6	0.1	40.7
35	-	-	-	-	0.2	42.1	0.1	41
36	-	-	-	-	0.2	42.2	0.2	41.3
37	-	-	-	-	0.2	42.3	0.2	41.3
38	-	-	-	-	0.2	42.5	0.2	41.7
39	-	-	-	-	0.2	42.5	0.2	42
40	-	-	-	-	0.2	42.5	0.2	42.3
41	-	-	-	-	0.2	42.6	0.2	42.7

42	-	-	-	-	0.3	42.7	0.2	42.8
43	-	-	-	-	0.3	42.6	0.2	42.2
44	-	-	-	-	0.3	42.9	0.3	42.5
45	-	-	-	-	0.3	43	0.3	42.7
46	-	-	-	-	0.3	43.4	0.3	43.1
47	-	-	-	-	0.3	43.5	0.3	43.6
48	-	-	-	-	0.3	43.5	0.3	43.6
49	-	-	-	-	0.3	43.6	0.3	43.9
50	-	-	-	-	0.3	43.6	0.3	44.5
51	-	-	-	-	0.3	43.8	0.4	44.7
52	-	-	-	-	0.4	43.8	0.4	44.9
53	-	-	-	-	0.4	44	0.4	44.4
54	-	-	-	-	0.4	44.1	0.5	44.1
55	-	-	-	-	0.4	44.3	0.5	44.1
56	-	-	-	-	0.4	44.3	0.5	44.5
57	-	-	-	-	0.4	44.5	0.6	45
58	-	-	-	-	0.4	44.4	0.6	45.1
59	-	-	-	-	0.5	44.7	0.7	45.4
60	-	-	-	-	0.5	44.6	0.7	45.8
61	-	-	-	-	0.5	44.9	0.8	46.6
62	-	-	-	-	0.5	45.1	0.8	47
63	-	-	-	-	0.5	44.8	0.8	47.4
64	-	-	-	-	0.5	45.2	0.9	47.7
65	-	-	-	-	0.5	44.3	1	47.8
66	-	-	-	-	0.5	45.5	1	48.1
67	-	-	-	-	0.6	45.7	1.1	48.6
68	-	-	-	-	0.6	45.9	1.2	47.6
69	-	-	-	-	0.6	46.3	1.3	47.9
70	-	-	-	-	0.6	46.4	1.4	48.4
71	-	-	-	-	0.6	46.5	1.5	48.5
72	-	-	-	-	0.7	46.7	1.6	48.6
73	-	-	-	-	0.7	46.8	1.8	48.8
74	-	-	-	-	0.7	46.9	2	49.1
75	-	-	-	-	0.7	46.6	2.2	49.7
76	-	-	-	-	0.8	46.7	2.4	50.7
77	-	-	-	-	0.8	46.6	2.6	50.5

Table A6: Power & Temperature of 15%, 20% & 25% duty cycle pulsed wave for varying thickness (**Duty cycle study**)

	15%(3.65mm)		20% (3.65mm)		20% (5.35mm)		25% (5.35mm)	
Time (Min)	Power (mW)	Temp (C)	Power (mW)	Temp (C)	Power (mW)	Temp (C)	Power (mW)	Temp (C)
1	0	31.7	0	32	0	29	0	29
2	0	33.4	0	34.6	0	30.5	0	31.1
3	0	34.7	0	35.8	0	31.9	0	32.8
4	0	35.1	0	36.7	0	32.6	0	33.6
5	0	36.4	0	37.6	0	33.5	0	34.1
6	0	36.7	0.1	38.3	0	34	0	34.5
7	0	37.7	0.1	38.7	0	34.5	0	35
8	0.1	37.4	0.1	38.5	0	34.9	0	35.1
9	0.1	38	0.1	38.3	0	35.1	0	35.7
10	0.1	38	0.1	39.3	0	34.1	0	35.5
11	0.1	38.2	0.1	39.2	0	34.7	0	35.6
12	0.1	39	0.1	39.4	0	34.9	0	35.5
13	0.1	38.7	0.1	39.7	0	35.3	0	35.6
14	0.1	39.5	0.1	39.9	0	35.4	0	35.8
15	0.2	39	0.1	40.4	0	35.7	0	35.9
16	0.2	39.9	0.2	40.7	0	35.9	0	36
17	0.2	40.9	0.2	41.2	0	36.2	0	36.2
18	0.3	40.5	0.2	41.6	0	36.2	0	36.5
19	0.3	40.6	0.3	41.8	0	36.6	0	36.4
20	0.3	41.6	0.3	42.4	0	36.6	0	36.4
21	0.3	41	0.3	42.5	0	36.8	0	36.5
22	0.4	41.5	0.3	42.7	0	37	0	36.7
23	0.5	42.4	0.3	43.1	0	37.1	0	36.7
24	0.6	42.6	0.4	42.9	0	37.2	0	36.9
25	0.6	42.6	0.4	43.3	0	37.2	0	36.5
26	0.7	42.8	0.5	43.7	0	36.8	0	36.7
27	0.7	43.3	0.5	44.2	0	36.7	0	36.9
28	0.8	43.8	0.6	44.2	0	36.9	0	36.9
29	0.9	43.6	0.6	44.7	0	37.1	0	37
30	1	44	0.7	45.1	0	37.1	0	37.2
31	1.1	44.5	0.7	45.4	0	37.2	0	37.5
32	1.2	44.6	0.8	46.1	0	37.5	0	37.5
33	1.3	45.7	0.9	46.4	0	37.5	0	37.4
34	1.4	46	1	46.5	0	37.9	0	37.3
35	1.5	45.4	1.1	46.6	0	38	0	37.5

36	1.6	45.7	1.2	46.8	0	38.2	0	37.6
37	1.8	46.5	1.3	47.4	0	38.2	0	37.8
38	1.9	46.4	1.5	48.4	0	38.3	0	37.9
39	2	46.6	1.6	47.6	0	38.4	0	38
40	2.1	47.1	1.8	47.7	0	37.9	0	37.8
41	2.2	47.3	2	48.2	0	37.9	0	37.7
42	2.3	47.8	2.1	48.2	0	38	0	37.5
43	2.4	48.3	2.3	48.9	0	38.2	0	37.7
44	2.6	47.8	2.4	48.7	0	38.6	0	38.1
45	2.8	47.9	2.7	48.9	0	38.6	0	37.9
46	3	48.2	2.8	48.9	0	39	0	38
47	3.3	48.4	3.2	49.3	0	39.1	38.2	0
48	3.6	48.5	3.4	49.9	0	39.2	38.2	0
49	3.7	49.2	3.5	50.6	0	39.2	38.4	0
50	3.9	49.2	3.7	51.1	0	38.9	38.5	0
51	4.1	50.2	4	51.1	0	39.4	38.5	0
52	4.4	50.2	4.3	50.9	0	39.5	38.6	0
53	4.7	50.2	4.6	51	0	39.6	38.5	0
54	4.9	50.7	4.8	50.7	0	39.7	38.7	0
55	5.1	51.6	5	50.8	0	39.1	38.8	0
56	5.5	51.4	5.4	51.6	0	39.4	38.8	0
57	5.6	51.8	5.5	51.1	0	39.2	38.8	0
58	5.9	52.4	5.7	51.5	0.1	39.5	39.2	0
59	6.2	51.2	6.1	51.8	0.1	39.4	39.4	0
60	6.5	51.2	6.3	53	0.1	39.7	39.6	0
61	-	-	-	-	0.1	39.7	39.2	0
62	-	-	-	-	0.1	39.8	39.9	0
63	-	-	-	-	0.1	39.7	40.1	0
64	-	-	-	-	0.1	40	40.1	0
65	-	-	-	-	0.1	40.2	40.1	0
66	-	-	-	-	0.1	40.3	40.2	0
67	-	-	-	-	0.1	40.4	40.2	0
68	-	-	-	-	0.1	40.4	40.5	0
69	-	-	-	-	0.1	40.6	40.1	0.1
70	-	-	-	-	0.1	40.4	40.1	0.1
71	-	-	-	-	0.1	40.4	40.1	0.1
72	-	-	-	-	0.1	40.6	40.4	0.1
73	-	-	-	-	0.1	40.5	40.2	0.1
74	-	-	-	-	0.1	40.5	40.3	0.1
75	-	-	-	-	0.1	40.3	40.3	0.1
76	-	-	-	-	0.1	40.6	40.5	0.1

77	-	-	-	-	0.1	40.7	40.5	0.1
78	-	-	-	-	0.1	40.7	40.6	0.1
79	-	-	-	-	0.1	41	40.6	0.1
80	-	-	-	-	0.1	41.1	40.8	0.1
81	-	-	-	-	0.1	41.1	40.8	0.1
82	-	-	-	-	0.1	41.4	40.9	0.1
83	-	-	-	-	0.1	41.4	40.9	0.1
84	-	-	-	-	0.1	41.6	41.1	0.1
85	-	-	-	-	0.1	41.6	0.1	41.2
86	-	-	-	-	0.1	41.5	0.1	41.4
87	-	-	-	-	0.1	41.4	0.1	41.3
88	-	-	-	-	0.1	41.7	0.1	41.4
89	-	-	-	-	0.1	41.8	0.1	41.4
90	-	-	-	-	0.1	42	0.1	41.5
91	-	-	-	-	0.1	42.2	0.1	41.5
92	-	-	-	-	0.2	42.1	0.1	41.2
93	-	-	-	-	0.2	42.2	0.1	41.5
94	-	-	-	-	0.2	42.2	0.1	41.5
95	-	-	-	-	0.2	42.6	0.1	41.6
96	-	-	-	-	0.2	42.7	0.1	41.7
97	-	-	-	-	0.2	42.5	0.1	41.8
98	-	-	-	-	0.2	42.6	0.1	41.7
99	-	-	-	-	0.2	42.4	0.1	41.5
100	-	-	-	-	0.2	42.8	0.2	42.1
101	-	-	-	-	0.2	42.6	0.2	42.2
102	-	-	-	-	0.2	42.5	0.2	42.3
103	-	-	-	-	0.2	42.6	0.2	42.1
104	-	-	-	-	0.2	42.9	0.2	42.4
105	-	-	-	-	0.2	43.1	0.2	42.6
106	-	-	-	-	0.2	43.1	0.2	42.6
107	-	-	-	-	0.2	43.1	0.2	42.8
108	-	-	-	-	0.2	43.2	0.2	42.6
109	-	-	-	-	0.3	43.4	0.2	42.8
110	-	-	-	-	0.3	43.3	0.2	42.9
111	-	-	-	-	0.3	43.2	0.2	42.9
112	-	-	-	-	0.3	43.2	0.2	42.8
113	-	-	-	-	0.3	43.2	0.2	43
114	-	-	-	-	0.3	43.5	0.2	43
115	-	-	-	-	0.3	43.7	0.3	42.9
116	-	-	-	-	0.3	43.9	0.3	43
117	-	-	-	-	0.3	43.9	0.3	43.2

118	-	-	-	-	0.3	44	0.3	43.3
119	-	-	-	-	0.3	44.1	0.3	43.5
120	-	-	-	-	0.3	44.5	0.3	43.7
121	-	-	-	-	0.4	44.4	0.3	43.5
122	-	-	-	-	0.4	44	0.3	43.7
123	-	-	-	-	0.4	44.2	0.3	44.1
124	-	-	-	-	0.4	44.5	0.3	43.9
125	-	-	-	-	0.4	44.7	0.4	44.1
126	-	-	-	-	0.4	44.7	0.4	44.4
127	-	-	-	-	0.4	44.6	0.4	44.7
128	-	-	-	-	0.4	44.4	0.4	44.8
129	-	-	-	-	0.5	44.7	0.4	45
130	-	-	-	-	0.5	44.7	0.4	44.8

Table A7: Power & Temperature characteristic of skin of varying thickness **(Skin Thickness study)**

	2.81 mm skin		3.55 mm skin				
Time (min)	Power (mW)	Temp (ºC)	Power (mW)	Temp (ºC)	Time (min)	Power (mW)	Temp (ºC)
1	0.2	32.2	0.2	34.9	44	4.3	53.6
2	0.5	33	0.2	34.9	45	4.5	54
3	0.7	35	0.2	35.4	46	4.5	54.2
4	1.6	38	0.2	37.2	47	4.7	54.7
5	3.9	40.8	0.3	39.5	48	5	55
6	3.7	42	0.3	39.3	49	5.6	55.1
7	5	42.8	0.3	40.1	50	6.5	54.4
8	5.6	43.3	0.5	40.3	51	5.8	54.1
9	6.8	43.5	0.6	41.6	52	6.8	55.5
10	6.5	43.5	0.6	41.7	53	7.3	55.7
11	8.8	43.3	0.7	42	54	8.1	54.5
12	9.3	45	0.9	43	55	7	54.8
13	10	44.4	1	44.8	56	7.7	55.1
14	10.4	44.8	0.8	45.4	57	7	56.5
15	8.8	45	1	46.6	58	8.1	57
16	8.2	45.5	1.1	46.7	59	8.1	57.1
17	11.3	46	1.1	46.6	60	8.4	56.9
18	12.5	46.8	1.1	46.4	61	8.8	56.8
19	13.2	47.4	1.2	47	62	8.8	57.3
20	13.5	46.9	1.1	46.9	63	9	57.5
21	14	46.9	1.7	48.2	64	9.3	58
22	14.5	47.2	1.8	48.3	65	10	57.8
23	15	47.2	1.8	49.6	66	9.1	58.5
24	15.8	47.2	1.8	49.6	67	12	58.8
25	16.2	47.9	1.8	49.5	68	12.5	59.7
26	16.6	48.4	1.6	50.2	69	12.2	60.2
27	18.1	47.9	2.1	50.2	70	12.5	60.3
28	20.9	48	2.3	50.2	71	13.7	60
29	16.5	48	2	50.3	72	13.4	60.7
30	20.1	48.5	2.2	50.7	73	16.5	60
31	21.2	48.2	2	51.2	74	16.4	60
32	24.7	48	2.9	51.5	75	16.7	61.5
33	27.2	47.9	3	51.6	76	16.5	61.4
34	27.7	48.4	2	51.8	77	17.6	61.7
35	27	49.2	2.9	52	78	19	61.4

36	33.5	50.1	3.3	52.4	79	19	62
37	33.1	48	3.4	52.6	80	20.2	63
38	34.8	49	3.9	52.7	81	20.7	62.9
39	37.3	49	4.2	53.2	82	21	63
40	40	48.6	3.7	53.4	83	22	63
41	-	-	4.1	54	84	23	63
42	-	-	4.5	54	85	23.5	63.4
43	-	-	4.8	54	79	19	62

Laser diode

MODEL	QFLD-1440-200S
PART NUMBER	FTAOZG1F09

Parameter	Value	Units
Internal Temperature	25	°C
Thermistor Resistance	10.0	kΩ
Optical Output Power	201	mW
Threshold Current	48	mA
Operating Current	682	mA
Operating Voltage	1.67	V
Monitor Current	0.3	mA
Monitor Dark Current	0	nA
Center Wavelength	1444.5	nm
Spectral Width	6.77	nm

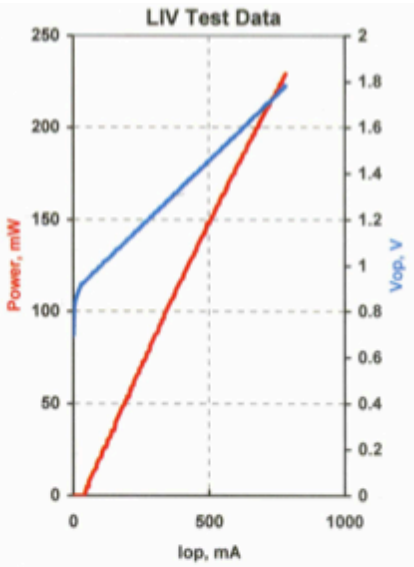

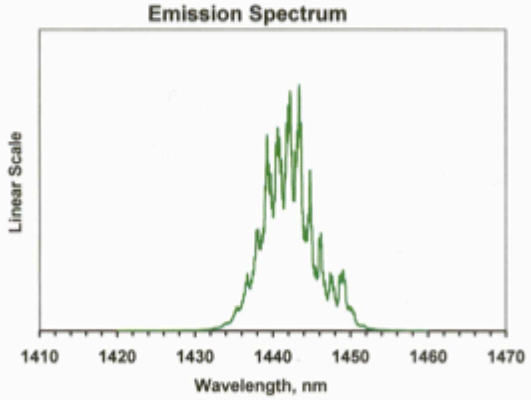

Fiber Type	SMF28
NA	0.13
Connector	FC/PC

Pin	Connection
1	TE Cooler (+)
2	Thermistor
3	PD Anode (-)
4	PD Cathode (+)
5	Thermistor
10	LD Anode (+)
11	LD Cathode (-)
14	TE Cooler (-)

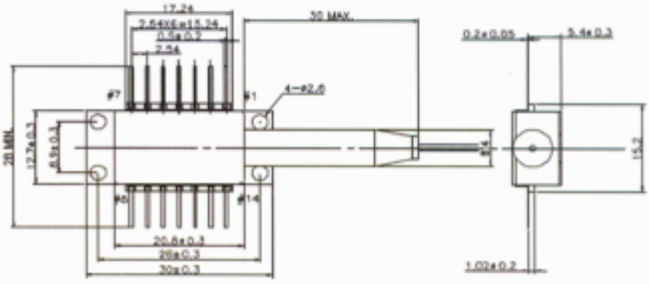

Spec Sheet: S122B Germanium Power Meter Optical Head

Description:

The S122B is an optical power meter head designed to be used directly with the ThorLabs PM100 and PM30 console system to measure light over the visible and near infrared wavelength range of 700 to 1800nm and provide a NIST traceable optical power measurement. The optical power meter head will detect light over the power range of 35nW to 35mW. An EPROM located in the DB9 mating connector will store the NIST calibrated spectral response curve required to provide an accurate power reading.

The S122B housing includes a threaded input that is compatible with any number of ThorLabs 1" threaded accessories. This allows convenient mounting of external optics, fiber adapters, light filters, and apertures. A 8-32 threaded mounting hole is provided to accommodate posts and post holders (an M4 adapter is included).

The removable annular IR viewing target allows conveniently centering the measured beam to the active area of the photo-diode. The target works from 400 to 640nm and 800 to 1700nm.

Specifications:

Spectra Range:	700 – 1800nm	Optical Power Range:	35nW – 35mW (@1550nm)
Sensor:	Germanium	Resolution:	1nW
Sensor Size:	10mm x 10mm sq. (0.39" x 0.39")	Measurement Standard:	NIST Traceable
		Measurement Uncertainty:	+/- 5%
Input Aperture:	9.5mm Diameter (0.374")	Operating Temperature:	5°C to 40°C
Distance to ND Filter:	1.5mm (0.060")	Storage Temperature:	-10°C to 70°C
Distance to Detector:	4.5mm (0.175")	Damage Threshold:	50W/cm²

Cleaning and Maintenance:

There are no serviceable parts in the S122B optical head. The housing may be cleaned by wiping with a soft damp cloth. When cleaning the aperture filter of the S122B, treat it as any other fine optic. Gently blow off any debris using compressed air and wipe gently with an optic tissue wetted with propanol. If you suspect a problem with your S122B please call ThorLabs and an engineer will be happy to assist you.

As long as the sensor has not been exposed to excessive optical power, the calibration should be very stable over long periods of time (well over a year). However, the detector should be calibrated once a year to ensure accuracy.

Console - Sensor Compatibility:

PM100:	Compatible from firmware version 1.62 (September 2005) Please contact ThorLabs for a free upgrade of the console firmware.
PM30:	Compatible
PM300:	Compatible
S100:	Not compatible, no upgrade possible

INFORMATION ONLY, NOT FOR MANUFACTURING

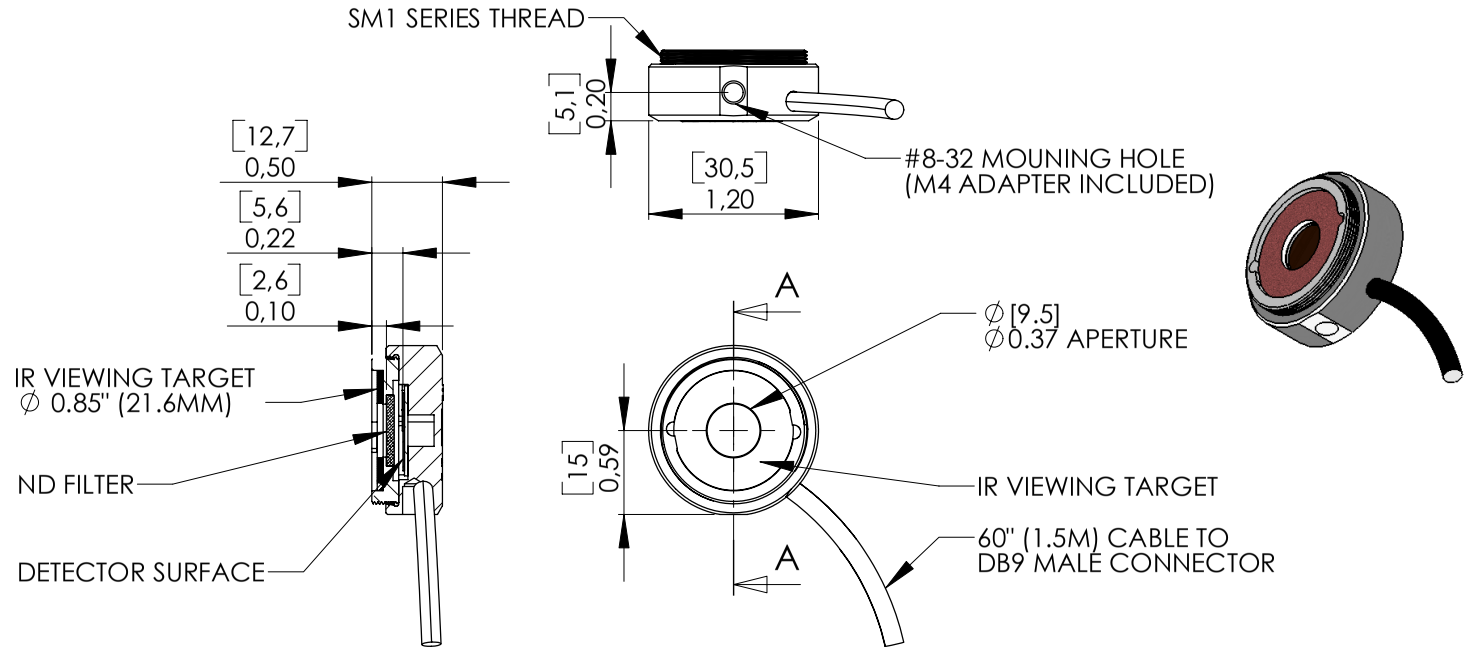

SECTION A-A

ALL DIMENSIONS IN PARANTHESES ARE MILLIMETERS

UNLESS OTHERWISE SPECIFIED: DIMENSIONS ARE IN INCHES TOLERANCES LINEAR: ±0.005 ANGULAR: ±30'	DEBUR AND BREAK SHARP EDGES	THORLABS Karlsfeld Germany
NAME / DATE: DRAWN Go 04/16/06; CHK'D Go 04/16/06; APPV'D Go 04/16/06	MATERIAL: N/A	TITLE: OPTICAL POWER METER HEAD
NO PART OF THIS DRAWING MAY BE REPRODUCED OR TRANSMITTED IN ANY FORM OR BY ANY MEANS INCLUDING PHOTOCOPYING OR RECORDING WITHOUT THE PRIOR WRITTEN PERMISSION OF THORLABS GMBH	FINISH / TREATMENT: N/A	PART NO. S120B, S121B, S122B REV B
© THORLABS GMBH		DWG NO. 13336-E01 SIZE A4
	DO NOT SCALE DRAWING	SCALE: 1:1 SHEET 1 OF 1

Infrared camera- A20M

ThermoVision™ A20M Technical Specifications

Imaging Performance	
Field of view/min focus distance	25° x 19° / 0.3 m
Detector type	Focal plane array (FPA) uncooled microbolometer
Spectral range	7.5 to 13 µm
Spatial resolution (IFOV)	2.7 mrad
Thermal sensitivity @ 50/60Hz	0.12° C at 30° C
Focusing	Manual, external motor focus optional
Image Presentation	
FireWire/Ethernet output	8/16-bit monochrome and 8-bit color
Video output	RS170 EIA/NTSC or CCIR/PAL composite video
Measurement	
Temperature ranges	Range 1: -20° C to +250° C (-4 to +482° F) Optional: +120° C to +900° C (+248 to +1652° F)
Accuracy (% of reading)	± 2°C or ± 2%
Measurement modes	Spot, Area, Difference
Automatic emissivity correction	Variable from 0.1 to 1.0
Individual emissivity settings	Individually settable
Measurement corrections	Reflected ambient, distance, relative humidity, external optics. Automatic, based on user input
Supplementary Lenses*	
Field of view/min. focus distance	12° Telescope (12° x 9°/1.2m) 45° Wide angle (45° x 34°/0.1m)
Lens recognition	Automatic lens recognition and measurement corrections

Power Source	
AC operation	AC adapter 110/220 VAC, 50/60Hz (included)
DC operation	12/24V nominal, <6W
Environmental	
Operating temperature range	-15°C to +50°C (5°F to 122°F)
Storage temperature range	-40°C to +70°C (-40°F to 158°F)
Humidity	Operating and storage 10% to 95%, non-condensing
Encapsulation	IP 40 (Determined by connector type)
Shock	Operational: 25G, IEC 68-2-29
Vibration	Operational: 2G, IEC 68-2-6
Physical Characteristics	
Weight	0.8 kg (1.7 lbs)
Size	157mm x 75mm x 80mm (6.2" x 2.9" x 3.1")
Tripod mounting	1/4"– 20

User Configuration Table

TYPE	FUNCTION	REMARK
Digital Input	TTL level • Shutter disable • Store image • Batch enable	Isolation and relay function in external module
Digital Output	TTL level • Spot/Area threshold ALARM • Internal temperature sensor ALARM • V-sync	Isolation and relay function in external module
Analog Output	• Spot/Area out: 0-5V • Internal temperature sensor out: 0-5V	Scaled to T_{low} - T_{high} Isolation in external module
Analog Input	• External temperature sensor out: 0-5V	Scaled to T_{low} - T_{high} Isolation in external module

CAMERA INTERFACES

Digital I/O ports—jackable screw terminal
3 output/1 input, 1 input/output selectable; function is user configurable*

Analog I/O ports—jackable screw terminal
2 output/1 input; function is user configurable*

RS-232 (DB-9)—connection to PC
Camera control

DC power in—2-pin jackable screw terminal
12/24V nominal

*See Configuration Table above

8-button keyboard

Ethernet jack (RJ45) or FireWire jack (IEEE-1394)

BNC—C-Video (NTSC/PAL)

2.5 mm DC power in
12/24V Nominal; camera needs only one power source

AFG3000 Series Characteristics

Characteristic	AFG3011	AFG3021B AFG3022B	AFG3101 AFG3102	AFG3251 AFG3252
Channels	1	1 / 2	1 / 2	1 / 2
Waveforms	Sine, Square, Pulse, Ramp, Triangle, Sin(x)/x, Exponential Rise and Decay, Gaussian, Lorentz, Haversine, DC, Noise			
Sine Wave	1 µHz to 10 MHz	1 µHz to 25 MHz	1 µHz to 100 MHz	1 µHz to 240 MHz
Sine wave in Burst Mode	1 µHz to 5 MHz	1 µHz to 12.5 MHz	1 µHz to 50 MHz	1 µHz to 120 MHz
Effective maximum frequency out	10 MHz	25 MHz	100 MHz	240 MHz
Amplitude Flatness (1 V_{pp})				
<5 MHz	±0.15 dB	±0.15 dB	±0.15 dB	±0.15 dB
5 MHz to 10 MHz	±0.3 dB	—	—	—
5 MHz to 20 MHz	—	±0.3 dB	±0.3 dB	±0.3 dB
20 MHz to 25 MHz	—	±0.5 dB	±0.3 dB	±0.3 dB
25 MHz to 100 MHz	—	—	±0.5 dB	±0.5 dB
100 MHz to 200 MHz	—	—	—	±1.0 dB
200 MHz to 240 MHz	—	—	—	±2.0 dB
Harmonic Distortion (1 V_{pp})				
10 Hz to 20 kHz	< -60 dBc	< -70 dBc	< -60 dBc	< -60 dBc
20 kHz to 1 MHz	< -55 dBc	< -60 dBc	< -60 dBc	< -60 dBc
1 MHz to 5 MHz	< -45 dBc	< -50 dBc	< -50 dBc	< -50 dBc
5 MHz to 10 MHz	< -45 dBc	< -50 dBc	< -37 dBc	< -37 dBc
10 MHz to 25 MHz	—	< -40 dBc	< -37 dBc	< -37 dBc
>25 MHz	—	—	< -37 dBc	< -30 dBc
THD	<0.2% (10 Hz – 20 kHz, 1 V_{pp})			
Spurious (1 V_{pp})				
10 Hz to 1 MHz	< -60 dBc	< -60 dBc	< -60 dBc	< -50 dBc
1 MHz to 10 MHz	< -50 dBc	—	—	—
1 MHz to 25 MHz	—	< -50 dBc	< -50 dBc	< -47 dBc
>25 MHz	—	—	< -50 dBc + 6 dBc/octave	< -47 dBc + 6 dBc/octave
Phase noise, typical	< -110 dBc/Hz at 10 MHz, 10 kHz offset, 1 V_{pp}	< -110 dBc/Hz at 20 MHz, 10 kHz offset, 1 V_{pp}		
Residual clock noise	-63 dBm	-63 dBm	-57 dBm	-57 dBm
Square Wave	1 µHz to 5 MHz	1 µHz to 12.5 MHz	1 µHz to 50 MHz	1 µHz to 120 MHz
Rise/Fall time	≤50 ns	≤18 ns	≤5 ns	≤2.5 ns
Jitter (RMS), typical	500 ps	500 ps	200 ps	100 ps
Ramp Wave	1 µHz to 100 kHz	1 µHz to 250 kHz	1 µHz to 1 MHz	1 µHz to 2.4 MHz
Linearity, typical	≤0.2% of peak output	≤0.1% of peak output	≤0.15% of peak output	≤0.2% of peak output
Symmetry	0.0% to 100.0%		0.0% to 100.0%	
Pulse Wave	1 mHz to 5 MHz	1 mHz to 12.5 MHz	1 mHz to 50 MHz	1 mHz to 120 MHz
Pulse width	80.00 ns to 999.99 s	30.00 ns to 999.99 s	8.00 ns to 999.99 s	4.00 ns to 999.99 s
Resolution	10 ps or 5 digits			
Pulse duty	0.001% to 99.999% (Limitations of pulse width apply)			
Edge transition time	50 ns to 625 s	18 ns to 625 s	5 ns to 625 s	2.5 ns to 625 s
Resolution	10 ps or 4 digits		10 ps or 4 digits	
Lead delay				
Range	(Continuous Mode): 0 ps to Period (Triggered/Gated Burst Mode): 0 ps to Period – [Pulse Width + 0.8 * (Leading Edge Time + Trailing Edge Time)]			
Resolution	10 ps or 8 digits			
Overshoot, typical	<5%			
Jitter (RMS), typical	500 ps	500 ps	200 ps	100 ps

Characteristic	AFG3011	AFG3021B AFG3022B	AFG3101 AFG3102	AFG3251 AFG3252
Other Waveforms	1 µHz to 100 kHz	1 µHz to 250 kHz	1 µHz to 1 MHz	1 µHz to 2.4 MHz
Noise Bandwidth (-3 dB)	10 MHz	25 MHz	100 MHz	240 MHz
Noise type	White Gaussian			
DC (into 50 Ω)	-10 V to +10 V	-5 V to +5 V	-5 V to +5 V	-2.5 V to +2.5 V
Arbitrary Waveforms	1 mHz to 5 MHz	1 mHz to 12.5 MHz	1 mHz to 50 MHz	1 mHz to 120 MHz
Arbitrary waveforms in Burst Mode	1 mHz to 2.5 MHz	1 mHz to 6.25 MHz	1 mHz to 25 MHz	1 mHz to 60 MHz
Effective analog bandwidth (-3 dB)	8 MHz	34 MHz	100 MHz	225 MHz
Nonvolatile memory	4 waveforms	4 waveforms	4 waveforms	4 waveforms
Memory: Sample rate	2 to 128 K: 250 MS/s	2 to 128 K: 250 MS/s	>16 K to 128 K: 250 MS/s 2 to 16 K: 1 GS/s	>16 K to 128 K: 250 MS/s 2 to 16 K: 2 GS/s
Vertical resolution	14 bits	14 bits	14 bits	14 bits
Rise/Fall time	≤80 ns	≤20 ns	≤8 ns	≤3 ns
Jitter (RMS)	4 ns	4 ns	1 ns at 1 GS/s 4 ns at 250 MS/s	500 ps at 2 GS/s 4 ns at 250 MS/s
Amplitude, 50 Ω Load	20 mV_{p-p} to 20 V_{p-p}	10 mV_{p-p} to 10 V_{p-p}	20 mV_{p-p} to 10 V_{p-p}	≤200 MHz: 50 mV_{p-p} to 5 V_{p-p} >200 MHz: 50 mV_{p-p} to 4 V_{p-p}
Amplitude, Open Circuit	40 mV_{p-p} to 40 V_{p-p}	20 mV_{p-p} to 20 V_{p-p}	40 mV_{p-p} to 20 V_{p-p}	≤200 MHz: 100 mV_{p-p} to 10 V_{p-p} >200 MHz: 100 mV_{p-p} to 8 V_{p-p}
Accuracy	±(2% of setting +2 mV) (1 kHz sine wave, 0 V offset, >20 mV_{p-p} amplitude)	±(1% of setting +1 mV) (1 kHz sine wave, 0 V offset, >10 mV_{p-p} amplitude)		
Resolution	0.1 mV_{p-p}, 0.1 mV_{rms}, 1 mV, 0.1 dBm or 4 digits			
Units	V_{p-p}, V_{rms}, dBm (sine wave only)			
Output impedance	50 Ω			
Load impedance setting	Selectable: 50 Ω, 1Ω to 10.0 kΩ, High Z (Adjusts displayed amplitude according to selected load impedance)			
Isolation	42 V_{pk} maximum to earth			
Short-circuit protection	Signal outputs are robust against permanent shorts against floating ground			
External voltage protection	To protect signal outputs against external voltages use fuse adapter 013-0345-xx			
DC offset range, 50 Ω load	±(10 V_{pk} – Amplitude$_{p-p}$/2)	±(5 V_{pk} – Amplitude$_{p-p}$/2)	±5 V_{pk} DC	±2.5 V_{pk} DC
DC offset range, open circuit	±(20 V_{pk} – Amplitude$_{p-p}$/2)	±(10 V_{pk} – Amplitude$_{p-p}$/2)	±10 V_{pk} DC	±5 V_{pk} DC
Accuracy	±(2% of |setting| + 10 mV + 1% of amplitude (V_{p-p}))	±(1% of |setting| + 5 mV + 0.5% of amplitude (V_{p-p}))		
Resolution	1 mV			

Modulation

AM, FM, PM

Characteristic	Description
Carrier Waveforms	All, except Pulse, Noise, and DC
Source	Internal/External
Internal Modulating Waveform	Sine, square, ramp, noise, ARB (AM: maximum waveform length 4,096; FM/PM: maximum waveform length 2,048)
Internal Modulating Frequency	2 mHz to 50.00 kHz
AM Modulation Depth	0.0% to +120.0%
Min FM Peak Deviation	DC
Max FM Peak Deviation	See chart, below

Modulation: Max FM Peak Deviation

Characteristic	AFG3011	AFG3021B AFG3022B	AFG3101 AFG3102	AFG3251 AFG3252
Sine	5 MHz	12.5 MHz	50 MHz	120 MHz
Square	2.5 MHz	6.25 MHz	25 MHz	60 MHz
ARB	2.5 MHz	6.25 MHz	25 MHz	60 MHz
Others	50 kHz	125 kHz	500 kHz	1.2 MHz

PM Phase Deviation – 0.0° to +180.0°

Frequency Shift Keying

Characteristic	Description
Carrier Waveforms	All, except Pulse, Noise, and DC
Source	Internal/External
Internal Modulating Frequency	2 mHz to 1.000 MHz
Number of Keys	2

Pulse Width Modulation

Characteristic	Description
Carrier Waveform	Pulse
Source	Internal/External
Internal Modulating Waveform	Sine, square, ramp, noise, ARB (maximum waveform length 2,048)
Internal Modulating Frequency	2 mHz to 50.00 kHz
Deviation	0% to 50.0% of pulse period

Sweep

Characteristic	Description
Waveforms	All, except Pulse, Noise, and DC
Type	Linear, logarithmic
Sweep Time	1 ms to 300 s
Hold/Return Time	0 ms to 300 s
Max Total Sweep Time	300 s
Resolution	1 ms or 4 digits
Total Sweep Time Accuracy, typical	≤0.4%
Min Start/Stop Frequency	All except ARB: 1 µHz ARB: 1 mHz
Max Start/Stop Frequency	See chart, below

Sweep: Max Start/Stop Frequency

Characteristic	AFG3011	AFG3021B AFG3022B	AFG3101 AFG3102	AFG3251 AFG3252
Sine	10 MHz	25 MHz	100 MHz	240 MHz
Square	5 MHz	12.5 MHz	50 MHz	120 MHz
ARB	5 MHz	12.5 MHz	50 MHz	120 MHz
Others	100 kHz	250 kHz	1 MHz	2.4 MHz

Burst

Characteristic	Description
Waveforms	All, except Noise and DC
Type	Triggered, gated (1 to 1,000,000 cycles or Infinite)
Internal Trigger Rate	1 µs to 500.0 s
Gate and Trigger Sources	Internal, external, remote interface

Auxiliary Inputs

Characteristic	Description
Modulation Inputs Channel 1, Channel 2	
Input range	All except FSK: ±1 V FSK: 3.3 V logic level
Impedance	10 kΩ
Frequency range	DC to 25 kHz (122 kS/s)
External Triggered/Gated Burst Input	
Level	TTL compatible
Impedance	10 kΩ
Pulse width	100 ns minimum
Slope	Positive/Negative, selectable
Trigger delay	0.0 ns to 85.000 s
Resolution	100 ps or 5 digits
Jitter (RMS), typical	Burst: <500 ps (Trigger input to signal output)
10 MHz Reference Input	
Impedance	1 kΩ, AC coupled
Required Input Voltage Swing	100 mV_{p-p} to 5 V_{p-p}
Lock Range	10 MHz ±35 kHz
External Channel 1 Add Input	AFG3101, AFG3102, AFG3251, AFG3252 only
Impedance	50 Ω
Input range	-1 V to +1 V (DC + peak AC)
Bandwidth	DC to 10 MHz (-3 dB) at 1 V_{p-p}

Auxiliary Outputs

Characteristic	Description
Channel 1 Trigger Output	
Level	Positive TTL level pulse into 1 kΩ
Impedance	50 Ω
Jitter (RMS), typical	AFG3011/21B/22B: 500 ps AFG3101/02: 200 ps AFG3251/52: 100 ps
Max Frequency	4.9 MHz (4.9 MHz to 50 MHz: A fraction of the frequency is output; >50 MHz: no signal is output)
10 MHz Reference Out	AFG3101, AFG3102, AFG3251, AFG3252 only
Impedance	50 Ω, AC coupled
Amplitude	1.2 V_{p-p} into 50 Ω load

Common Characteristics

Characteristic	Description		
Frequency Setting Resolution	1 µHz or 12 digits		
Phase (except DC, Noise, Pulse)			
Range	-180° to +180°		
Resolution	0.01° (sine), 0.1° (other waveforms)		
Internal Noise Add	When activated, output signal amplitude is reduced to 50%		
Level	0.0% to 50% of amplitude (V_{p-p}) setting		
Resolution	1%		
Main Output	50 Ω		
Effective Frequency Switching Speed	2 ms using remote control (sequencing not available)		
Internal Frequency Reference			
Stability	All except ARB: ±1 ppm, 0 °C to 50 °C ARB: ±1 ppm ± 1 µHz, 0 °C to 50 °C		
Aging	±1 ppm per year		
Remote Programming	GPIB, LAN 10BASE-T / 100BASE-TX, USB 1.1 Compatible with SCPI-1999.0 and IEEE 488-2 standards		
Configuration times, typical	**USB**	**LAN**	**GPIB**
Function change	95 ms	103 ms	84 ms
Frequency change	2 ms	19 ms	2 ms
Amplitude change	60 ms	67 ms	52 ms
Select user ARB	88 ms	120 ms	100 ms
Data download time for 4000 point waveform data, typical	20 ms	84 ms	42 ms
Power Source	100 to 240 V, 47 to 63 Hz, or 115 V, 360 to 440 Hz		
Power Consumption	Less than 120 W		
Warm-up Time, typical	20 minutes		
Power-on Self Calibration, typical	<16 s		
Acoustic Noise, typical	<50 dBA		
Display	AFG3021B: 5.6 in. Monochrome LCD All others: 5.6 in. Color LCD		
User Interface and Help Language	English, French, German, Japanese, Korean, Simplified and Traditional Chinese, Russian (user selectable)		

Physical Characteristics

Benchtop Configuration

Dimensions	mm	in.
Height	156.3	6.2
Width	329.6	13.0
Depth	168.0	6.6
Weight	**kg**	**lb.**
Net	4.5	9.9
Shipping	5.9	12.9

Environmental and Safety Characteristics

Characteristic	Description
Temperature	
Operating	0 °C to +50 °C
Nonoperating	-30 °C to +70 °C
Humidity	
Operating	≤ +40 °C: ≤80% > +40 °C to 50 °C: ≤60%
Altitude	Up to 10,000 ft./3,000 m
EMC Compliance	
European Union	EN 61326:1997 Class A EN 61000-3-2:2000, and EN 61000-3-3:1995 IEC 61000-4-2:1999, -4-3:2002, -4-4:2004, -4-5:2005, -4-6:2003, -4-11:2004
Australia	EN 61326:1997
Safety	UL 61010-1:2004 CAN/CSA C22.2 No. 61010-1:2004 IEC 61010-1:2001

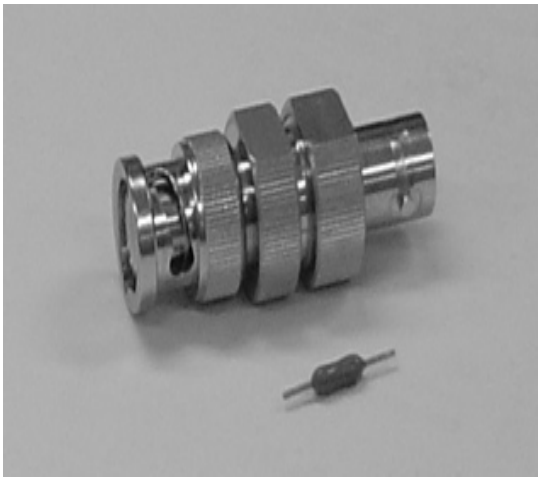

BNC Fuse Adapter and 0.125 A Fuse

Ordering Information

AFG3011, AFG3021B, AFG3022B, AFG3101, AFG3102, AFG3251, AFG3252

Arbitrary/Function Generator

Includes: Quick-start user manual, power cord, USB cable, CD-ROM with programmer manual, service manual, LabView and IVI drivers, CD-ROM with ArbExpress™ software, and NIST-traceable calibration certificate. Please specify power plug when ordering.

International Power Plugs

Option	Description
Opt. A0	North America power
Opt. A1	Universal EURO power
Opt. A2	United Kingdom power
Opt. A3	Australia power
Opt. A5	Switzerland power
Opt. A6	Japan power
Opt. A10	China power
Opt. A11	India power
Opt. A99	No power cord or AC adapter

Note: Includes front-panel overlay.

Manual Options

Option	Description
Opt. L0	English (071-1631-xx)
Opt. L1	French (071-1632-xx)
Opt. L2	Italian (071-1669-xx)
Opt. L3	German (071-1633-xx)
Opt. L4	Spanish (071-1670-xx)
Opt. L5	Japanese (071-1634-xx)
Opt. L7	Simple Chinese (071-1635-xx)
Opt. L8	Traditional Chinese (071-1636-xx)
Opt. L9	Korean (071-1637-xx)
Opt. L10	Russian (071-1638-xx)
Opt. L99	No manual

Service

Option	Description
Opt. C3	Calibration Service 3 Years
Opt. C5	Calibration Service 5 Years
Opt. CA1	Single calibration event or coverage for the designated calibration interval, whichever comes first
Opt. D1	Calibration Data Report
Opt. D3	Calibration Data Report 3 Years (with Opt. C3)
Opt. D5	Calibration Data Report 5 Years (with Opt. C5)
Opt. R5	Repair Service 5 Years

Warranty

Three-year warranty on parts and labor.

Recommended Accessories

Accessory	Description
Rackmount Kit	RM3100
Fuse adapter, BNC-P to BNC-R	013-0345-xx
Fuse set, 3 pcs, 0.125 A.	159-0454-xx
BNC cable shielded, 3 ft.	012-0482-xx
BNC cable shielded, 9 ft.	012-1256-xx
GPIB cable, double shielded	012-0991-xx

Temperature control Output

Load resistance	> 10 kΩ
Output voltage	0 ... ± 10 V
Transmission coefficient IC sensors	50 mV / °C ± 5%
Transmission coeff. thermistor (20 kΩ / 200 kΩ range)	500 mV/ kΩ / 50 mV/kΩ ± 5%

Temperature window protection

Setting range T_{WIN}	0.5 °C ... 20 °C
Setting range R_{WIN} (20 kΩ / 200 kΩ range)	50 Ω ... 2 kΩ / 500 Ω ... 20 kΩ

Computer Interface

Setting resolution	16 Bit
Measurement resolution	12 ... 18 Bit [1)]

1.5.2 Technical data ITC510

General Data

Line voltage	100 V / 115 V / 230 V (-10%, +15 %) (fixed)
Line frequency	50 ... 60 Hz
Max. power consumption	150 VA
Supply mains overvoltage	Overvoltage category II (Cat II)
Operating temperature [2]	0 ... +40°C
Storage temperature	-40°C ... +70°C
Relative Humidity	Max. 80% up to 31°C, decreasing to 50% at 40 °C
Operation altitude	< 3000 m
Pollution Degree (indoor use only)	2
Warm up time for rated accuracy	≤ 10 min
Weight	< 7 kg
Dimensions	220 x 120 x 377 mm^3

Current control

Range of laser current I_{LD}	0 ... ± 1 A
Compliance voltage	> 6 V
Setting resolution (manual / remote control)	100 µA / 15 µA
Measurement resolution (manual / remote control)	100 µA / 10 µA
Accuracy	± 1 mA
Noise without ripple (10 Hz ... 10 MHz, rms, typ.)	< 5 µA
Ripple (50/60 Hz, rms, typ.)	< 3 µA
Transients (typ.)	< 1 mA
Drift (24 hours, 0…10Hz, at constant ambient temperature, typ.)	< 30 µA
Temperature coefficient	≤ 50 ppm/°C

Power control

Range of monitor current I_{PD}	5 µA ... 2 mA [1)]
Setting resolution (manual / remote control)	0.1 µA / 0.03 µA
Measurement resolution (manual / remote control)	0.1 µA / 0.01 µA
Accuracy	± 2 µA
Photodiode bias voltage	0 ... 10 V

Laser voltage

Measurement principle	4-wire
Measurement range	0 ... 10 V
Measurement resolution (manual / remote control)	1 mV / 0.1 mV
Accuracy	± 20 mV

Analog control output

Load resistance	≥ 10 kΩ
Output voltage for 0 ... $I_{LD\ MAX}$	0 ... ± 10 V [2)]
Transmission coefficient	10 V/A ± 5%

LD Current limit

Setting range I_{LIM}	0 ... ≥ 1 A
Measurement resolution (manual / remote control)	100 µA / 10 µA
Accuracy	± 2.5 mA

Analog modulation input

Input impedance	10 kΩ
Small signal 3 dB bandwidth (CC mode)	DC ... 200 kHz
Laser diode modulation coefficient (CC mode)	100 mA/V ± 5%
Laser diode modulation coefficient (CP mode)	0.2 mA/V ± 5%

Current output TEC element

Control range	- 4 A ... + 4 A
Maximum output power	32 W
Compliance voltage	> 8 V
Measurement resolution (manual / remote control)	1 mA / 0.1 mA
Measurement accuracy	± 20 mA
Noise and ripple (typ.)	< 2 mA
Measurement resolution TEC voltage (manual / remote control)	1 mV / 0.1 mV
Measurement accuracy TEC voltage	± 40 mV

TEC Current limit

Setting range	0 ... ≥ 4 A
Measurement resolution (manual / remote control)	1 mA / 0.1 mA
Accuracy	± 40 mA

Temperature sensors AD590, AD592, LM135, LM335

Control range (AD590, LM135)	- 45 °C ... + 145 °C
Control range (AD592)	- 25 °C ... + 105 °C
Control range (LM335)	- 40 °C ... + 100 °C
Setting resolution (manual / remote control)	0.01 °C / 0.003 °C
Measurement resolution (manual / remote control)	0.01 °C / 0.001 °C
Accuracy	± 0.1 °C
Temperature stability (24 hours)	≤ 0.001 °C

Thermistor (2 kΩ / 20 kΩ range)

Measurement current	100µA / 10 µA
Control range	10 Ω ... 19.99 kΩ / 100 Ω ... 199.9 kΩ
Setting resolution (manual control)	1 Ω / 10 Ω
Setting resolution (remote control)	0.3 Ω / 3 Ω
Measurement resolution (manual control)	1 Ω / 10 Ω
Measurement resolution (remote control)	0.1 Ω / 1 Ω
Accuracy	± 5 Ω / ± 50 Ω
Temperature stability (24 hours) [1)]	≤ 0.5 Ω / ≤ 5 Ω

Temperature control input

Input resistance	10 kΩ
Control voltage	-10 ... +10 V
Transmission coefficient IC-sensors	2 °C/V ±5%
Transmission coefficient thermistor (20 kΩ / 200 kΩ range)	0.2 kΩ/V / 2 kΩ/V ±5%

Temperature control Output

Load resistance	> 10 kΩ
Output voltage	0 ... ± 10 V
Transmission coefficient thermistor	500 mV/ kΩ / 50 mV/kΩ ± 5%
Transmission coefficient IC sensors	50 mV / °C ± 5%

Temperature window protection

Setting range T_{WIN}	0.5 °C ... 20 °C
Setting range R_{WIN} (20 kΩ / 200 kΩ range)	50 Ω ... 2 kΩ / 500 Ω ... 20 kΩ

Computer Interface

Setting resolution	16 Bit
Measurement resolution	12 ... 18 Bit [2)]

[1)] Due to the nonlinear conversion from Ω to °C the stability in °C depends on the operating conditions and the characteristics of the thermistor. E.g. for a typical thermistor at a set point of 10kΩ (25°C), a 0.5Ω stability translates into about 1mK temperature stability. At a set point of 5kΩ (38°C), the stability is about 2mK.

[2)] in High Resolution mode, at reduced measurement speed

REFERENCES

[1] C. M. Lakovos N. Nomikos, Nicholas C. Vamvakopoulos, "Protective and Damaging Aspects of Healing: A Review," *Wounds,* vol. 18, pp. 177-185, 2006.

[2] Y. D. T. S. McLennan S, "Molecular aspects of wound healing in diabetes," *Primary Intention,* vol. 14, pp. 8-13, 2006.

[3] H. Brem and M. Tomic-Canic, "Cellular and molecular basis of wound healing in diabetes," *The Journal of Clinical Investigation,* vol. 117, pp. 1219-1222, 2007.

[4] D. T. Nguyen, D. P. Orgill, and G. F. Murphy, *Biomaterials for treating skin loss*. Cambridge, UK: Woodhead Publishing Limited, 2009.

[5] J. Quinn, et al, "Quinn, James, et al. "Tissue adhesive versus suture wound repair at 1 year: randomized clinical trial correlating early, 3-month, and 1-year cosmetic outcome." Annals of emergency medicine 32.6 (1998): 645-649.," *Annals of Emergency Medicine,* vol. 32, pp. 645-649, 1998.

[6] A. G. D. Wayne K Stadelmann, Gordon R Tobin, "Physiology and healing dynamics of chronic cutaneous wounds," *The American Journal of Surgery,* vol. 176, pp. 26S-28S, 1998.

[7] L. V. W. Kim S. Midwood, Jean E. Schwarzbauer, "Tissue repair and the dynamics of the extracellular matrix," *The International Journal of Biochemistry & Cell Biology,* vol. 36, pp. 1031-1037, 2004.

[8] J. B. S. Howard Y Chang, Ash A Alizadeh,Ruchira Sood,Rob B West,Kelli Montgomery,Jen-Tsan Chi,Matt van de Rijn,David Botstein,Patrick O Brown, "Gene Expression Signature of Fibroblast Serum Response Predicts Human Cancer Progression: Similarities between Tumors and Wounds," *PLOS,* vol. 2, 2004.

[9] H. G. Garg, and Michael T. Longaker, *Scarless wound healing.* Newyork: Marcel Dekker, Inc, 2000.

[10] R. J. Conlan MJ, Cobb CM., "Biostimulation of wound healing by low-energy laser irradiation. A review," *Journal of Clinical Periodontology,* vol. 23, pp. 492-496, 1996.

[11] K. P. Maiya AG, Nayak BS, "Photo-stimulatory effect of low energy helium-neon laser irradiation on excisional diabetic wound healing dynamics in wistar rats," *Indian Journal Dermatology,* vol. 54, pp. 323-329, 2009.

[12] P. P. Enoch S. (2004). *Cellular, molecular and biochemical differences in the pathophysiology of healing between acute wounds, chronic wounds and wounds in the elderly*. Available: http://www.worldwidewounds.com/2004/august/Enoch/Pathophysiology-Of-Healing.html

[13] H. N. A. Yasuhiro Matsumura, "Toxic effects of ultraviolet radiation on the skin," *Toxicology and Applied Pharmacology,* vol. 195, pp. 298-308, 2004.

[14] B. B. Törmä H, Vahlquist A., "UV irradiation and topical vitamin A modulate retinol esterification in hairless mouse epidermis," *Acta Derm Venereol.,* vol. 68, pp. 291-299, 1988.

[15] A. C. Guyton, *BASIC HUMAN PHYSIOLOGY: NORMAL FUNCTION AND MECHANISMS OF DISEASE*. Philadelphia: W. B. Saunders Company, 1971.

[16] G. Karp, *Cell and Molecular Biology : Concepts and Experiments* 5ed. New Jersey: John Wiley & Sons, Inc., 2007.
[17] G. A. Teresa Audesirk, Bruce Byers, *Life on Earth*, 5 ed. New Jersey: Prentice Hall, 2005.
[18] Y. AR, "Chromophores in human skin.," *Phys Med Biol,* vol. 42, pp. 789-802, 1997.
[19] J. M. S. a. G. Kumar, "Turbulent nature of refractive-index variations in biological tissue," *Optics Letters,* vol. 21, pp. 1310-1312, 1996.
[20] S. R. Kollias N, Zeise L, Chedekel MR., "Photoprotection by melanin.," *J Photochem Photobiol B.,* vol. 9, pp. 135-160, 1991.
[21] S. Q. D. Edward A. Edwards, "The pigments and color of living human skin," *American Journal of Anatomy,* vol. 65, pp. 1-33, 1939.
[22] T. I. Karu, "EFFECTS OF VISIBLE RADIATION ON CULTURED CELLS," *Photochemistry and Photobiology,* vol. 52, pp. 1089-1098, 1990.
[23] B. R. Anders JJ, Woolery SK, Van de Merwe WP, "Low power laser irradiation alters the rate of regeneration of the rat facial nerve," *Lasers in Surgery and Medicine,* vol. 13, pp. 72-82, 1993.
[24] O. N. Navarrete Álvaro ML, Rodriguez L, Boemo R, Fuentes JF, Mateo A, Ortiz P, "Pilot Study on the Efficiency of the Biostimulation with Autologous Plasma Rich in Platelet Growth Factors in Otorhinolaryngology: Otologic Surgery (Tympanoplasty Type I)," *ISRN Surgery,* vol. 2011, p. 4, 2011.
[25] J. T. Eells, M. T. T. Wong-Riley, J. VerHoeve, M. Henry, E. V. Buchman, M. P. Kane*, et al.*, "Mitochondrial signal transduction in accelerated wound and retinal healing by near-infrared light therapy," *Mitochondrion,* vol. 4, pp. 559-567, 9// 2004.
[26] E. M. D. R. D. Lins, K. C. Lucena, M. H. Catão, A.F. Granville-Garcia, and L. G. Carvalho Neto, "Biostimulation effects of low-power laser in the repair process," *Anais Brasileiros de Dermatologia,* vol. 85, pp. 849-855, 2010.
[27] T. B. B. I. Lange, and G. Hüttmann, "Temperature dependence of light absorption in water at holmium and thulium laser wavelengths," *Applied Optics,* vol. 41, pp. 5797-5803, 2002.
[28] R. M. a. P. A. Payne, *Bioengineering and the skin*. Hingham, MA: Kluwer Academic Publishers, 1981.
[29] M. R. Mohamed Henini, *Handbook of Infra-red Detection Technologies* Oxford, UK: Elsevier Science Publishers, 2002.